

**N-glycan profiling of medulloblastoma in patients at different  
proteome subtypes of disease**

**Dissertation**

for the acquisition of the academic degree

**Doctor rerum naturalium (Dr. rer. nat.)**

at the

Faculty of Mathematics, Informatics and Natural Science

Department of Chemistry

University of Hamburg

Submitted by

**Bojia Peng, M. Sc.**

From Hunan, China

Hamburg

2023

**Reviewers of the dissertation:**

Prof. Dr. Hartmut Schlüter,

Prof. Dr. Dr. Christian Betzel

**In the presence of the examination commission members:**

Prof. Dr. Hartmut Schlüter,

Prof. Dr. Markus Fischer,

Dr. Thomas Hackl,

Prof. Huali Shen

**Date of disputation:**

14.02.2024

The research for this thesis was carried out in the Section Mass Spectrometry Proteomics, headed by Prof. Dr. Hartmut Schlüter, Diagnostic Center at the University Medical Centre Hamburg-Eppendorf (UKE) from November 2020 to November 2023.

## List of publications

1. Voss H, Godbole S, Schlumbohm S, Dottermusch M, Schuhmann Y, Neumann P, Schlüter H, Schüller U, **Peng B**, Barwikowski P, Krisp C, Neumann JE. OTHR-42. Missing data tolerant integration of proteomic datasets enables the identification and characterization of brain cancer subtypes. *Neuro Oncol.* 2022 Jun 3;24(Suppl 1):i156–7.
2. Voß H, Godbole S, Schlumbohm S, Schumann Y, **Peng B**, Mynarek M, & Neumann JE. Multiomic profiling of medulloblastoma reveals subtype-specific targetable alterations at the proteome and N-glycan level. *BioRxiv* 2023:2023.2001.2009.523234.

# Table of contents

List of publications .....	I
Table of contents.....	II
List of Abbreviations .....	IV
Abstract.....	1
Zusammenfassung .....	2
1. Introduction .....	3
1.1 Medulloblastoma .....	3
1.2 N-glycosylation in cancer.....	10
1.3 Aim of the project.....	23
2. Materials and methods.....	24
2.1 Materials .....	24
2.2 Patient samples .....	26
2.3 Proteins extraction from FFPE .....	27
2.4 Total Protein Determination by Bicinchoninic Acid Assay (BCA Assay).....	27
2.5 Protein digestion.....	27
2.6 N-glycan release .....	28
2.7 Purification of N-glycans.....	28
2.8 Reduction of N-glycans .....	28
2.9 Classical solid-phase permethylation of N-glycans.....	28
2.10 LC-MS and MS/MS Analysis.....	29
2.11 Processing of proteome raw data .....	30
2.12 Processing of N-glycome raw data.....	30
2.13 Statistical analysis and visualization .....	30
3. Result.....	32
3.1 Diversity of N-glycome profiling in different subgroups of medulloblastoma.....	34
3.2 Distribution of the N-glycosylation features in six subgroups of medulloblastoma.....	38
3.3 Quantitative changes in N-glycan profiles in six subgroups of medulloblastoma .....	41

3.4 Comparison of N-glycosylation-related proteins in six subgroups of medulloblastoma ...	44
3.5 Comparative Analysis of N-glycans between pWNT and pG3myc group.....	47
4. Discussion.....	53
4.1 N-glycan profiles detected by HPLC-MS/MS from FFPE.....	54
4.2 N-glycan diversity across different medulloblastoma subtypes .....	55
4.3 High-mannose N-glycans are correlated with pG4 .....	56
4.4 Clinical importance of bisected, poly-LacNAc modified, and tetra-antennary N-glycans in non-WNT/non-SHH medulloblastoma.....	57
4.5 Abnormal sialylation and fucosylation are potential medulloblastoma tumor biomarkers	59
4.6 Aberrant N-glycan as malignant progression markers between pWNT and pG3myc.....	61
5. Conclusion .....	64
6. References .....	65
7. Supplemental material .....	82
S1 The identified 302 N-glycans from medulloblastoma patients at MS1 and MS2 levels.....	82
8. Acknowledgment .....	120
9. Risk and safety.....	121
10. Declaration.....	124

## List of Abbreviations

<b>Abbreviation</b>	<b>Meaning</b>
ACN	Acetonitrile
Ambica	Ammonium bicarbonate
ANOVA	Analysis of Variance
CID	Collision induced dissociation
DDA	Data-dependent acquisition
DMSO	Dimethyl sulfoxide
Dol-P	Dolichol phosphate
Dol-P-P-GlcNAc	Dolichol pyrophosphate N-acetylglucosamine
DTT	Dithiothreitol
ECM	Cell-extracellular matrix
EGFR	Epidermal growth factor receptor
EMT	Epithelial–mesenchymal transition
ER	Endoplasmic reticulum
ESI	Electrospray ionization
FA	Formic acid
FDR	False discovery rate
FFPE	Formalin-fixed, paraffin-embedded
Fuc	Fucose
Gal	Galactose
GSEA	Gene Set Enrichment Analysis
HCC	Hepatocellular carcinoma
HCD	Higher-energy C-trap dissociation
Hex	Hexose
HexNAc	N-acetyl hexosamine
HPLC	High-performance liquid chromatography
IAA	Iodoacetamide
iBAQ	intensity-based absolute quantification
ICH3	Methyl iodide
LacNAc	N-acetylglucosamine
LC	Liquid chromatography
LCA	Large cell anaplastic

m/z	Mass to charge ratio
MALDI	Matrix-assisted laser desorption/ionization
min	Minute
MS	Mass spectrometry
NaOH	Sodium hydroxide
NEU	Neuraminidases
NeuAc	N-acetylneuraminic acid
OPLS-DA	Orthogonal partial least squares discriminant analysis
OST	Oligosaccharide transferase complex
PNGase F	N-glycosidase F
red-HexNAc	Reduced N-acetylhexosamine
RP	Reversed-Phase
RT	Room temperature
SD	Standard deviation
SHH	Sonic hedgehog-activated
SPE	Solid-phase extraction
TACAs	Tumor-associated cancer antigens
TEAB	Triethyl ammonium bicarbonate
WNT	Wingless-activated

## **Abstract**

Medulloblastoma, the most prevalent malignant central nervous system tumor in pediatric patients, although associated with high survival rates, presents enduring side effects from current therapies. It is crucial to unravel the biology behind the progression of different subtypes of medulloblastoma. A well-known hallmark of cancer is altered glycosylation. Profiling the N-glycosylation patterns in medulloblastoma has the potential to unveil novel targets for therapeutic intervention and diagnostic applications. In this study, an in-depth N-glycomic and proteomic analysis of six proteome subgroups of medulloblastoma was conducted using nano-liquid chromatography coupled with electrospray ionization mass spectrometry. This approach enables the resolution of the separation of isomers and performs structural characterization, uncovering profound N-glycomic diversity within the studied medulloblastoma patients with the elucidation of a number of 302 N-glycans. N-glycan profiles can distinguish medulloblastoma proteome subtypes. Furthermore, the associations between glycosylation features and glycosylation-related proteins were studied. The relative abundance of bisected and poly-LacNAc modified N-glycans was higher in the worst prognostic non-pWNT/non-pSHH in comparison with low-risk of pWNT/pSHH. Additionally, tetra-antennary N-glycans' relative abundance was more expressed in non-pWNT/non-pSHH. In pG3myc patients, the prevalence of sialylated and fucosylated N-glycans was notably elevated, whereas pG4 patients exhibited the highest levels of high-mannose N-glycans. It is noteworthy that the expression of aberrant N-glycans was influenced by N-glycan synthesis pathways in both pWNT and pG3myc subgroups. This study provides a comprehensive characterization of the N-glycome of different medulloblastoma subgroups, which may contribute to the future discovery of novel glyco-biomarkers of medulloblastoma.



## Zusammenfassung

Das Medulloblastom ist der häufigste bösartige Tumor des Zentralnervensystems bei pädiatrischen Patient\*innen. Obwohl das Medulloblastom mit hohen Überlebensraten assoziiert ist, haben Patient\*innen mit anhaltenden Nebenwirkungen der derzeitigen Therapien zu kämpfen. Es ist von entscheidender Bedeutung, die biologischen Prozesse hinter dem Fortschreiten der verschiedenen Subtypen des Medulloblastoms zu entschlüsseln. Ein bekanntes Merkmal von Krebs ist eine veränderte Glykosylierung. Die Erstellung von Profilen der N-Glykosylierungsmuster beim Medulloblastom hat das Potenzial, neue therapeutische Interventionen und diagnostische Anwendungen aufzudecken. In dieser Studie wurde eine umfangreiche N-Glykosylierungs- und Proteomanalyse von sechs Proteom-Untergruppen des Medulloblastoms unter Verwendung von Nano-Flüssigchromatographie gekoppelt mit Elektrospray-Ionisations-Massenspektrometrie durchgeführt. Dieser Ansatz ermöglicht eine hohe Auflösung der Isomerentrennung und deren strukturelle Charakterisierung, wodurch eine große N-Glykom-Vielfalt innerhalb der untersuchten Medulloblastom Patient\*innen aufgedeckt und 302 verschiedene N-Glykane gefunden werden konnte. Anhand von N-Glykanprofilen können Medulloblastom-Proteom-Subtypen unterschieden werden. Darüber hinaus wurden die Zusammenhänge zwischen Glykosylierungsmerkmalen und glykosylierungsbezogenen Proteinen untersucht. Die relative Häufigkeit von bisected und poly-LacNAc-modifizierten N-Glykanen war bei der Gruppe mit der schlechtesten Prognose (nicht-pWNT/nicht-pSHH) höher als bei der Gruppe mit dem niedrigsten Risiko (pWNT/pSHH). Darüber hinaus war die relative Häufigkeit von tetra-antennären N-Glykanen bei nicht-pWNT/nicht-pSHH stärker ausgeprägt. Bei pG3myc-Patient\*innen war die Prävalenz von sialylierten und fucosylierten N-Glykanen deutlich erhöht, während pG4-Patient\*innen die höchsten Werte von N-Glykanen mit hohem Mannosegehalt aufwiesen. Bemerkenswert ist, dass die Expression von abweichenden N-Glykanen sowohl in den pWNT- als auch in den pG3myc-Untergruppen von den N-Glykan-Synthesewegen beeinflusst wurde. Diese Studie liefert eine umfassende Charakterisierung des N-Glykosystems verschiedener Medulloblastom-Untergruppen, was zur zukünftigen Entdeckung neuer Medulloblastom Glyko-Biomarker beitragen kann.

# 1. Introduction

## 1.1 Medulloblastoma

Medulloblastoma is a prevalent malignancy within the pediatric population, representing an estimated 25% of all intracranial neoplasms and approximately 50% of posterior fossa cancers [1, 2]. Histomorphologically, medulloblastoma is categorized as an embryonal tumor of the cerebellum, the origins of this condition can be traced to specific populations of neuronal stem or progenitor cells during the early stages of life (Figure 1). Presently, there are several therapeutic approaches for medulloblastoma. Nonetheless, the prognosis remains daunting, as nearly 30% of patients do not survive this relentless disease, while those grapple with profound, long-term sequelae that significantly impede their quality of life [3]. Efforts to improve both the efficacy of treatment modalities and the quality of life for survivors remain imperative in the realm of medulloblastoma research and management.

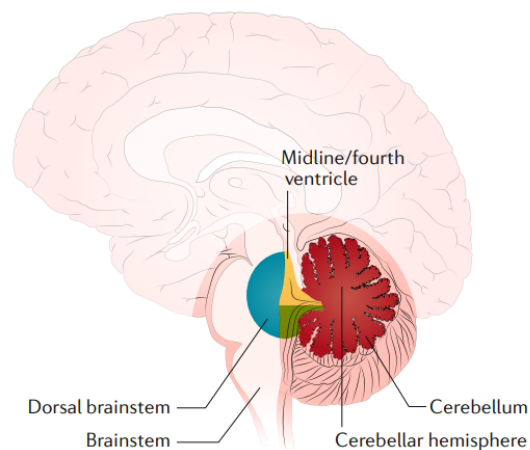


Figure 1. Location of medulloblastoma [4].

### 1.1.1 Epidemiology of Medulloblastoma

Medulloblastoma, the most prevalent childhood intracranial embryonal tumor, accounts for a substantial 63% of such cases, with an annual incidence rate of approximately 5 cases per 1 million individuals [2]. This malignancy predominantly affects children, with the majority of diagnoses occurring at a median age of 9 years, and the highest incidence rates found between the ages of 3 and 7 years. [5]. Interestingly, a secondary peak in incidence emerges among adults, constituting roughly a quarter of cases [6]. Despite therapeutic advancements, concerns persist regarding the long-term morbidity associated with treatment [7-10]. In adults, the incidence of medulloblastoma is exceptionally rare, occurring at a rate of merely 0.05 cases per 100 000

individuals [11]. Gender-wise, males are disproportionately affected, with a male-to-female ratio of 1.8:1, although this ratio may vary among different medulloblastoma subgroups [12, 13]. Alarmingly, approximately 18% of patients encounter subsequent neoplasms within 30 years of their medulloblastoma diagnosis, potentially owing to hereditary predisposition [14]. Notably, available population-based studies reveal no substantial disparities in medulloblastoma incidence across different ethnicities or geographical regions [15, 16].

### **1.1.2 Molecular classification of medulloblastoma**

Medulloblastoma is defined by a spectrum of critical genetic events, with recurrent high-level MYC amplifications representing a prominent gene-level alteration in this malignancy. MYC emerges as a frequently perturbed oncogene within medulloblastoma, and regrettably, children afflicted by MYC-amplified medulloblastoma often exhibit poor responses to current therapeutic interventions.

Early gene expression array studies confirmed that medulloblastoma was molecularly distinct from other embryonal brain tumors, such as atypical teratoid rhabdoid tumor and supratentorial primitive neuroectodermal tumor [17]. Subsequent molecular investigations have unveiled discrete molecular subgroups within medulloblastoma, leading to the consensus subgroup classifications of wntless-activated (WNT), sonic hedgehog-activated (SHH), and non-WNT/non-SHH (comprising Group 3 and Group 4) (Table 1) [18-24]. These consensus subgroup delineations have garnered widespread adoption within both the basic and clinical research realms, profoundly influencing the approach to studying and managing medulloblastoma [23]. Recent proteomic analyses have further refined subgroup distinctions within non-WNT/non-SHH and SHH medulloblastomas. These subgroups are characterized by specific molecular programs, as elucidated through multi-omic profiling encompassing proteomic and phosphoproteomic analyses, as well as investigations into transcription, translation, and synaptic and immunological processes [25, 26]. These comprehensive insights into the molecular landscape of medulloblastoma have the potential to revolutionize the understanding of this disease and guide more precise and effective therapeutic strategies.

Table 1. Molecular Classification of Medulloblastoma [4].

Molecular subtype	WNT	SHH	Group 3	Group 4
<b>Proportion of medulloblastoma</b>	10-15%	25%	25%	35%
<b>Age distribution</b>	10-12 years old	Bimodal, < 5 -> 16 years old	< 3 years old	Children
<b>Male/Female ratio</b>	1:1	1:1	2:1	3:1
<b>Location</b>	Midline, fourth ventricle	Cerebellar Hemispheres, vermis	Midline, fourth ventricle	Midline, fourth ventricle
<b>Histology</b>	Classic, rarely LCA	DN, Classic, LCA	Classic, rarely LCA	Classic, rarely LCA
<b>Metastasis</b>	5-10%	15-20%	45%	30-40%
<b>Recurrence</b>	Rare	Local	Metastasis	Metastasis
<b>Driver genes</b>	CTNNB1(90%) DDX3X (50%) SMARCA4 (25%) TP53(12.5%)	TERT (83%) PTCH1 (45%) TP53 (13%) SUFU (10%) SMO (9%) MYCN (8%) GLI2 (5%)	GF1/GFI1B (30%) MYC (10-20%) PVT1 (12%) SMARCA4 (11%) OTX2 (10%)	KDM6A (13%) SNCAIP (10%) MYCN (6%) CDK6 (83%) GF1/GFI1B (5-10%)
<b>Chromosome Aberration</b>	Monosomy 6 (>80%)	Loss 9q (PTCH1 locus)	Isochromosome 17q	Isochromosome 17q
<b>MYC status</b>	+	+	+++	-
<b>5-year survival</b>	>90%	70%	40-60%	75%

### 1.1.2.1 WNT

WNT-activated medulloblastomas, constituting approximately 10% of diagnoses, exhibit the most favorable prognosis in pediatric cases, boasting an impressive 5-year survival rate exceeding 95% [20, 27, 28]. However, this optimistic outlook is notably less pronounced among adults [29]. These tumors primarily manifest in older children, typically beyond the age of 4, with no gender predilection [21, 30]. Remarkably, they tend to present with limited metastatic spread at the time of diagnosis.

WNT-activated tumors are distinguished by a distinctive gene expression signature and the activation of the canonical WNT signaling pathway [31-33]. A noteworthy observation is that

most WNT medulloblastomas carry somatic activating mutations in exon 3 of CTNNB1<sup>[34]</sup>. These mutations result in the stabilization of  $\beta$ -catenin and its subsequent translocation to the nucleus <sup>[35, 36]</sup>. In cases lacking somatic CTTNB1 mutations, the presence of pathogenic germline APC variants necessitates genetic testing for Turcot syndrome <sup>[14]</sup>. The constitutive activation of the WNT pathway in these tumors may arise from either increased  $\beta$ -catenin stability or impaired degradation mechanisms, offering valuable insights into the underlying molecular mechanisms of this distinctive medulloblastoma subtype.

#### 1.1.2.2 SHH

SHH-activated medulloblastomas constitute both infants (below three years) and adults (above 16 years), while representing only about 15% of cases among children aged 3 to 16 <sup>[37]</sup>. Compared to WNT-driven tumors, SHH tumors manifest substantial biological, pathological, and clinical diversity <sup>[38, 39]</sup>. Prognostic outcomes in SHH tumors hinge upon a complex interplay of genetic factors and clinicopathologic parameters <sup>[40]</sup>.

Characteristically, SHH tumors harbor alterations in genes integral to the SHH signaling pathway, where canonical activation entails ligand-dependent mechanisms <sup>[41-43]</sup>. Cytogenetic aberrations observed in SHH tumors lead to haploinsufficiency of PTCH1 and SUFU <sup>[34, 44-46]</sup>. Furthermore, the presence of TP53 mutations in SHH medulloblastoma, particularly in children and adolescents, signifies a dismal prognosis <sup>[47]</sup>. Within the SHH subgroup, distinct molecular subtypes have emerged, exhibiting varying characteristics and survival rates <sup>[23]</sup>.

In contrast to WNT-activated medulloblastoma, SHH-activated medulloblastoma exhibits pronounced molecular and clinical heterogeneity <sup>[27, 44, 48]</sup>. Within the realm of SHH medulloblastoma, a nuanced classification into molecular subtypes has emerged, revealing distinctions in cytogenetics, demographic profiles, and overall survival rates. The divergence between DNA methylation and proteomics data becomes evident, underlining their differential sensitivity to specific biological processes. DNA methylation profiles may offer insights into the developmental state of the cells of origin at the inception of oncogenesis, while proteomic data capture the dynamic interplay of post-transcriptional phenomena, encompassing RNA stability, protein stability, translational regulation, and intricate signaling pathways <sup>[49, 50]</sup>. Recent proteomic investigations have unveiled two discernible proteome subgroups within SHH medulloblastoma, denoted as pSHHs and pSHHt <sup>[25, 26]</sup>. Remarkably, these proteome subgroups exhibit minimal correlation with histological characteristics or patient age. Notably, pSHHs are marked by SHH pathway-activating mutations, enriched synaptic pathways, and a

distinct metabolic profile. Conversely, pSHHt samples exhibit expression signatures and molecular alterations that align with the canonical activation of the SHH pathway. Collectively, these multifaceted insights underscore the intricate and diverse landscape of SHH-activated medulloblastoma, both in terms of molecular subtypes and their complex biological characteristics.

#### 1.1.2.3 Non-WNT /non-SHH

The 2016 World Health Organization classification system combined Group 3 and Group 4 medulloblastomas into a unified subgroup denoted as non-WNT/non-SHH medulloblastoma [23, 51]. Despite their common categorization, Group 3 and Group 4 medulloblastoma remain distinctive entities characterized by marked genetic diversity, although they share certain specific genetic aberrations [27, 39, 51, 52].

Non-WNT/non-SHH medulloblastoma often manifests a mosaic of features drawn from both Group 3 and Group 4, with classic histology being a frequent observation, sometimes featuring histological patterns such as rosette formation or nodule formation [53]. Based on large cell anaplastic (LCA) characteristics, non-WNT/non-SHH medulloblastoma predominantly aligns with Group 3 [54]. Notably, immunoreactivity of  $\beta$ -catenin in non-WNT/non-SHH tumors manifests as cytoplasmic rather than nuclear [55]. A diagnostic approach involving specific antibodies has been developed to effectively distinguish between WNT, SHH, and non-WNT/non-SHH medulloblastoma subgroups [56]. It is noteworthy that non-WNT/non-SHH tumors often present with metastatic disease, a prevalent feature at the time of diagnosis. Regrettably, these non-WNT/non-SHH medulloblastomas exhibit the bleakest overall prognosis compared to SHH and WNT medulloblastoma, with Group 3 tumors displaying an overall survival rate of less than 60% [57]. This comprehensive account elucidates the intricate nature of non-WNT/non-SHH medulloblastoma, spanning their classification, histological features, immunoreactivity, and clinical prognosis within the broader landscape of medulloblastoma subgroups.

##### 1.1.2.3.1 Group 3

Group 3 medulloblastoma represents approximately 20% of all cases, with a notably higher prevalence, reaching 45%, among infants [37]. Typically characterized by LCA histology, they primarily afflict infants and children, displaying a higher incidence in males [58]. Group 3 medulloblastoma frequently presents with a strikingly elevated rate of metastatic disease at the time of diagnosis, affecting nearly 40% of cases [59]. A salient feature of Group 3

medulloblastoma is the over-expression of the MYC gene, often attributed to amplification or aberrant expression, which distinguishing them from other medulloblastoma groups. MYC, encoding the proto-oncogene C-MYC, assumes a pivotal role in cell cycle progression, apoptosis, and cellular transformation <sup>[60]</sup>. The MYC-PVT1 fusion event has been implicated in MYC over-expression within Group 3 tumors <sup>[51]</sup>.

Genomic instability prevails in Group 3 tumors, manifesting as an unbalanced genome with a multitude of chromosomal and genetic aberrations. Notably, genomic rearrangements involving enhancer regions, leading to the overactivation of GFI1 and GFI1B oncogenes, are pervasive in Group 3 medulloblastoma <sup>[61]</sup>. Amplifications of MYC, PVT1, and OTX2 genes are observed in a substantial proportion of Group 3 tumors. Furthermore, isochromosome 17q is a recurrent genetic anomaly, occurring in approximately 25% of all Group 3 medulloblastoma, and is associated with an ominous prognosis <sup>[40]</sup>. This comprehensive delineation underscores the intricate genetic landscape of Group 3 medulloblastoma, elucidating their clinical characteristics and highlighting the significance of MYC dysregulation and genomic alterations within this medulloblastoma subgroup.

Group 3 medulloblastomas exhibit considerable clinical diversity, with the activation of the MYC oncogene holding significant therapeutic implications <sup>[18, 27, 34, 39]</sup>. Prior investigations have underscored the utility of transcriptional and gene expression profiles in distinguishing between low- and high-risk Group 3 patients <sup>[18, 39]</sup>. Nevertheless, it is noteworthy that genomic, epigenomic, and transcriptional data alone do not provide direct insights into MYC activation, a process that can manifest through various mechanisms. Recent strides in the field have enabled the direct measurement of MYC post-translational modifications, culminating in the refined categorization of Group 3 tumors into distinct clusters, namely pG3 and pG3myc <sup>[25, 26]</sup>. Pathway-level scrutiny reveals that pG3myc tumors manifest heightened MYC activity relative to their counterparts in the pG3 cluster. pG3 tumors are typified by classic histology, a notable enrichment in processes related to transcription, translation, and DNA repair pathways. Conversely, pG3myc patients exhibit elevated expression of potential biomarkers associated with high-risk non-WNT/non-SHH medulloblastoma, along with an enrichment in proteins linked to RNA processing, SUMOylation, and Ubiquitinylation. These findings shed light on the intricate landscape of Group 3 medulloblastoma, delineating distinct subgroups based on MYC activation and associated molecular processes, thereby informing potential therapeutic strategies and prognostic considerations.

#### 1.1.2.3.2 Group 4

Group 4 medulloblastomas represent the largest molecular subgroup<sup>[51]</sup>. These tumors are associated with an intermediate prognosis, akin to SHH medulloblastoma, and can affect individuals across all age groups, with a prominent incidence peak observed between 5 and 15 years of age<sup>[62]</sup>. Group 4 medulloblastoma demonstrates a predilection for males and can exhibit both classic histologic subtype and LCA characteristics<sup>[63]</sup>. Notably, approximately one-third of Group 4 medulloblastoma patients present with metastases, serving as a robust prognostic indicator linked to unfavorable outcomes<sup>[51]</sup>. This subgroup is marked by several prevalent somatic alterations, including PRDM6 enhancer hijacking, MYCN amplification, hotspot somatic mutations in KBTBD4, and recurring genetic changes in essential genes such as KDM6A, OTX2, ZMYM3, KMT2C, ZIC1, and CDK6<sup>[51, 64]</sup>. Furthermore, Group 4 tumors frequently display copy number alterations on chromosome 17<sup>[65]</sup>. It is noteworthy that a subset of non-WNT/non-SHH tumors, not aligning with Group 3 or Group 4 classifications, is characterized by activated GFI oncogenes, underscoring the intricate diversity within this subgroup<sup>[61]</sup>.

#### 1.1.3 Therapeutic strategies for medulloblastoma

Current therapeutic strategies for medulloblastoma entail a multifaceted approach encompassing maximal safe tumor resection, chemotherapy, and radiation therapy for select patients<sup>[30, 66-68]</sup>. The degree of tumor resection has been consistently correlated with improved progression-free survival and overall survival. However, the feasibility of surgical options and the attainable resection grade are influenced by the tumor's inherent aggressiveness and infiltrative characteristics<sup>[67]</sup>. Surgery stands as the widely accepted primary treatment modality, though debates persist regarding adjuvant therapy protocols. Post-surgical chemotherapy is commonly advocated, bolstered by recent meta-analysis findings, albeit not without ongoing discourse. The advent of molecular subclassification for medulloblastomas has ignited discussions on tailoring adjuvant treatments based on precise risk stratification<sup>[69]</sup>. Ongoing clinical trials are diligently investigating risk-benefit profiles, including the prospect of de-escalation or intensification therapies tailored to specific subgroups. In parallel, the development and validation of targeted drug therapies directed against molecular drivers are in progress, underscoring the paramount importance of accurate subgroup identification to steer clear of both inadequately and overly aggressive treatments. These dynamic developments underscore the evolving landscape of medulloblastoma management and the pursuit of increasingly tailored therapeutic interventions<sup>[52]</sup>.



## 1.2 N-glycosylation in cancer

Glycosylation is a multifaceted post-translational modification process that encompasses the connection of carbohydrate residues to non-carbohydrate entities, culminating in the formation of a glycocalyx on cell surfaces (Figure 2). This intricate modification exerts regulatory control over a substantial portion of cell proteins, influencing various eukaryotic processes [70]. The phenomenon of aberrant glycosylation is well-documented in both experimental models and human cancer, with numerous glycosylated epitopes serving as tumor-associated cancer antigens (TACAs) [71]. Among the diverse glycosylation types, N-linked and O-linked glycosylation are the most prevalent. In particular, aberrant N-glycosylation emerges as a recurrent feature in cancer, playing pivotal roles in tumor growth, cell signaling, migration, invasion, metastasis, angiogenesis, and immune evasion [72]. These N-glycan alterations have the capacity to modulate critical physiopathological processes underpinning tumorigenesis and cancer progression [73, 74]. Consequently, N-glycans hold promise as prospective clinical biomarkers and therapeutic targets [74-76]. While the debate continues regarding whether aberrant N-glycosylation is a cause or consequence of carcinogenesis, mounting evidence suggests its frequent association with oncogenic transformation and its pivotal role in facilitating tumor invasion and metastasis.

## Glycocalyx

Forest of cell-surface glycoconjugates

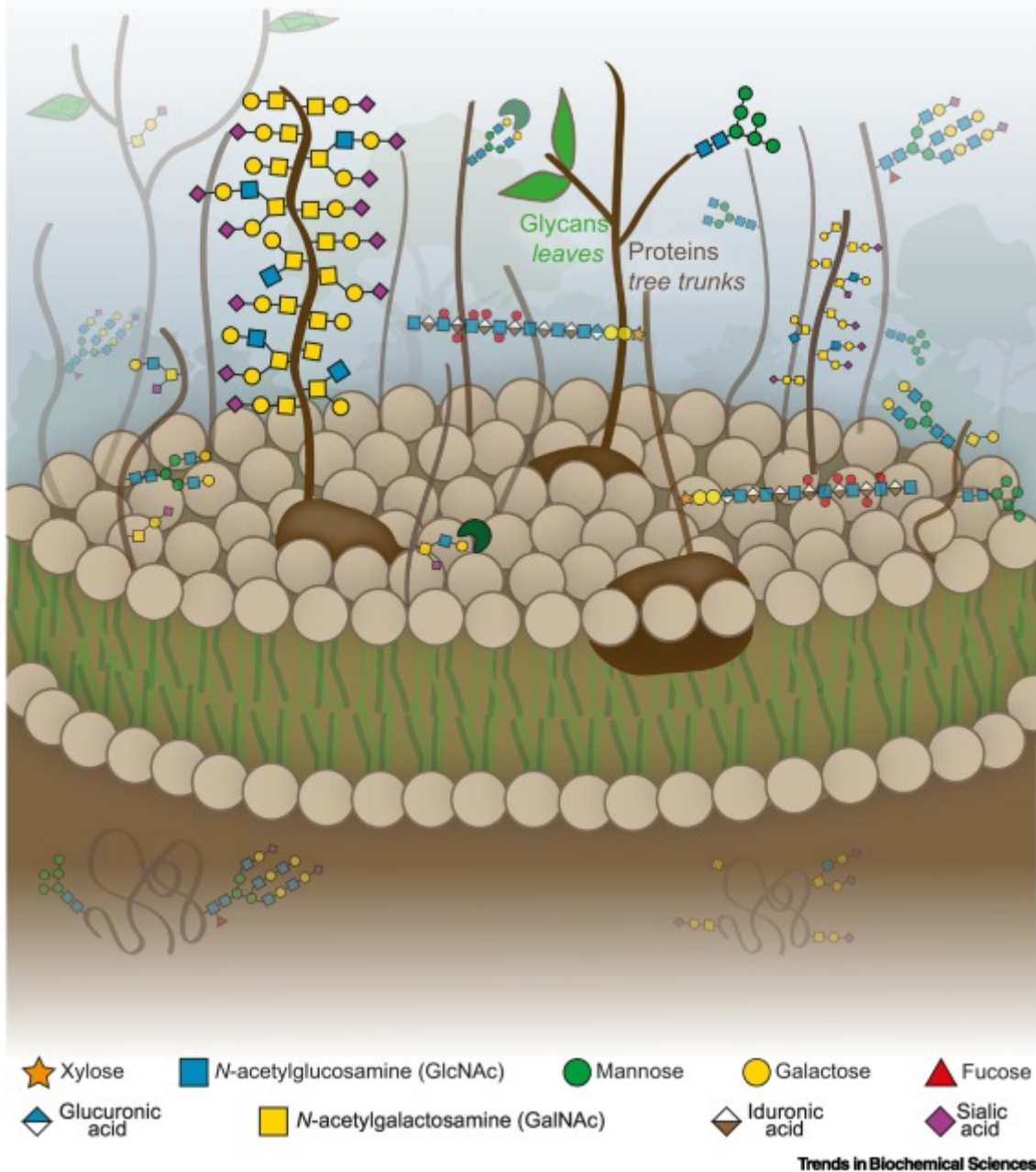


Figure 2. Glycosylation on the cell membrane <sup>[77]</sup>.

### 1.2.1 Synthesis of N-glycan in Eukaryotes

N-linked glycosylation initiates at the consensus sequence Asn-X-Ser/Thr, representing a co-translational process integral to protein synthesis, and commences in the cytoplasmic compartment of the endoplasmic reticulum (ER) membrane (Figure 3). This intricate process is initiated by transferring GlcNAc-P from UDP-GlcNAc to dolichol phosphate (Dol-P), facilitated by GlcNAc-1-phosphotransferase, ultimately yielding dolichol pyrophosphate N-acetylglucosamine (Dol-P-P-GlcNAc) <sup>[78, 79]</sup>. Subsequently, another GlcNAc residue and five

Man (mannose) residues are added in sequence, leading to the creation of the Man5GlcNAc2-P-P-Dol precursor. This precursor translocates across the ER membrane with the assistance of an enzyme known as 'flippase'. The maturation of the N-glycan lipid-linked oligosaccharide, Glc3Man9GlcNAc2-P-P-Dol, ensues through the sequential addition of glycan residues contributed by Dol-P-Glc and Dol-P-Man<sup>[80]</sup>. The entirety of this 14-sugar N-glycan precursor synthesis is orchestrated by glycosyltransferases operating within the asparagine-linked glycan pathway. Upon completion, this glycan precursor is transferred 'en bloc' to a conserved Asn-X-Ser/Thr sequon on a folded protein by the oligosaccharide transferase complex (OST)<sup>[81]</sup>.

Within the ER, N-glycans tethered to proteins undergo a sequence of processing steps pivotal to their maturation. These steps primarily entail the enzymatic trimming of glucose and mannose residues situated at the free-reducing end, a process orchestrated by specific glycosidases, including glucosidase I and II<sup>[82]</sup>. Glucosidase I functions to remove the  $\alpha$ 1-2 linked glucose residue, while glucosidase II acts on the remaining two  $\alpha$ 1-3 linked glucose. It's noteworthy that inhibiting glucosidase I can result in the retention of glucose residues, leading to the generation of partially trimmed glycoproteins due to the action of ER  $\alpha$ -mannosidase I. This progression ultimately yields mature glycoproteins adorned with Glc3Man7–9GlcNAc2 structures. Subsequently, the majority of glycoproteins exit the ER carrying eight or nine Man residues. Additional trimming of  $\alpha$ 1-2Man residues takes place in the Golgi, facilitated by  $\alpha$ 1-2 mannosidases. This Golgi-driven trimming culminates in the formation of the Man5GlcNAc2 intermediate. It is noteworthy that not all glycoproteins undergo entire processing to Man5GlcNAc2, resulting in incompletely processed glycoproteins bearing N-glycans with Man5–9 GlcNAc2 moieties, commonly referred to as high mannose-type glycans<sup>[83]</sup>.

The processing of N-linked glycans proceeds within the medial-Golgi, marking a crucial stage in glycan maturation. During this phase, GlcNAcT-I plays a pivotal role by adding an N-acetylglucosamine residue to the C2 position of the  $\alpha$ 1-3 mannose arm within the core Man5GlcNAc2 structure<sup>[84]</sup>. Subsequently,  $\alpha$ -mannosidase II acts to remove the remaining terminal mannose residues, yielding the formation of GlcNAcMan3GlcNAc2. Following this enzymatic step, GlcNAcT-II intervenes by adding a second N-acetylglucosamine residue to the C-2 position of the  $\alpha$ 1-6-linked mannose arm, thus generating the common precursor for biantennary, complex N-glycans<sup>[85]</sup>. In instances where  $\alpha$ -mannosidase II fails to trim GlcNAcMan5GlcNAc2, hybrid glycans emerge, characterized by the persistence of peripheral  $\alpha$ 1–3Man and  $\alpha$ 1–6Man residues. These complex N-glycans can undergo further extensions with the addition of branches (antennae) at the C-4 and C-6 positions of the mannose arms, a

process mediated by specific enzymes. Highly branched N-glycan structures are often augmented with galactose (Gal) residues and capped through the transfer of sialic acids at the terminal non-reducing end. Additional modifications, including bisecting-type N-glycans, core fucosylation, and terminal fucosylation, contribute to the remarkable structural diversity and complexity exhibited by N-glycan moieties [86, 87].

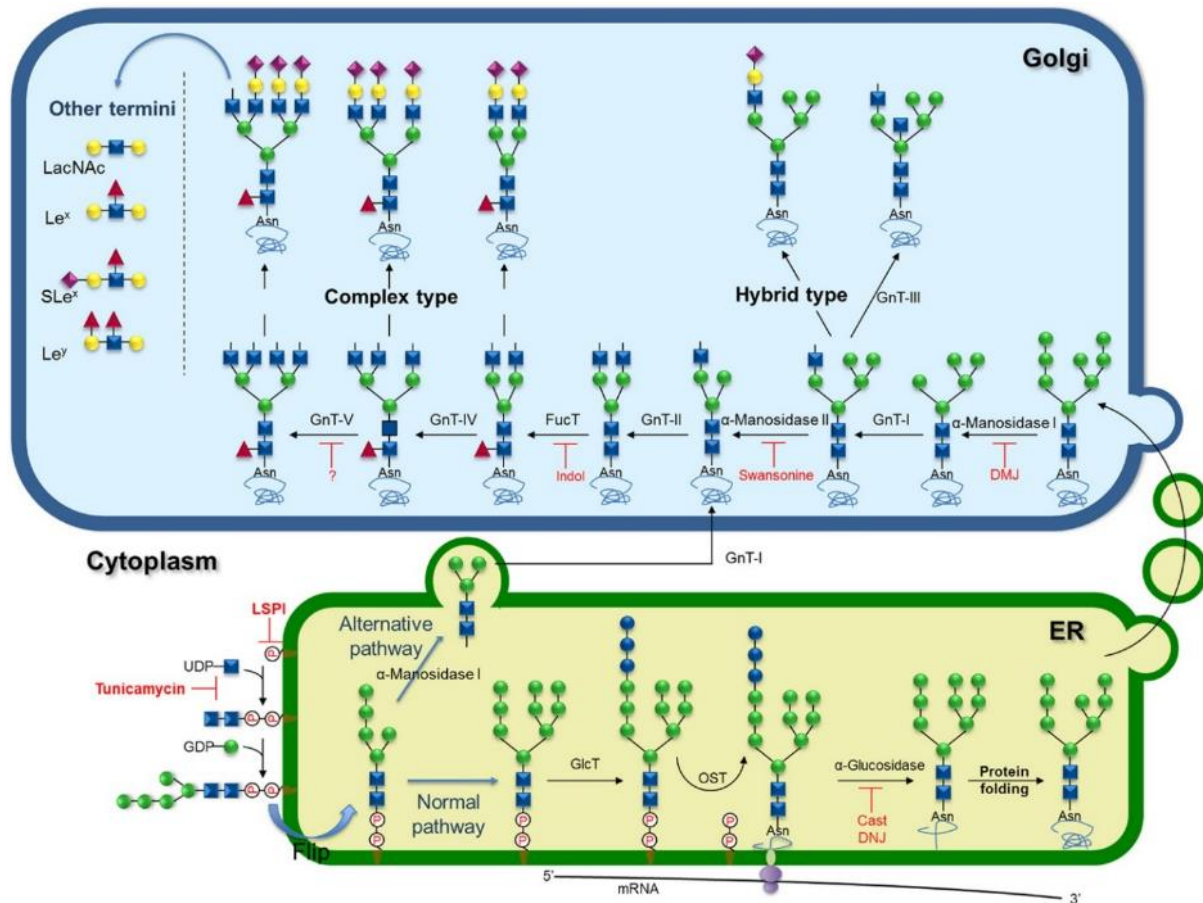


Figure 3. Schematic representation of biosynthesis and processing of N-linked oligosaccharides [88].

### 1.2.2 The role of N-glycan in cancer

N-glycosylation assumes a notable yet relatively enigmatic role in the processes of tumor invasion and metastasis. This facet of glycosylation research has historically received limited attention from the majority of cell biologists engaged in cancer investigations [89, 90]. The complexity inherent to N-glycan's structural intricacies and functional implications within the context of cancer largely underpins this dearth of attention. In stark contrast, the roles played by specific genes and proteins in shaping cancer cell phenotypes, as well as their involvement in related molecular events, have enjoyed more comprehensive definition and scrutiny within the field<sup>[74]</sup>. As the further sections, it is anticipated that forthcoming sections will delve into a

comprehensive exploration of N-glycosylation's major roles in driving the aberrant expression of N-glycan structures and the consequential impact on tumor progression.

#### 1.2.2.1 High-mannose N-glycans

High-mannose-type glycans, a distinct subgroup of N-glycans, play indispensable roles in facilitating the transit of properly folded proteins from the ER to the Golgi apparatus [91, 92]. In the context of cancer, these high mannose N-glycans assume a dual role, primarily associated with cell migration and metastasis [93-95]. Emerging evidence underscores their heightened expression in high-grade hepatocellular carcinoma (HCC), a hallmark of malignancy in this context [96]. Additionally, a correlation emerges between the upregulation of high-mannose glycans and the process of epithelial–mesenchymal transition (EMT) in HCC cells, an indicator of heightened metastatic potential [97]. Beyond HCC, the prevalence of high mannose glycans extends to colorectal cancer cell lines, encompassing both poorly differentiated and metastatic variants [98, 99]. This prevalence significantly impacts critical cellular processes, as high mannose N-glycans actively stimulate cell migration, modulate protein interactions, and enhance cellular adhesion to vascular walls across diverse cancer types, including cholangiocarcinoma, glioblastoma stem cells, and breast cancer cells [94, 100-102].

#### 1.2.2.2 $\beta$ 1,6-branched N-glycans

The enzymatic activity of GnT-V, responsible for introducing N-acetylglucosamine *via* a  $\beta$ 1–6 linkage to core mannose residues, governs the formation of  $\beta$ 1–6 branches on N-linked oligosaccharides [103](Figure 4). Remarkably, alterations in the expression profiles of these  $\beta$ 1,6-branched N-glycans have been intimately linked to key hallmarks of cancer progression, including heightened replicative potential, tissue invasion, and metastasis [104-106]. This association underscores their potential significance as crucial determinants in cancer development and metastasis, potentially serving as prognostic markers [107-109]. Furthermore, the increased branching of N-glycans demonstrates an intriguing capacity to diminish intercellular adhesion among epithelial cells, a phenomenon that could potentially foster tumor progression [110-112]. Notably, MGAT5-mediated modification of E-cadherin, a pivotal cell-cell adhesion molecule, with  $\beta$ 1,6-branched N-glycans leads to the destabilization of E-cadherin-mediated cell-cell adhesion [113]. This molecular transformation, in turn, actively contributes to tumor progression and fuels the EMT process [114, 115], thereby providing further insights into the intricate role of glycosylation in the pathophysiology of cancer [116].

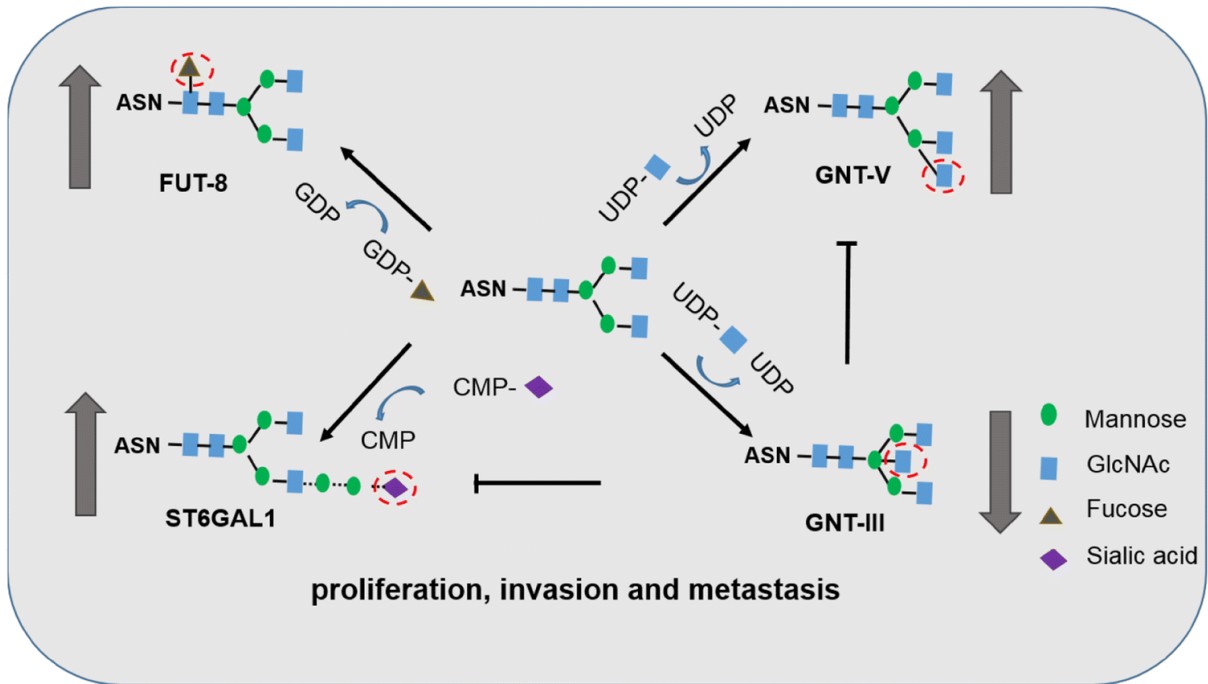


Figure 4. The cross-talk between various glycosyltransferases <sup>[117]</sup>.

### 1.2.2.3 Bisected N-glycans

The addition of bisecting GlcNAc, a distinctive modification found on hybrid or complex N-glycans catalyzed by the enzyme  $\beta$ 1,4-N-acetylglucosaminyltransferase III (MGAT3)<sup>[118]</sup> (Figure 4), has gained prominence in recent research for its profound impact on tumor progression and metastasis <sup>[84, 119]</sup>. Intriguingly, MGAT3 overexpression in highly metastatic B16 melanoma cells suppresses lung colonization and reduces  $\beta$ 1-6GlcNAc branching <sup>[120]</sup>. Furthermore, investigations have revealed an augmented expression of complex N-glycans featuring  $\beta$ 1-6 GlcNAc modification in breast and colorectal carcinomas, demonstrating a direct correlation with the progression of cancer stages <sup>[121, 122]</sup>. Bisecting GlcNAc structures are observed in highly metastatic epithelial ovarian cancer cells by elevated MGAT5 expression <sup>[123]</sup>. Mechanistically, GlcNAc-modified N-glycans play a significant role in promoting cancer cell metastasis via sialic acid modifications and their interaction with galectins, which form lattices regulating the endocytosis of signaling receptors <sup>[119]</sup>. Additionally, the introduction of bisecting N-glycan modifications in human glioma cells and neuronal cells leads to a reduction in the binding affinity between the epidermal growth factor receptor (EGFR) and EGF, subsequently leading to increased EGFR endocytosis <sup>[124-127]</sup>. In breast cancer models, E-cadherin, an essential component for metastasis, has been identified as harboring bisecting GlcNAc modifications, which negatively modulate the tyrosine phosphorylation of  $\beta$ -catenin, thus shedding light on their regulatory role in cancer progression <sup>[128-130]</sup>.

#### 1.2.2.4 Poly-N-acetyllactosamine modified N-glycans

N-acetyllactosamine (LacNAc), a disaccharide comprising GlcNAc and Gal linked through a  $\beta$ 1-4 linkage, serves as the foundational unit for more complex glycan structures. The addition of GlcNAc moieties onto LacNAc, primarily mediated by the enzyme MGAT5, results in the formation of poly-N-acetyllactosamine <sup>[131]</sup> (Figure 4). This glycan motif is subject to further modifications, including sialylation and fucosylation, with a significant proportion of  $\alpha$ 2-6-sialic acid attachments occurring on N-acetyllactosamine moieties <sup>[132]</sup>. Dysregulation in the expression of LacNAc and its polymers on both O- and N-glycans has been closely associated with various malignancies, encompassing thyroid papillary carcinomas, melanomas, and hepatocarcinomas, potentially facilitating metastatic processes <sup>[133, 134]</sup>. Moreover, the intricate interplay between the galectin family and LacNAc plays a pivotal role in tumor immune evasion. For instance, poly-N-acetyllactosamine structures, which are extended forms of LacNAc, facilitate the binding of galectin-3 to MHC class I-related chain A, thereby promoting the survival of bladder tumor cells and preventing their elimination by natural killer cells <sup>[135, 136]</sup>. Additionally, galectin-1, expressed within cancer-associated fibroblasts, has been implicated in enhancing the invasiveness of gastric cancer cells by engaging LacNAc on the cell surface through  $\beta$ 1 integrin interactions. These insights underscore the multifaceted involvement of LacNAc and its derivatives in cancer biology, shedding light on their significance as potential therapeutic targets <sup>[137, 138]</sup>.

#### 1.2.2.5 Sialylated N-glycans

Sialic acid, a crucial nine-carbon sugar located at the termini of glycans, is instrumental in mediating vital cell-cell and cell-extracellular matrix (ECM) interactions through the process of sialylation, which diversifies sialylated glycans. Sialylation, the process of adding sialic acid residues to glycans, occurs at GalNAc or Gal units within both N- and O-linked glycan structures, contributing to the structural diversity of sialylated glycans <sup>[139]</sup> (Figure 4). Notably, the introduction of sialic acid imparts a negative charge to glycoproteins, profoundly influencing their conformation, oligomerization, and interactions with other proteins under physiological pH conditions <sup>[140, 141]</sup>. Consequently, alterations in sialylation patterns have been intricately associated with various pathological conditions, prominently including cancer <sup>[142]</sup>. In bladder tumors, sialoglycoforms take precedence. Sialylation of cell-ECM adhesion molecules, such as integrins, is a driving force behind heightened metastatic potential in multiple cancer types, reshaping their adhesive properties <sup>[143]</sup>. Sialylation can also disrupt interactions involving Gal-3 and its binding partners, thereby influencing a spectrum of cellular

processes<sup>[144]</sup>. Overexpression of sialylation stands as a hallmark of the progressive landscape of pancreatic ductal adenocarcinoma, underpinning liver metastasis and conferring a dismal prognosis for affected patients <sup>[145-147]</sup>. The enhancement of sialylation processes not only facilitates CD44-mediated adhesion to selectins but also enhances integrin-mediated cellular mobility, hinting at its instrumental role in promoting metastasis through the metabolic control of protein sialylation <sup>[148]</sup>. These multifaceted facets of sialic acid's involvement underscore its significance as a pivotal player in cancer biology, offering promising avenues for therapeutic intervention.

#### 1.2.2.6 Fucosylated N-glycans

Fucosylation, an essential process in glycosylation driven by fucosyltransferases, involves the transfer of fucose from GDP-fucose to specific substrates <sup>[149]</sup> (Figure 4). It predominantly contributes to the synthesis of terminal glycan structures, marking the culmination of glycosylation <sup>[150]</sup>. Fucosylation can be categorized into two main types: core fucosylation and antenna fucosylation, depending on the location of fucose within the glycan structure. This intricate process involves thirteen types of fucosyltransferases, primarily located in the Golgi apparatus, responsible for N-linked fucosylation. In physiological contexts, fucosylated glycoproteins assume pivotal roles in determining ABO blood groups, sustaining microbial equilibrium, and modulating cognitive processes. Notably, ABO blood group antigens represent well-established instances of fucosylated glycans <sup>[151]</sup>. However, aberrant fucosylation in pathological conditions is linked to the increased proliferation, migration, invasion, and metastasis of cancer cells <sup>[74]</sup>. Elevated N-glycans with fucose residues have emerged as a valuable biomarker for the detection of colorectal carcinogenesis <sup>[133]</sup>. Moreover, reduced core fucosylation of E-cadherin contributes to the activation of EMT in lung cancer <sup>[152]</sup>. Additionally, terminal fucosylated glycans produced by luminal breast cancer cells interact with lectin receptors on myeloid cells, thereby contributing significantly to tumor progression <sup>[153]</sup>. Finally, fucosylated carbohydrate epitopes, exemplified by CD15 and sialylated CD15, play pivotal roles in blood-brain barrier disruption and the transmigration of cancer cells into the brain parenchyma, ultimately promoting the development of brain metastases <sup>[154]</sup>.

### 1.2.3 Glycans as therapeutic targets in cancer

Decades of dedicated research into carbohydrates have culminated in the emergence of glycan-based therapeutics, holding substantial promise in the realm of cancer treatment <sup>[155]</sup>. The integration of glycans as a therapeutic modality signifies a notable advancement in the ongoing battle against cancer. A wealth of recent literature, comprising various comprehensive reviews,



delves into the subject of glycan-based therapeutics within the context of cancer treatment [71]. Notably, Ferreira et al. have undertaken a comprehensive exploration of the diverse therapeutic avenues offered by glycans [156]. Their work encompasses a broad spectrum of possibilities, encompassing immunotherapy, antibody-based interventions, glycan mimetics, and innovative nano-vehicles, collectively shedding light on the multifaceted landscape of glycan-based approaches to cancer therapeutics (Figure 5).

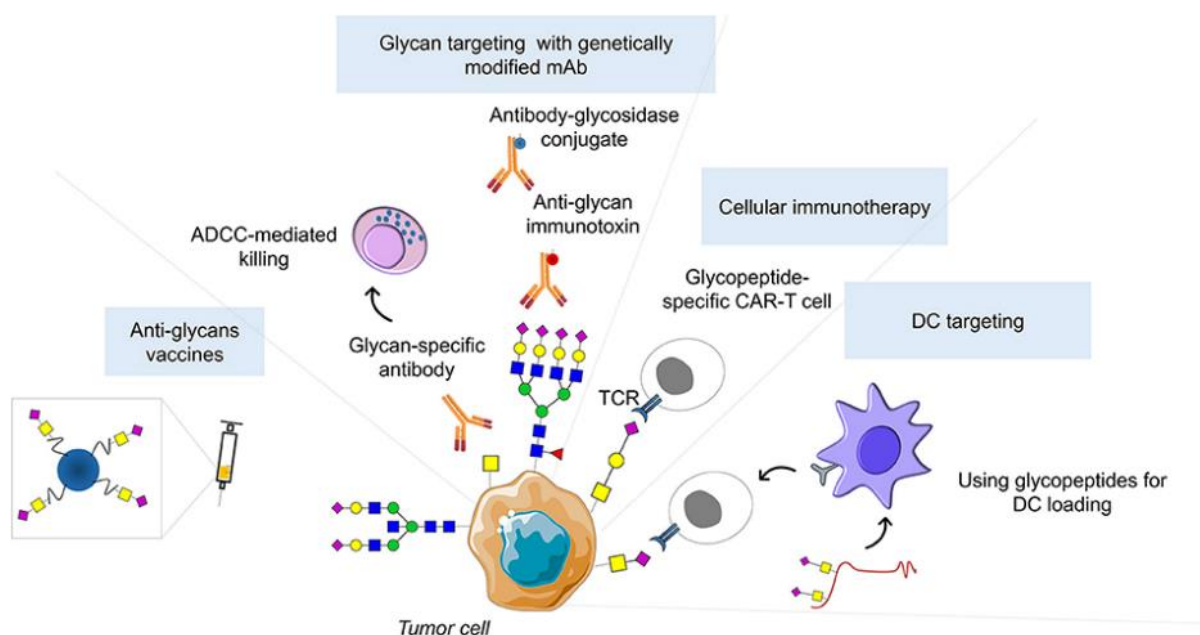


Figure 5. Glycan-based therapeutic strategies [157].

TACA constitutes a pivotal focal point in the pursuit of cancer vaccination development [158]. The ability of carbohydrates to trigger an immune response is enhanced by connecting them to immunologically active proteins. An exemplary milestone in glycan-based cancer therapeutics is the synthesis of the Globo H hexasaccharide vaccine, meticulously conjugated to keyhole limpet hemocyanin [159, 160]. This innovative endeavor marks a transformative stride in the field [161, 162]. Glycan-based antibodies have a dual role, not only guiding nascent nanotherapies but also steering the development of genetically engineered T cells armed with chimeric antigen receptors [163]. Another promising avenue involves the disruption of tumor-associated glycan-lectin interactions, with the potential to bolster the efficacy of immunotherapies [164]. A novel strategy has emerged, centered on the targeting of dendritic cells using glycopeptides, presenting an intriguing approach to induce antitumor immunity [165]. The realm of anticancer multicomponent glycoconjugate vaccines, integrating glycan antigens with T-cell peptide epitopes or immunostimulant epitopes, has proven adept at evading cancer

immunotolerance<sup>[166, 167]</sup>. Concurrently, the exploration of small molecule inhibitors targeting glycosylation machinery holds promise as a therapeutic strategy to impede cancer progression. Clinical trials now encompass a spectrum of glycosylation inhibitors, extending their potential impact to various cancer types, including melanoma, non-small cell lung cancer, squamous cell carcinoma of the head and neck, and colorectal cancer<sup>[74]</sup>.

#### **1.2.4 Mass spectrometry (MS) -based qualitative and quantitative N-glycomics**

In contemporary glycosylation research, analytical strategies play a pivotal role in the comprehensive characterization of N-glycans. These strategies are instrumental in unraveling the intricate structural identity of N-glycans, encompassing critical information such as monosaccharide composition, branching patterns, and linkage details<sup>[168]</sup>. The foundational step in this analytical process entails the liberation of N-glycans from glycoproteins, an operation facilitated by the enzyme PNGase F. Subsequently, the characterization of these liberated N-glycans unfolds through the application of diverse techniques that have evolved and matured over the past few decades<sup>[169]</sup>. These analytical approaches collectively empower researchers to delve deep into the glycomic landscape.

##### **1.2.4.1 N-glycan purification**

The pursuit of efficient N-glycomic analyses necessitates a preliminary purification and enrichment of glycans as a prerequisite to MS analysis<sup>[170]</sup>. This crucial purification step becomes imperative due to the inherently low abundance of N-glycans within biological samples, compounded by the presence of various interfering substances that can obfuscate glycan detection<sup>[171]</sup>. However, the challenge lies in sample preparation, where a variety of chemicals, including salts, reducing agents, labeling agents, and detergents, are frequently employed. Paradoxically, some of these agents, while serving their intended purposes, can inadvertently suppress glycan signals, thereby limiting the sensitivity of the analysis<sup>[172]</sup>. To circumvent these challenges, solid-phase extraction (SPE) emerges as an efficient technique for N-glycan extraction, exploiting variances in hydrophobicity to segregate glycans from the complex milieu<sup>[173]</sup>. Notably, commonly utilized SPE materials such as C18 and charcoal exhibit remarkable selectivity for N-glycans<sup>[174]</sup>. The affinity of charcoal for carbohydrate structures enables the differentiation and separation of distinct glycan types, rendering it invaluable for glycan fractionation<sup>[175]</sup>. Nevertheless, it is essential to acknowledge that SPE purification bears a significant drawback, namely incomplete trapping and elution of N-glycans, which can result in undesirable sample loss, thereby warranting careful consideration in N-glycomic analytical workflows.

#### 1.2.4.2 N-glycan Derivatization

Native N-glycans, particularly those bearing acidic moieties, exhibit inherent hydrophilicity and possess low proton affinity characteristics. These attributes collectively contribute to their limited ionization efficiency when subjected to positive mode MS analysis. To surmount this challenge and bolster the sensitivity of N-glycan detection, it becomes imperative to augment their hydrophobicity through derivatization processes [176, 177]. Notably, native sialylated and fucosylated glycans face a precarious fate during ionization and subsequent MS analysis due to their intrinsic instability [178]. Consequently, derivatization emerges as a vital strategy, serving to stabilize these N-glycan structures and preserve their integrity throughout the analytical workflow. This meticulous approach aids in unveiling the intricate details of N-glycan composition and structure, enabling a comprehensive and nuanced understanding of their roles in various biological contexts.

Permethylation and reductive amination stand out as highly effective methods for the derivatization of N-glycans, specifically tailored for MS analysis [179]. Permethylation, in particular, has been meticulously developed to meet the unique demands of MS-based N-glycomics. This approach offers the dual advantages of enhancing N-glycan stability and bolstering ionization efficiency during MS analysis, all without the introduction of extraneous chromophores or fluorophores [180]. To further streamline and optimize the derivatization process, a solid-phase permethylation protocol has been introduced. This innovation not only reduces reaction time but also significantly enhances derivatization efficiency, particularly for sialylated glycans, thereby elevating overall throughput in glycan analysis [181]. Additionally, reductive amination of glycans' free-reducing ends plays a crucial role in the elimination of glycan  $\alpha$  and  $\beta$  anomers, a critical step to mitigate complexities in liquid chromatography (LC) analysis [182]. This chemical modification introduces a discernible mass difference to the reducing end GlcNAc, facilitating its clear distinction from other internal GlcNAc moieties, thereby advancing the precision and accuracy of glycan characterization by LC-MS techniques.

#### 1.2.4.3 N-glycan separation

The efficient characterization of N-glycan isomers, mainly those present in minute quantities within biological specimens, is contingent upon the application of effective separation techniques, which are instrumental in facilitating comprehensive analysis. This necessity becomes even more pronounced when dealing with the intricate landscape of complex N-glycan structures, replete with compositional and linkage isomers that further exacerbate the analytical challenge [183]. Conventionally, condensed phase separation methods, such as LC and

Capillary Electrophoresis, have been integral to the fields of proteomics and glycomics. However, despite their proven utility, the separation of N-glycan isomers continues to present formidable hurdles, mainly attributable to the inherent microheterogeneity of N-glycans. To circumvent these limitations, various LC-MS approaches have emerged, including Reversed-Phase (RP) [184, 185], Hydrophilic Interaction Chromatography [186], Porous Graphitic Carbon [187], and Mesoporous Graphitic Carbon [188]. These innovative methodologies have been harnessed to enhance the precision of isomeric N-glycan separation, offering promising avenues for the advancement of glycomics research.

RP-LC stands as a prominent technique in the separation of derivatized glycans, predominantly relying on noncovalent interactions occurring between the analyte and the column packing materials [189]. In this context, C18 often assumes the role of the stationary phase within RP-LC columns designated for glycan separations. Nano-LC, a specialized iteration of LC, emerges as an advantageous approach for glycan analysis, proffering heightened sensitivity, enhanced separation efficiency, and improved resolution [190, 191]. The employment of permethylation as a prevalent derivatization method in RP-LC N-glycan separation serves to augment the hydrophobicity of N-glycans [192]. Notably, the hydrophobic moieties introduced through permethylation exhibit a direct correlation with the N-glycan's structural attributes, thereby engendering a more predictable retention of permethylated N-glycans on a C18 stationary phase [193]. Pioneering research efforts have culminated in the development of an advanced nano-LC nano-spray tandem MS technique meticulously tailored for the analysis of human milk oligosaccharides. This innovative method encompasses the RP-LC separation of permethylated samples, coupled with collision-induced dissociation (CID) MS/MS fragmentation [194]. Notably, this approach has proven instrumental in the profiling of milk glycans, facilitating the extraction of valuable structural insights and enabling the nuanced separation of isomeric variations through the meticulous fragmentation of permethylated human milk oligosaccharides.

#### 1.2.4.4 MS-Based N-glycomics

MS-based N-glycomics has emerged as the preeminent analytical approach, offering unparalleled sensitivity, high-throughput capabilities, and comprehensive insights into the characterization of N-glycans and N-glycomes. A watershed moment in glycomics research was marked by the commencement of a multi-institute glycomic profiling study in 2007, jointly undertaken by the Human Proteome Organization and the Human Disease Glycomics/Proteome Initiative [195]. This collaborative effort yielded a pivotal finding,

affirming the efficacy of MS-based analysis as an efficient means for the identification and quantification of oligosaccharides in N-glycomic investigations <sup>[196]</sup>. Central to the continued progress of N-glycan analysis are advances in ionization techniques, which hold the key to the development of ever more efficient MS tools <sup>[197]</sup>. Mainly, the presence of labile residues such as sialic acid and fucose necessitates the application of soft ionization techniques that induce minimal fragmentation. This preference has elevated Matrix-assisted laser desorption/ionization (MALDI) and Electrospray ionization (ESI) as favored options for N-glycan analysis <sup>[198]</sup>. The utility of ESI is further magnified when coupled with separation methodologies like LC and Capillary Electrophoresis, facilitating the examination of intricate N-glycan mixtures with exceptional sensitivity and reproducibility <sup>[199]</sup>. Nonetheless, it is noteworthy that despite these remarkable advantages, the structural analysis of N-glycans can pose challenges, principally due to the scarcity of high-throughput analysis software solutions currently available in the field.

### **1.3 Aim of the project**

Medulloblastomas are aggressive pediatric brain tumors of which distinct subtypes are defined mainly using transcriptome analysis, next-generation sequencing, and examination of DNA methylation. Proteomic analysis, encompassing post-translational modifications, provides a direct representation of a tumor's phenotype, offering a distinct advantage over nucleic acids and enabling precise identification of clinically significant phenotypes and actionable functional alterations, while also revealing potential common therapeutic targets in medulloblastomas that may arise from genomic and epigenomic changes. In this study, six proteome medulloblastoma subgroups were utilized, pWNT, pSHHs, pSHHt, pG3myc, pG3 and pG4 (p=proteome, s=synaptic profile, t= transcriptional profile).

In contrast to nucleic acids and protein distribution, N-glycan possesses the capability to intricately dissect cancer-related signaling networks and identify cell physiology that can be targeted with precision. This study utilized quantitative N-glycome as a valuable technique to investigate and characterize the N-glycan patterns and glycosylation-related protein and changes associated with different medulloblastoma subtypes. In the current study, N-glycans were derivatized by reduction and permethylation, and followed by RPLC-MS/ MS measurement. This study followed the hypothesis that based on N-glycan biosynthesis and quantification of N-glycan abundance, insights into the dysregulated N-glycan patterns and potential therapeutic targets for different proteome subtypes of medulloblastoma.

This study had four main objectives. Firstly, it was aimed to examine N-glycan diversity across six medulloblastoma subgroups. Secondly, the focus was on analyzing the relative abundance of N-glycosylation traits across different subgroups. Thirdly, the focus was on glycosylation-associated proteins such as N-glycan synthesis and ECM proteins depending on different molecular subtypes of medulloblastoma. Lastly, the focus was on the dysregulated N-glycan and biosynthesis pathway between pWNT and pG3myc. This research aimed to expand the understanding of the N-glycan profiles that play vital roles in medulloblastoma.

## 2. Materials and methods

### 2.1 Materials

Table 2: List of chemicals and enzymes used.

Chemicals and enzymes	Manufacturer
n-heptane	Merck (142-82-5, Darmstadt, Germany)
Acetonitrile (ACN), LC-MS grade	Merck (75-05-8, Darmstadt, Germany)
Triethyl ammonium bicarbonate (TEAB)	Thermo Fisher (90114, Waltham, Massachusetts, USA)
Sodium Deoxycholate (SDC)	Sigma-Aldrich (D6750-10G, St. Louis, Missouri, USA)
Formic acid (FA)	Honeywell Fluka (94318, North Carolina, US)
Ammonium bicarbonate (AmbiCa)	Sigma-Aldrich (09830, St. Louis, Missouri, USA)
Dithiothreitol (DTT)	Sigma-Aldrich (D0632, St. Louis, Missouri, USA)
Iodo acetamide (IAA)	Sigma-Aldrich (I-6125, St. Louis, Missouri, USA)
Sequencing grade modified Trypsin	Promega (V5111, Madison, Wisconsin, USA)
N-glycosidase F (PNGase F)	Promega (V48331, Madison, Wisconsin, USA)
Acetic acid	Carl Roth (UN 2789, Karlsruhe, Germany)
Borane-ammonia complex	Sigma-Aldrich (682098, St. Louis, Missouri, USA)
Dimethyl sulfoxide (DMSO)	Sigma-Aldrich (SZBC1660V, St. Louis, Missouri, USA)
Sodium hydroxide (NaOH) beads	Honeywell Fluka (71691, North Carolina, US)
Methyl iodide (ICH <sub>3</sub> )	Sigma-Aldrich (18507, St. Louis, Missouri, USA)
Chloroform	Merck (67-66-3, Darmstadt, Germany)
Ethanol	Th. Geyer (2273.1000, Renningen, Germany)
Methanol	Sigma-Aldrich (67-56-1, St. Louis, Missouri, USA)
Water	Th. Geyer (455.1000, Renningen, Germany)

Table 3: List of disposables used.

Disposables	Manufacturer
Amicon Ultra 0.5 ml 3K centrifugal filters	Merck Millipore (UFC500396, Billerica, Massachusetts, USA)
Pierce™ BCA Protein Assay Kit	Thermo Fisher (2161296, Waltham, Massachusetts, USA)
SepPak C18 1cc 100 mg	Waters (WAT023590, Milford, Massachusetts, USA)

Table 4: List of devices used.

Devices	Manufacturer
Probe sonicator Sonoplus	Bandelin electronic GmbH & Co. KG (Berlin, Germany)
Centrifuge 5424	Eppendorf (Hamburg, Germany)
Microplate Reader	Tecan Life Sciences (Männedorf, Switzerland)
SpeedVac concentrator	Thermo Fisher (Waltham, Massachusetts, USA)
Thermomixer compact	Eppendorf (Hamburg, Germany)

Table 5: List of chromatography instruments used.

Chromatography Instruments	Manufacturer
Dionex Ultimate 3000	Thermo Fisher (Waltham, Massachusetts, USA)

Table 6: List of chromatography columns used.

Chromatography columns	Manufacturer
Acclaim PepMap 100 C18 trap, 100 $\mu\text{m}$ x 2 cm, 5 $\mu\text{m}$ , 100 Å	Thermo Fisher (Waltham, Massachusetts, USA)
Acclaim PepMap 100 C18 analytical column, 75 $\mu\text{m}$ x 50 cm, 2 $\mu\text{m}$ , 100 Å	Thermo Fisher (Waltham, Massachusetts, USA)



Table 7: List of mass spectrometry instruments used.

Mass spectrometry instruments	Manufacturer
Orbitrap Fusion™ Tribrid™ Mass Spectrometer	Thermo Fisher (Waltham, Massachusetts, USA)

Table 8: List of software used.

Software	Manufacturer/Developer
MaxQuant 1.6.2.10	Mann and Cox Lab Group
Perseus 1.6.15.0	Mann and Cox Lab Group
ProteomeDiscoverer 2.0	Thermo Fisher (Waltham, Massachusetts, USA)
Skyline 21.1.0.278	MacCoss Lab Group
GlycoWorkbench 2.1	Alessio Ceroni, Kai Maass and David Damerell
Xcalibur Qual Browser 4.2.28.14	Thermo Fisher (Waltham, Massachusetts, USA)
Xcalibur Freestyle 1.4	Thermo Fisher (Waltham, Massachusetts, USA)
R 4.2.2	John Chambers and colleagues
GSEA 4.1	UC San Diego and Broad Institute
GraphPad Prism 8.0	Harvey Motulsky (San Diego, CA, USA)
SIMCA Software 14.1	MKS Umetrics AB
Cytoscape environment 3.8.2	National Institute of General Medical Sciences
EnrichmentMap 3.3	Merico D, Isserlin R, Stueker O, Emili A, Bader GD
AutoAnnotate 1.3	Mike Kucera and colleagues

## 2.2 Patient samples

Archival Formalin-fixed, paraffin-embedded (FFPE) specimens from medulloblastoma patients who had undergone surgery at various neuropathology units in Germany within the years 1976-2021, were used in the study, in line with ethics requirements laid down in an appropriate version of the 1964 Declaration of Helsinki. All samples underwent anonymization. Samples were sectioned from the FFPE tissue blocks using standard laboratory protocols.

### **2.3 Proteins extraction from FFPE**

FFPE medulloblastoma sections underwent a meticulous deparaffinization procedure, which included three 10-min heptane incubations, followed by centrifugation at room temperature (RT) for 10 min at 14 000 g. Subsequent rehydration of these sections was meticulously executed through three incubations in ethanol (each time for 10 min), followed by centrifugation at RT for 10 min at 14 000 g. After the supernatant was removed, samples were resuspended by 200  $\mu$ L of lysis buffer containing 100 mM TEAB and 1% SDC and incubated at 99°C for 1 h on a thermomixer. For homogenization and DNA degradation, sonication was performed for ten pulses at 30% power with a probe sonicator. Then, the extracts were centrifuged for 1 min at 14 000 g at RT and stored at -20°C until use.

### **2.4 Total Protein Determination by Bicinchoninic Acid Assay (BCA Assay)**

To determine ascertain the protein concentration within the samples, the Pierce™ BCA Protein Assay Kit was employed. A set of protein standards was prepared from concentrated albumin standards. The next step entailed the formulation of a working solution, an amalgamation achieved through the meticulous mixing of BCA Reagent B with BCA Reagent A. 200  $\mu$ L of the prepared working solution was subsequently introduced into both protein standard solutions and sample solutions. Subsequently, these solution mixtures were subjected to a controlled incubation period of 30 minutes at a constant temperature of 37 °C, with the experimental environment shielded from external light sources. Post-incubation, precise absorbance measurements were exactly recorded at a wavelength of 562 nm, thus concluding the essential protocol for protein concentration determination.

### **2.5 Protein digestion**

Each sample lysate, containing 60  $\mu$ g of proteins, was adjusted to a final volume of 100  $\mu$ L by lysis buffer. To initiate protein processing, disulfide bonds were reduced by adding 10  $\mu$ L of 100 mM DTT to the sample-buffer mixture, followed by 30-min incubation at 37 °C on a thermomixer. Alkylation was carried out by adding 10  $\mu$ L of 200 mM IAA to the mixture and then incubating it for 30 min at 37 °C in the dark using a thermomixer. After incubation, protein digestion was carried out by adding trypsin to each sample in a ratio of 1:100 and incubated at 37°C for 16 hours. Digestion reaction was quenched by adding 1% FA and vortexed for 30 s. After centrifugation at 14 000 g for 10 minutes, the supernatant was carefully transferred to a new tube and subsequently subjected to vacuum drying using a SpeedVac concentrator. The desiccated peptides were stored until further measurement.

## **2.6 N-glycan release**

As previously mentioned, 100 ug of proteins from each sample (n=18) were utilized. The samples were then reduced and alkylated. Samples were concentrated fivefold using Amicon Ultra Centrifugal Filters with buffer exchange in 100 mM ammonium bicarbonate. Each sample was supplemented with twenty units of PNGase F, followed by incubation at 37 °C for 24 hours. After incubation, samples were boiled at 95 °C for 5 min on a thermomixer and cooled at -20 °C for 10 min. Protein digestion was performed by adding trypsin to each sample at a ratio of 1:100 and incubating at 37°C for 24 hours. An additional ten units of PNGase F were added into each tube and moved on 37 °C thermomixer to incubated for 24 h. Samples were vacuum-dried using a SpeedVac concentrator and stored at -40 °C.

## **2.7 Purification of N-glycans**

Following PNGase F digestion, the released N-glycans underwent a purification process employing Sep-Pak C18, as outlined by Morelle et al. [200]. Initially, the Sep-Pak C18 cartridge was conditioned through five incubations in methanol, followed by equilibration with 5 mL of 5% (v/v) acetic acid solution. The sample was reconstituted with 200 µL of 5% (v/v) acetic acid, transferred into the column, and subsequently purified N-glycans were eluted with 1 mL of 5% (v/v) acetic acid, repeated five times. Samples were further subjected to vacuum drying using a SpeedVac concentrator and stored at -40 °C.

## **2.8 Reduction of N-glycans**

To eliminate the  $\alpha$  and  $\beta$  anomers from the reducing end of the released N-glycans, the dried samples were incubated with 40 µL of 10 mg/mL Borane-ammonia complex at 60 °C for 1.5 h on a Thermomixer using a rotation speed of 1000 rpm. Afterward, samples were vacuum-dried and then redissolved in 300 µL of methanol. Ammonium hydroxide and ammonium carbonate were eliminated through the repeated evaporation of methanol using a SpeedVac concentrator until no white reagents were noticeable in the tube.

## **2.9 Classical solid-phase permethylation of N-glycans**

The N-glycans were permethylated by an optimized solid-phase procedure. Briefly, samples were dissolved in 110 µL of DMSO/water (in a ratio of 1:100) solution and 70 µL of methyl iodide, followed by a 10-min incubation with 200 mg of NaOH beads on a Thermomixer at RT. The reaction solution was moved to a tube after incubation and subsequent supernatant collection through centrifugation. With the addition of another 300 µL of DMSO, the supernatant was collected through centrifugation to the previous 1.5 mL Eppendorf tube. The

quenching of permethylation and oxidation reactions was accomplished by introducing 5% (v/v) acetic acid into the mixture solution. Afterward, the retrieval of permethylated N-glycans was achieved through a chloroform-water method. The chloroform phases were vacuum-dried and stored at -40 °C for further measurement.

## **2.10 LC-MS and MS/MS Analysis**

Reduced permethylated N-glycans and label-free peptides were dissolved in 0.1% FA solution and subsequently transferred to a glass vial before injection into a Dionex UltiMate 3000 UPLC system. Purification and desalting of permethylated reductive N-glycans and peptides were carried out using an RP C18 trapping column with a solvent composition of 2% solvent B (0.1% (v/v) FA in ACN) and 98% solvent A (0.1% (v/v) FA). Subsequently, an analytical RP C18 column facilitated chromatographic separation. Peptide separation and elution were accomplished through a linear gradient, transitioning from 1% to 30% of solvent B over a duration of 70 min, while maintaining a constant flow rate of 0.3  $\mu$ L/min. The peptides were analyzed using a quadrupole-orbitrap-ion trap mass spectrometer operating in data-dependent acquisition (DDA) mode. For MS1 scanning, an orbitrap mass analyzer with a resolution of 120 000 FWHM was employed, accompanied by an AGC target of  $2.0 \times 10^6$ , and a m/z scan range set from 400 to 1300. During higher-energy C-trap dissociation (HCD)-MS/MS, the most intense precursor ions were selected for fragmentation, isolated using a 1.6 m/z isolation window, and subjected to HCD with a normalized collision energy of 30%. The resulting fragments were detected using an orbitrap resolution of 15 000 FWHM, an AGC target of  $1 \times 10^5$ , and a max accumulation time of 60.00 ms.

For measuring permethylated N-glycan, a 115 min gradient was used, in which solvent B started with 2%, increasing to 30% in 10 min, to 75% in 70 min, and finally to 95 min. Eluting N-glycans were analyzed using a quadrupole-orbitrap-iontrap mass spectrometer in DDA mode. For MS1 scanning, an orbitrap mass analyzer was performed with an orbitrap resolution of 120 000 FWHM; an AGC target was  $2.0 \times 10^6$ ; and the m/z scan range was set from 400 to 2000. For CID-MS/MS, the most intense precursor ions were selected for fragmentation and isolated using an isolation window of 2 m/z; the normalized collision energy of CID was set to 35%; the fragments were detected at an orbitrap resolution of 17 500 FWHM; the AGC target was  $1.0 \times 10^4$ ; max accumulation time was 20.00 ms.

## 2.11 Processing of proteome raw data

LC–MS/MS data underwent processing using the Andromeda algorithm, integrated with MaxQuant, wherein the protein identification strategy entailed searching measured MS2 spectra against theoretical fragment spectra of tryptic peptides derived from a murine Swiss-Prot FASTA database (as of February 2020) containing 17,015 entries. Each sample was treated as an independent experiment, with meticulous consideration given to specific modifications, including carbamethylation of cysteine residues, methionine oxidation, protein N-terminal acetylation, initiator methionine removal, and glutamine to pyroglutamate conversion, as variable modifications. Peptides meeting the criteria of a minimum length of 6 amino acids and a maximum mass of 6000 Da were identified with a mass tolerance of 10 ppm and a restriction of a maximum of two missed trypsin cleavage sites. For accurate peptide identification, matching between runs was employed within specified time windows, and error tolerances for precursor and fragment spectra searches were predefined. Peptide identification employed a stringent false discovery rate (FDR) threshold of <0.01 through a decoy database approach. Label-free quantification ensued with meticulous criteria for peptide selection and quantification, encompassing both razor and unique peptides.

## 2.12 Processing of N-glycome raw data

The raw N-glycan data was initially visualized using Xcalibur Qual Browser, and all detected molecular masses and  $m/z$  were extracted by MaxQuant. Potential monosaccharide compositions for N-glycan precursors were determined using an In-house Python script <sup>[201]</sup>. The variable N-glycan compositions and structures were based on MS/MS results. Manual assignments were made to correlate peaks in MS/MS spectra with all possible N-glycan fragment mass lists from GlycoWorkbench. The depiction of all N-glycan structures adhered to the Symbol Nomenclature for Glycans guidelines and was drawn using GlycoWorkbench <sup>[202, 203]</sup>. Skyline software was used for all N-glycan quantitation. Peak areas for each quantified N-glycan were exported in Excel.

## 2.13 Statistical analysis and visualization

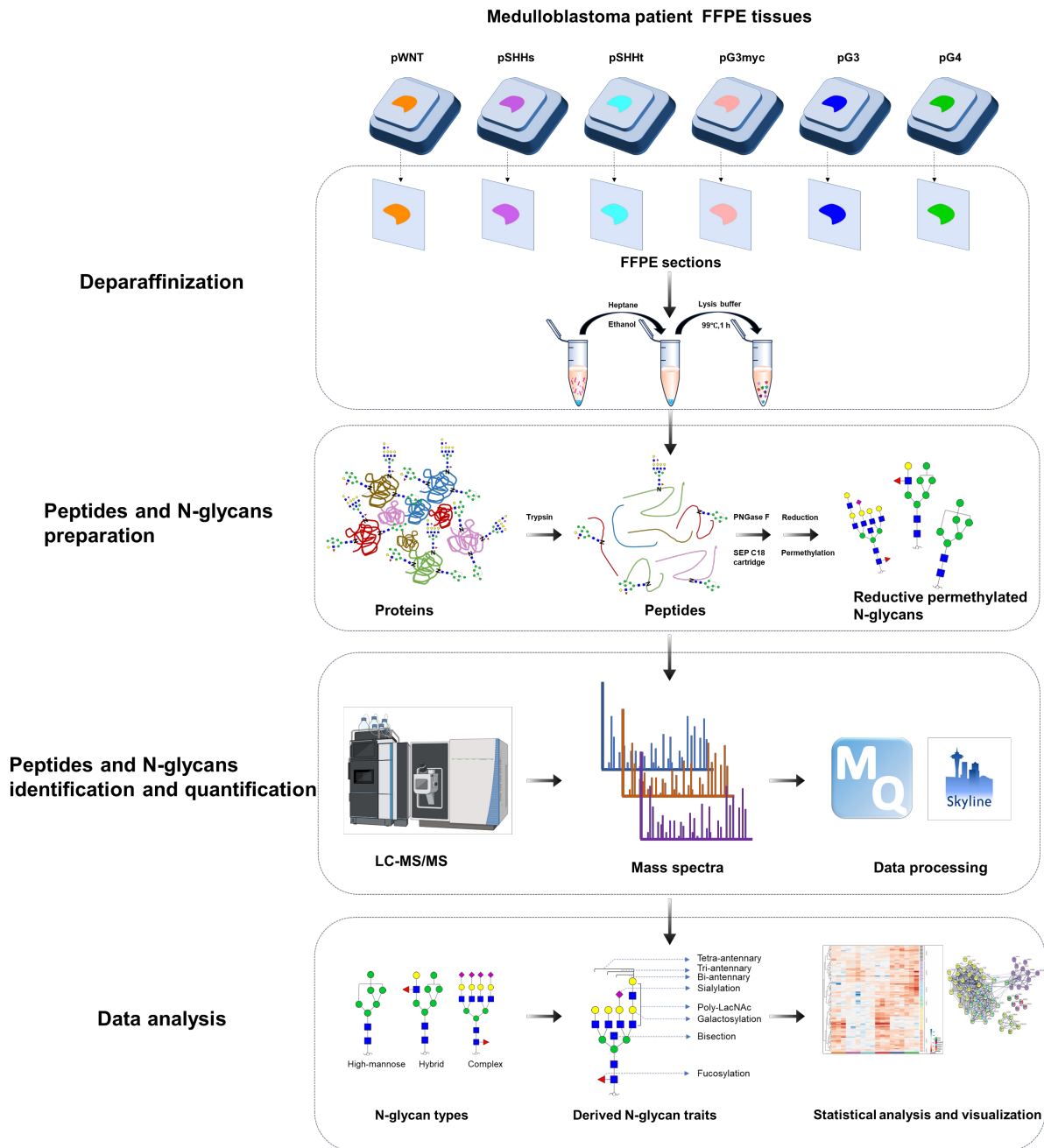
Relative protein abundances were subjected to log<sub>2</sub> transformation and normalization to the total protein content per sample in Perseus. This procedure aimed to correct for variations in sample-to-sample injected amounts. Gene Set Enrichment Analysis (GSEA), based on Reactome, was performed using GSEA software, involving 1000 permutations structured around gene sets and employing a weighted enrichment statistic based on the signal-noise ratio

for gene ranking <sup>[204]</sup>. The GSEA results were effectively visualized using Cytoscape <sup>[205]</sup> with the EnrichmentMap application <sup>[206]</sup>, focusing on gene sets that met predefined criteria (FDR < 0.25 and a *p*-value < 0.1). To cluster gene sets, AutoAnnotate was applied <sup>[207]</sup>, utilizing the Markov cluster algorithm (MCL) and the gene-set-similarity coefficient for edge weighting within the clustering process.

N-glycan compositions were succinctly represented using abbreviations like hexose (Hex), N-acetylhexosamine (HexNAc), reduced N-acetylhexosamine (red-HexNAc), fucose (Fuc) and N-acetylneuraminic acid (NeuAc). The results were presented as mean ± standard deviation (SD) for each of the three samples (n = 3). Relative quantification of individual N-glycan species within the samples was accomplished by calculating the percentage of each N-glycan relative to the total N-glycome, which included direct N-glycan traits pertaining to individual N-glycan compositions, as well as derived traits based on shared structural characteristics, such as high-mannose, hybrid-type, and complex-type, the number of antennas, bisecting GlcNAc and sialylation, fucosylation, galactosylation, and poly-LacNAc motifs <sup>[208]</sup>. Significantly, the summation of N-glycan composition abundances was conducted to compute derived glycosylation traits. For distributions of N-glycan levels across different medulloblastoma subgroups, the N-glycan data was log-transformed, and the median normalization was applied across columns to address variations in injection amounts. Afterward, N-glycans with at least 50% valid values in 18 samples were considered, and further missing values were filled with MissForest imputation. Analysis of Variance (ANOVA) (*p*-value < 0.05) was employed to assess the statistical difference in significant N-glycan abundance changes between patients with different medulloblastoma subtypes. To further demonstrate the separation between different group patients, orthogonal partial least squares discriminant analysis (OPLS-DA) was performed to reveal the class separation between the groups and to identify the N-glycans responsible for class separation. Moreover, the heat map of the Pearson correlation coefficients, based on N-glycan abundance, was constructed with Perseus software to explore inter-individual variation in N-glycan expression visually. The Student's *t*-test (*p*-value < 0.05 and fold change difference more than 1.5) was used to determine the statistically significant dysregulation of N-glycans. The dynamic range of N-glycan abundance across different medulloblastoma subgroups was based on an intensity-based absolute quantification (iBAQ) algorithm. Traditional statistical analysis was performed using GraphPad Prism and R, and SIMCA Software was used for OPLS-DA.

### 3. Result

To examine N-glycome diversity and proteome profiles according to different subgroups of medulloblastoma, 18 medulloblastoma patient samples were prepared for the N-glycomics experiment and 62 samples for the proteomic experiment (Figure 6). In this study, the proteins were extracted from FFPE tissue by dewaxing with heptane and ethanol, followed by additional SDC buffer. Moreover, reductive permethylated N-glycans and Proteins were detected by RPLC-MS/MS analysis. To assess N-glycosylation changes across all subgroups of medulloblastoma, glycosylation-related proteins were identified by GSEA, and identified N-glycans were classified into three common N-glycan types as well as derived glycosylation features based on the N-glycan biosynthesis, such as galactosylation, sialylation, fucosylation, bisection, and antennary. Finally, the pWNT, pSHHs, pSHHt, pG3myc, pG3 and pG4 group N-glycomes and proteomes were characterized by comparing the quantitative N-glycans and glycosylation-related proteins across different medulloblastoma subgroups by ANOVA, OPLS-DA, T-test, N-glycan biosynthesis and GSEA.



**Figure 6. Scheme of N-glycomics and proteomics workflow of six medulloblastoma subgroups.** Medulloblastoma tissues, preserved using FFPE techniques, were sectioned into multiple fragments for further analysis. After paraffinization, proteins were isolated with lysis buffer and denatured. Each sample underwent trypsin digestion and PNGase F cleave. Native N-glycans were purified by SEP C18 cartridge, and reduced and permethylated by Borane-ammonia complex and protocol of classical solid-phase permethylation. Reductive permethylated N-glycans and peptides were measured by RPLC-MS/MS measurement, and followed by identification and quantification. Direct N-glycan and derived N-glycosylation features were characterized for exploring the role of glycosylation in medulloblastoma.



### 3.1 Diversity of N-glycome profiling in different subgroups of medulloblastoma

A total of 302 N-glycans were found in medulloblastoma samples across all subgroups (Supplemental material S1). To obtain a comprehensive overview of glycomics profiling, each N-glycan composition was plotted with the main glycan classification. Based on the biosynthetic pathway, N-glycans compositions were ordered from high mannose to complex and hybrid N-glycans. Identified N-glycans were mainly complex type (n=260), while just a few numbers of high-mannose and hybrid type N-glycans (n=11, 31) were identified among six groups (Figure 7A). For the characterization of N-glycans traits in identified N-glycan profiles, the high-mannose type of identified N-glycans contained Man3 to Man9 consisting of mannose and two numbers of HexNAc in combination with few numbers of Fuc residues, the composition of the hybrid type of identified N-glycans have consisted of the main proportion of mannose and combined with few numbers of HexNAc, Fuc, Gal and Neu5Ac, and the composition of the complex type of identified N-glycan were mainly proportion of HexNAc, Gal, Fuc, and Neu5Ac and combined with three numbers of mannose.

At the qualification level of N-glycome, the number of N-glycans in non-WNT/ non-SHH subgroups are significantly higher than in pWNT, pSHHs and pSHHt group. 162, 139, and 110 common N-glycans with three samples were identified in pWNT, pSHHs and pSHHt subgroup, respectively (Figure 7B). Additionally, 232, 190, and 231 common N-glycans with three samples were identified in pG3myc, pG3, and pG4 subgroup.

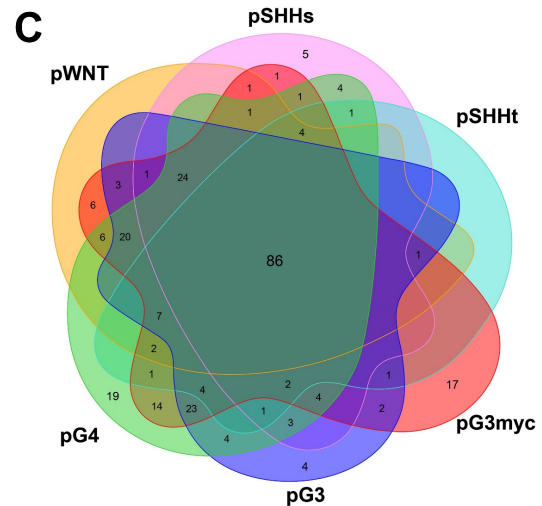
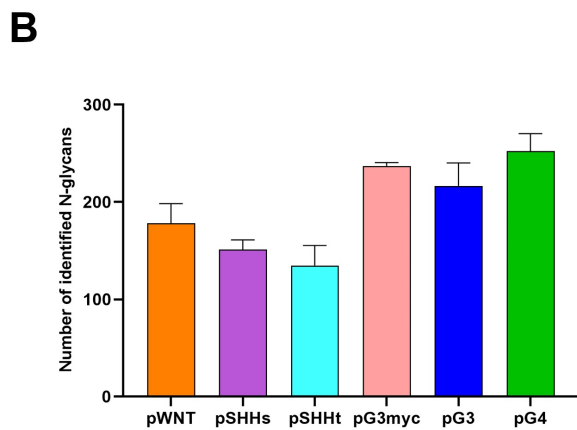
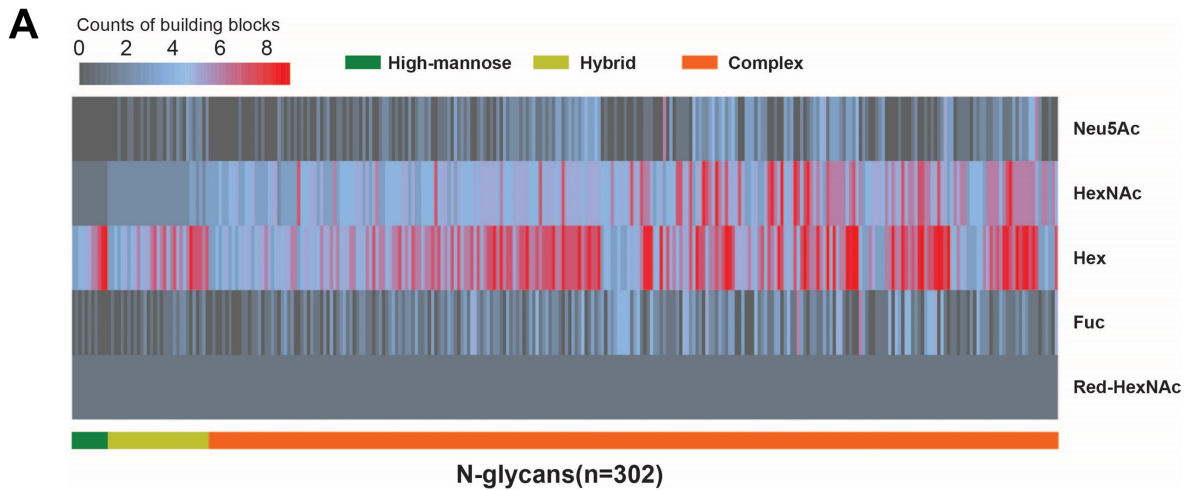
A Venn diagram showing that the differences in N-glycan profiles among the six groups is presented in Figure 7C. In total, there were 86 conserved N-glycans shared with all six subgroups, and each group had its own unique N-glycan, except for pSHHt and pWNT groups. There were five exclusive N-glycans in the pSHHs group, namely N14311, N06421, N25311, N06311 and N16521. N36531, N04331, N05731, N05541, N34501, N45611, N08701, N23721, N07461, N36541, N25431, N07711, N22701, N28711, N05341, N07721 and N35831 were only present in the pG3myc group. N06411, N16511, N16711 and N17901 were unique N-glycan in the pG3 group. N17811, N36611, N36711, N26711, N23621, N07801, N06611, N34631, N26921, N25621, N15541, N05851, N26831, N46711, N16821, N27451, N06741, N46811 and N26611 were unique N-glycan in the pG3 group.

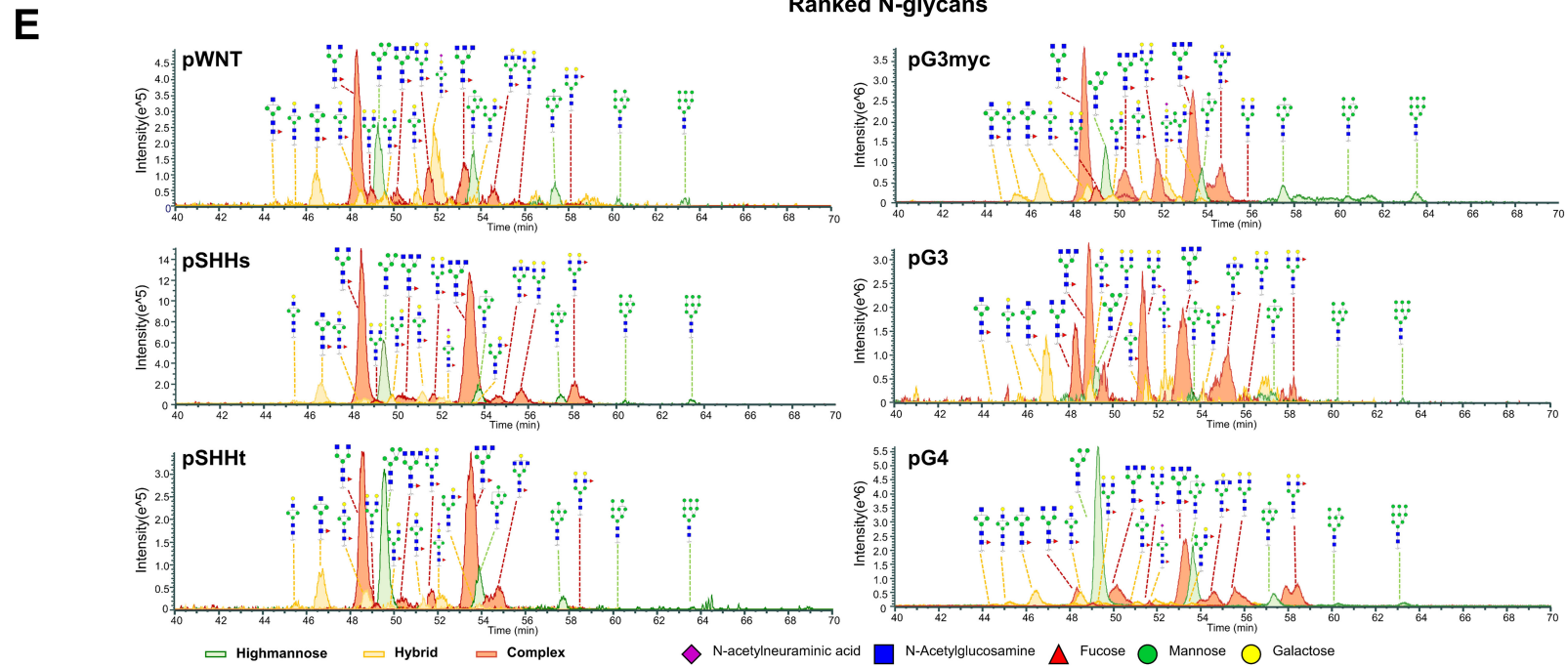
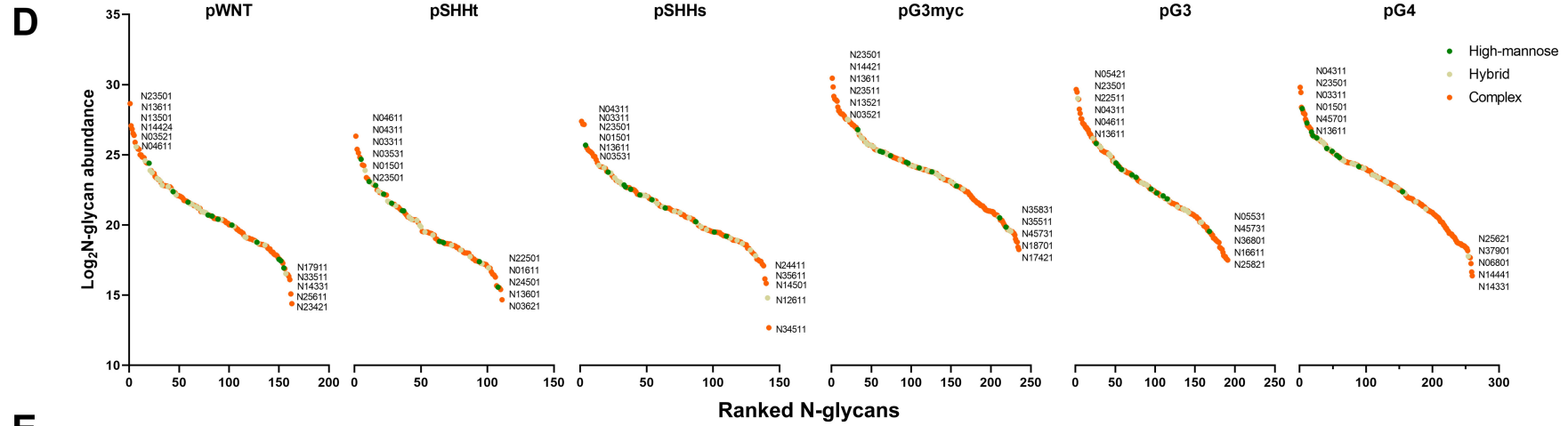
In order to assess the distribution of N-glycan abundance in each of the subgroups of medulloblastoma, the iBAQ algorithm were utilized. The dynamic range of N-glycan

abundance within among six subgroups was around 19 orders of magnitude (Figure 7D). The top six of the highest abundance of N-glycans in pWNT group are N23501, N13611, N13501, N14424, N03521 and N04611 from 28.64 to 25.88, but the top five of lowest-ranked N-glycans in pWNT group are N17911, N33511, N14331, N25611 and N23421 from 16.46 to 14.39. In pSHHs subgroup, the top six of the highest abundant N-glycans are N04311, N03311, N23501, N01501, N13611 and N03531 from 27.40 to 25.35, and the top five of lowest abundant N-glycans are N24411, N35611, N14501, N12611 and N34511 from 17.09 to 12.68. In the pSHHt subgroup, the top six of the highest abundant N-glycans are N04611, N04311, N03311, N03531, N01501 and N23501 from 26.35 to 24.29, and the top five of lowest abundant N-glycans are N22501, N01611, N24501, N13601 and N03621 from 15.68 to 14.68. In pG3myc subgroup, the top six of highest abundant N-glycans are N23501, N14421, N13611, N23511, N13521 and N03521 from 30.47 to 28.91, and top five of lowest abundant N-glycans are N35831, N35511, N45731, N18701 and N17421 from 19.01 to 18.26. In the pG3 subgroup, the top six of highest abundant N-glycans are N05421, N23501, N22511, N04311, N04611 and N13611 from 29.67 to 27.96, and the top five of lowest abundant N-glycans are N05531, N45731, N36801, N16611 and N25821 from 17.76 to 17.50. In the pG4 subgroup, the top six of highest abundant N-glycans are N04311, N23501, N03311, N01501, N45701 and N13611 from 29.83 to 27.99, and top five of lowest abundant N-glycans are N25621, N37901, N06801, N14441 and N14331 from 17.71 to 16.39. Furthermore, the highly abundant N-glycans were observed across all subgroups, such as N23501, N13611 and N03521. In the iBAQ result according to N-glycan classification, the most and least abundant N-glycans among all groups were complex-type glycans, but a high-mannose-type N-glycan (N01501) was the second most abundant N-glycan in both of pSHHs and pG4 subgroups and a hybrid-type N-glycan (N22511) was a third most abundant N-glycan in pG3 subgroup.

N-glycomic profiling with mass spectra allows for comprehensive analysis of N-glycan structure and quantification level in different medulloblastoma subgroups. Representative Extracted compound chromatograms (ECCs) show that 15 representative N-glycans observed significant differences among all groups (Figure 7E). The intensity of representative N-glycans in non-WNT/ non-SHH subgroups was significance increased in comparison to pWNT, pSHHs and pSHHt group. Representative N-glycan structures were assigned to each peak. Three hybrid N-glycans (N02311, N02511 and N02411) and three complex N-glycans (N03501, N03511 and N04311) were found in two peaks, while all high-mannose N-glycans were found in a single peak. Furthermore, N02511 and N04311 have two isomeric structures in mass

spectra because of core and antenna fucosylation. However, N02311 and N03501 had only one peak in the mass spectrum of pSHHt, and the peaks disappeared at the retention time of around 44 and 55 minutes, respectively. N03511 with antenna Fuc at 58 minutes in pG3 groups' mass spectra were lost in mass spectra.





**Figure 7. Overview of the N-glycome profiles of six subgroups of medulloblastoma.** A. The heat map of identified 302 N-glycan compositions in medulloblastoma patients. The counts of building blocks indicate the number of each monosaccharide. All N-glycans are classified into three N-glycan traits (the green represents the high-mannose type of N-glycan, the dark yellow is the hybrid type of N-glycan, and the orange is the complex type of N-glycan). B. The number of identified N-glycans in each subgroup of medulloblastoma (Error bars represent mean values with SD). C. All quantified N-glycans among six subgroups are displayed, plotting their log-transformed relative abundances against their rank in the dynamic range and combination with the list of highest and lowest abundant N-glycans. The green plot represents high-mannose type of N-glycan, the dark yellow plot is hybrid type of N-glycan, and the orange plot is complex type of N-glycan. Sugar code: N- No. Neu5Ac- No. Neu5Ac- No. HexNAc- No. Hex No. red-HexNAc. D. Venn diagram of the number of N-glycans shared by pWNT (orange), pSHHs (orchid), pSHHt (turquoise), pG3myc (red), pG3 (blue) and pG4 (lime-green). Overlapping parts represent shared N-glycans, and non-overlapping parts represent unique N-glycans. E. ECCs, showing the five N-glycans with the highest intensity across three N-glycan traits, were obtained from a randomly patient in each subgroup of medulloblastoma using Xcalibur Freestyle 1.4. Each peak represents an individual N-glycan structure, the green peak was the high-mannose type of N-glycan, the yellow peak was hybrid N-glycan and the orange peak was complex N-glycan.

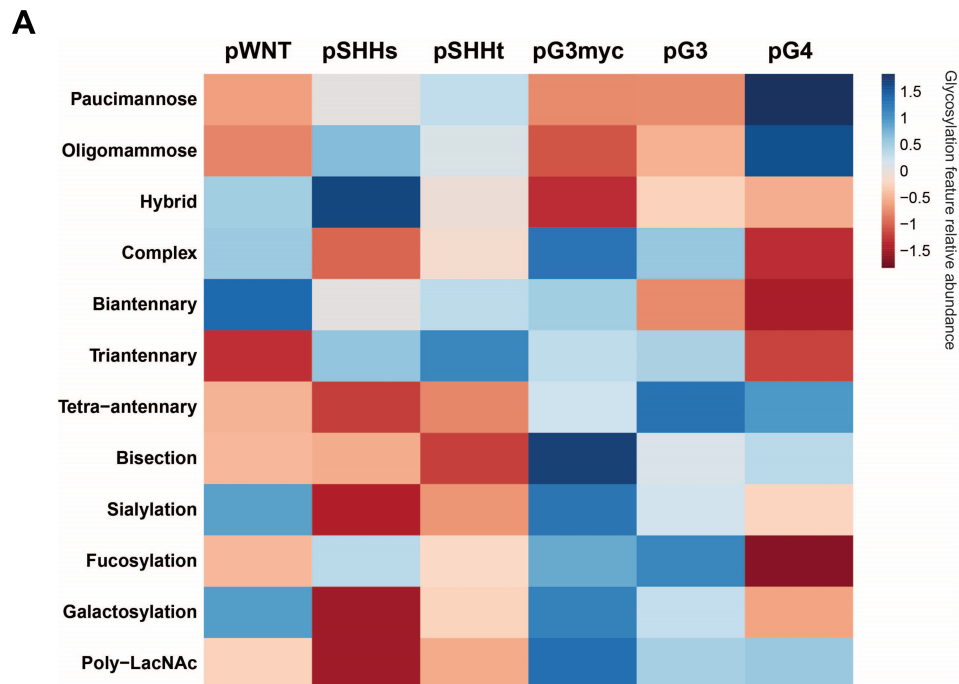
### 3.2 Distribution of the N-glycosylation features in six subgroups of medulloblastoma

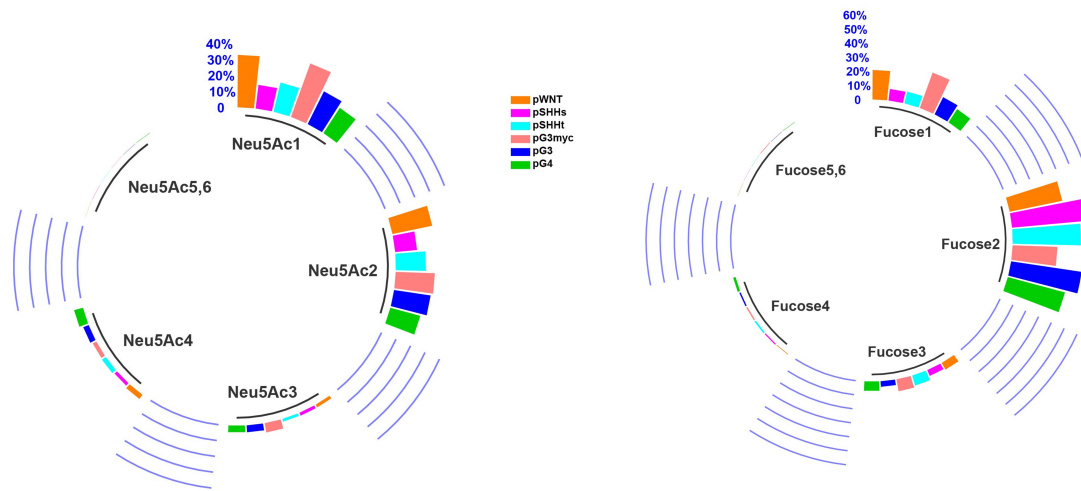
The distribution of N-glycomic phenotypes of medulloblastoma subgroups was relatively quantified and classified into different glycosylation feature groups based on specific N-glycan types (paucimannose, oligo-mannose, hybrid and complex), the number of antennas (biantennary, tri-antennary, tetra-antennary), presence of bisecting GlcNAc as well as glycan epitopes (sialylation, fucosylation and poly-LacNAc motifs), as shown in Figure 8A. pG4 group expressed the highest abundance of paucimannose-type N-glycans (2.87%), followed by the pSHHt group (1.44%) and pSHHt group (1.21%), and then pWNT group (0.57%), pG3 group (0.46%) and pG3myc group (0.45%) expressed the lowest abundance of paucimannose-type N-glycan. Among Oligo-mannose species, N-glycans with compositions Man4, Man5, Man 6, and Man 8 were significantly more abundant in the pG4 group. Oligo-mannose-type N-glycans were most abundant in the pG4 group (12.38%), followed by pSHHs group (8.7%) and pSHHt

group (6.46%), and then pG3 group (3.92%), pWNT group (2.78%) and pG3myc group (1.64%). Hybrid-type was the lowest abundant in the pG3myc group (7.78%). Interestingly, the relative abundance of Hybrid-type in non-pWNT/non-pSHH (pG3=9.47%, pG4=9.07%) was less than pWNT/ pSHH (pSHHt = 9.81%, pWNT = 10.71%, pSHHs = 12.57%). With regard to complex type, pG3myc group (90.13%) expressed the most abundance in comparison to all other subgroups (pG3 (86.13%), pWNT (85.93%), pSHHt (82.28%), pSHHs (77.51%) and pG4 (75.67%). Furthermore, biantennary-type was the lowest abundant in the pG4 group (31.53%) and pG3 group (31.53%). Meanwhile, the pG4 group expressed the second lowest abundance of tri-antennary-type N-glycans (23.33%). The highest abundance of this glycosylation feature was found in pSHHt (29.24%) compared to all other subgroups. Remarkably, the relative abundance of tetra-antennary-type in non-pWNT/non-pSHH group (pG3 = 14.56%, pG3myc = 20.44%, pG4=18.55%) was more than pWNT/ pSHH group (pWNT = 10.70%, pSHHt = 9.11%, pSHHs=6.80%). Contrary to pWNT/ pSHH group, non-pWNT/ non-pSHH group expressed a higher abundance of bisecting type N-glycan (pG3myc=3.56%, pG3=1.79%, pG4=2.04%). The relative abundance of galactosylated N-glycans was highly expressed in all groups. pG3myc group expressed the most abundance in this feature (92.19%), while pSHHs group had the lowest galactosylation-type abundance (56.26%). Comparing the relative abundance of poly-LacNAc modified N-glycans between medulloblastoma subgroups, the highest abundance of this feature of N-glycans for pG3myc group (3.76%), followed by pG3 group (2.65%) and pG4 group (2.75%), but the lowest abundance of that was pSHHs group (0.09%). The relative abundance of poly-LacNAc feature in pWNT (1.72%) and pSHHt (1.34%) expressed twice less than pG3myc group.

Concerning sialylation and fucosylation, sialylation was found to be highest in the pG3myc group (68.52%), followed by the pWNT group (63.38%), and lowest in the pSHHs group (32.43%). Fucosylation was detected to be lowest in the pG4 group (61.39%), followed by pWNT group (64.6%) and pSHHt group (65.3%), but highest in pG3myc group (68.04%) and pG3 group (68.87%). To explore the relationship between N-glycan containing different numbers of sialic acid or Fuc and medulloblastoma subgroup, a more in-depth analysis of the quantification of N-glycans with Neu5Ac was performed across all medulloblastoma subgroups in Figure 8B. Interestingly, the relative abundance of N-glycans containing mono-Neu5Ac and di-Neu5Ac in pWNT group (32.85%, 25.44%) was similar to pG3myc group (35.59%, 24.53%). The relative abundance of glycosylation (mono-Neu5Ac and di-Neu5Ac) showed no difference between the pSHHt group (18.74%, 18.87%) and pG4 group (18.79%,

19.36%). However, the relative abundance of N-glycans containing from 3 to 6 Neu5Ac residues was higher expressed in non-pWNT/ non-pSHH group in comparison to pWNT/ pSHH group. With regard to the fucosylated N-glycans, the relative abundances of N-glycans with one Fuc were increased in the pG3myc group (26.60%) compared to all other subgroups. The N-glycans containing di-Fuc were most abundant in the pSHHs group (53.50%), followed by pG3 group (50.52%), pSHHt (48.36%) and pG4(41.88%), and the lowest abundant in pG3myc group (31.75%). pG3myc group expressed the most abundance of fucosylated N-glycans with tri-fucose and five to six Fuc residues (7.31%, 0.31%), while the pG3 group (3.87%) expressed the lowest abundance of N-glycans containing tri-Fuc among six subgroups. Furthermore, a significantly higher abundance of fucosylated N-glycans with four fucoses was detected in pG4 group, followed by pSHHt group (1.04%), pG3 group (0.89%), pG3myc group (0.82%), pSHHs group (0.72%) and pWNT group (0.33%). To note, the relative abundance of fucosylated N-glycans containing five and six Fuc in non-pWNT/ non-pSHH group (pG4=0.12%, pG3=0.07%) was higher than in pWNT/ pSHH group (pWNT=0.06%, pSHHt=0.06%, pSHHs=0.003%).



**B**

**Figure 8. The quantitative comparison of N-glycosylation features in six medulloblastoma subgroups.** A. Heat map displaying the average quantification of 12 N-glycosylation features for different subgroups of medulloblastoma. The abundance for each glycan species was normalized to the abundance of total identified glycans. Data from biological replicates ( $n = 3$ ) were used (pWNT, pSHHt, pSHHs, pG3myc, pG3, pG4). Moreover, the average relative abundance of each glycosylation feature was normalized, with the high relative abundance of the glycosylation feature depicted in blue and the low relative abundance of the glycosylation feature depicted in red. B. Circular bar chart shows the relative abundance of N-glycans containing the different numbers of Neu5Ac and Fuc residues in different medulloblastoma subgroups. Relative quantification was obtained by normalizing the abundance of individual N-glycan to the total identified N-glycan abundance. All comparisons were based on the average of relative abundance. Data from biological replicates ( $n = 3$ ) were used (pWNT, pSHHt, pSHHs, pG3myc, pG3, pG4).

### 3.3 Quantitative changes in N-glycan profiles in six subgroups of medulloblastoma

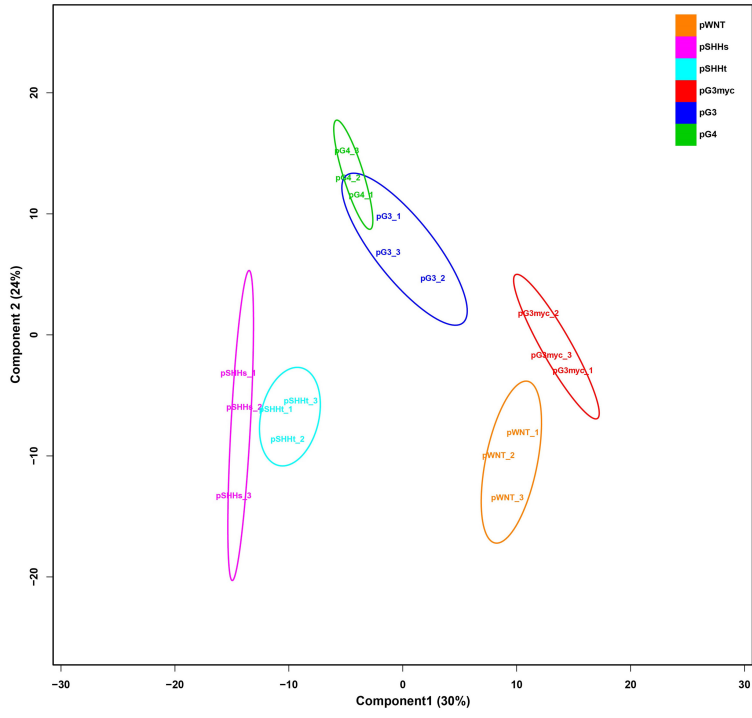
OPLS-DA was performed to evaluate the differential expressions of N-glycan profiles among pWNT, pSHHt, pSHHs, pG3myc, pG3 and pG4. Before univariate analysis, N-glycans with at least 50% valid values in 18 samples were included, and further missing values were filled with MissForest imputation. The score plot of OPLS-DA was constructed to present an overall view of the N-glycome (194 N-glycans), as shown in Figure 9A. In general, the score plot of the



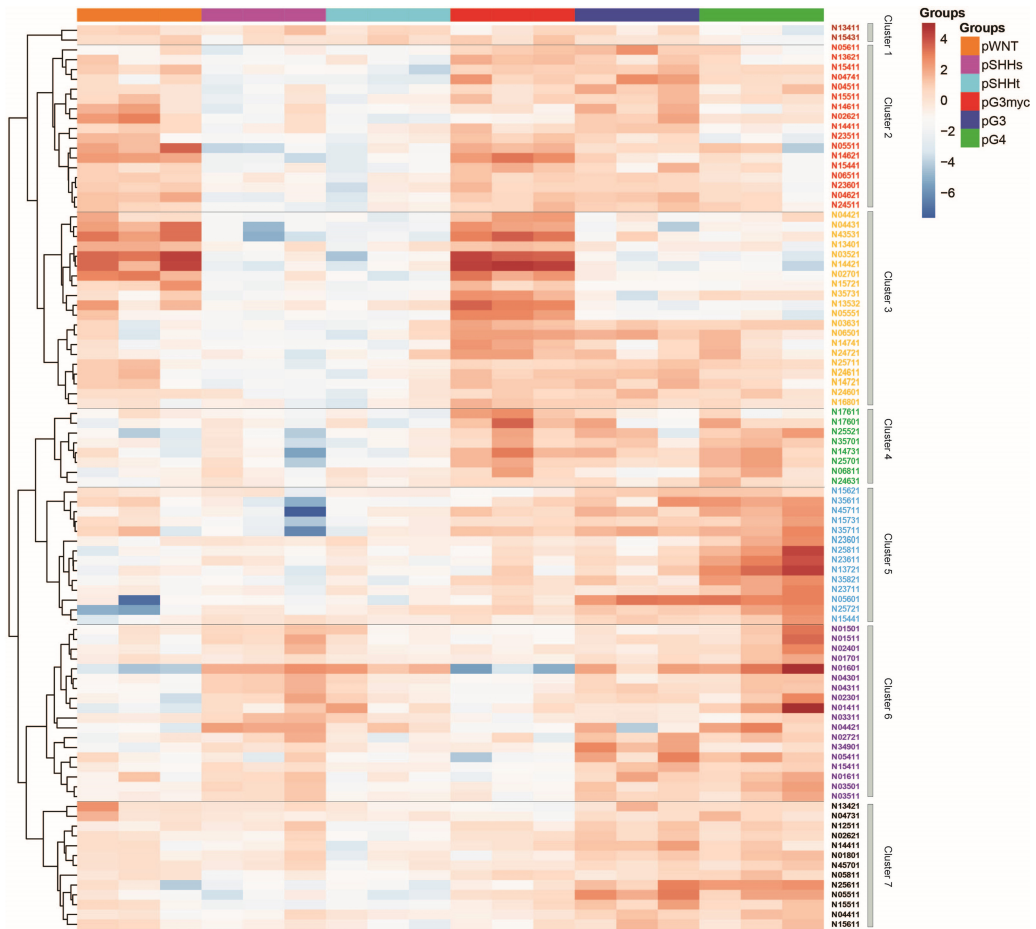
OPLS-DA displayed a clear separation of different subgroups of medulloblastoma (component 1 = 30%, component 2 = 24%), even though the pG3 group showed less overlap with pG4 group. The OPLS-DA of glycome data showed cumulative values of  $R^2(X)=82.1\%$ ,  $R^2(Y)=90.2\%$  and  $Q^2=66.6\%$ .

In order to gain a broader understanding of the N-glycan profile difference and similarity levels among different medulloblastoma subgroups, after ANOVA statistical test, 92 significantly expressed N-glycans across all subgroups were plotted as clusters in the heat map (Figure 9B). All altered N-glycans in six subgroups of medulloblastoma were divided into seven cluster groups. Furthermore, N-glycans in each cluster group contained similar glycosylation features, such as complex, sialylation, fucosylation, galactosylation and highly branched. Interestingly, cluster 6 has a high number of high-mannose type of N-glycans (N01501, N01511, N01701, N01601 and N01411), and N01801, a high-mannose type of N-glycan, was found in cluster 7, but other clusters were not included high-mannose N-glycan. The N-glycans in cluster 4 and cluster 5 were almost all complex-type glycans containing sialic acid with tetra-antennary, while cluster 6 contained only two sialylated and complex-type N-glycans (N34901, N15411). In addition, sialylated N-glycans containing poly-LacNAc were found in cluster 2, cluster 3 and cluster 4 (N02621, N16801, N17611, N17601, N06811), while sialylated hybrid appeared in cluster 5 and cluster 7 (N13721, N23711, N12511). Fucosylated N-glycans containing bisecting GlcNAc were found in cluster 2 and cluster 4 (N13621, N02621, N17611, N17601). Cluster 1 included only two N-glycans, which are complex and fucosylated.

**A**



**B**



**Figure 9. Comparison of Medulloblastoma subgroup based on N-glycan expression.** A. OPLS-DA scores plots based on N-glycan profiles of medulloblastoma patients samples from six subgroups. The 95% confidence interval areas are highlighted in different colors for pWNT, pSHHs, pSHHt, pG3myc, pG3 and pG4, respectively. B. Heatmap for the hierarchical clustering of 92 significant N-glycans differentially abundant after ANOVA test of  $p < 0.05$ . Each column represents a medulloblastoma patient and each row represents a N-glycan. The scale bar indicates z-scores of standardized N-glycan values. Red and blue are represented higher or lower expressions, respectively. Rows correspond to clusters obtained from all altered N-glycans. Sugar code: N- No. Neu5Ac- No. Neu5Ac- No. HexNAc- No. Hex No. red-HexNAc.

### 3.4 Comparison of N-glycosylation-related proteins in six subgroups of medulloblastoma

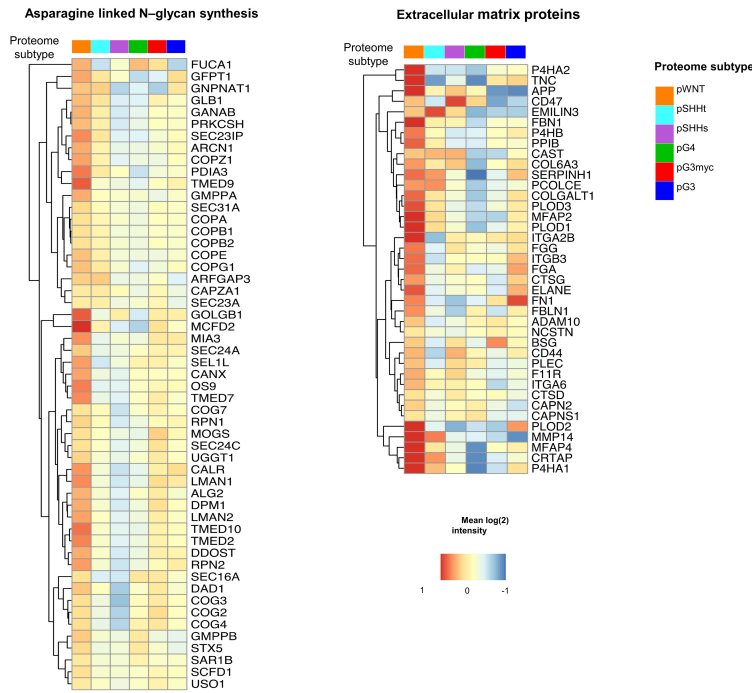
Aberrant N-glycosylation has emerged as a promising biomarker for cancer, with fundamental changes in the N-glycosylated patterns of cell surface and secreted proteins during cancer progression. The N-glycomic results showed that N-glycan patterns were changed across six subgroups of medulloblastoma. To comprehensively understand glycosylation changes in medulloblastoma, hallmark gene sets of N-Asparagine-linked Glycan synthesis and extracellular matrix proteins were downloaded. In the proteomic result, 53 proteins related to asparagine-linked N-glycan synthesis were found after gene enrichment analysis ( $NES_{Glycan}=2.2$ ,  $p_{Glycan} \leq 0.001$ ) (Figure 10A). Those related proteins were more abundant in pWNT compared to all other subgroups. Specifically, aberrant proteins were involved in the entire process, from N-glycan precursor synthesis in the ER to N-glycan modifications in the Golgi apparatus. Interestingly, based on the hallmark gene set of extracellular matrix proteins, 39 extracellular matrix proteins were more abundant in the pWNT group than all other subgroups ( $NES_{EMP}=1.7$ ,  $p_{EMP}=0.02$ ).

According to previous reports, the proteome profiles demonstrated the closest similarity between the high-risk pG3myc group and the excellent survival pWNT group. To explore the molecular mechanism in pG3myc and pWNT, the roles of differentially expressed proteins were analyzed based on GESA. The top 10 enriched gene sets of the pG3myc group as shown in Figure 10B, protein folding, association of Tric/CCT with target proteins, and mitochondrial translation. On the other hand, compared to the pG3myc group, asparagine-linked N-

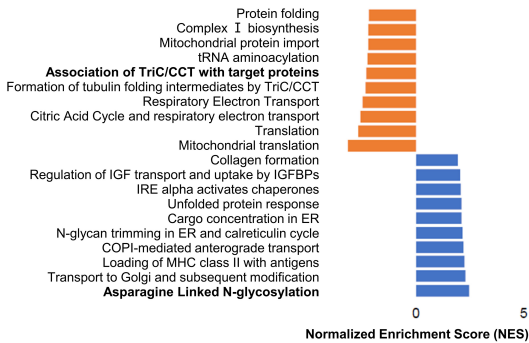
glycosylation-associated factors were more abundance in pWNT group, followed by transport to Golgi and subsequent modification and N-glycan trimming in ER and calreticulin cycle.

Furthermore, these significantly different abundance proteins associated with N-glycosylation were mapped to reveal the protein-protein interaction networks via STRING (Figure 10C). Six proteins (ALG2, DPM1, GLB1, GMPPA, GMPPB, and NAGK) were involved in the precursor synthesis of the first step of protein N-glycosylation. SEL1L, OS9, RPN2, RPN1, DDOST, CALR, UGGT1, MOGS, GANAB, PRKCSH, PDIA3, and MAN1B1 were involved in N-glycan trimming in ER by Calnexin /Calreticulin cycle for controlling the folding quality of glycosylated proteins. GMPPA and DPM1 were involved in catalyzing the formation of GDP-mannose. GLB1, NAGK, GMPPB, GMPPA, and DPM1 were engaged in synthesis of substrates in N-glycan biogenesis. CANX, CAPZB, CAPZA1, DCTN3, DCTN1, DYNC1H1, DYNC1LI2, TUBB6, SEC23A, SEC24C, SEC31A, SAR1B, and SEC24A were associated with the pathway of MHC class II Antigen presentation. NAPA, TEMD10, SCFD1, STX5, SEC23A, TEMD2, USO1, RAB1A, SAR1B, SEC23IP, SEC24A, SEC24C, SEC31A, MCFD2, LAMN1, SEC16A, and LMAN2 were associated with the pathway of COPII mediate vesicle transport. Additionally, 45 different expressed proteins were involved in transport to the Golgi and subsequent modifications. For instance, COPE, COPB2, COPA, COPZ1, and COPG1 were cytosolic protein complexes that a critical factor in Golgi membranes budding and the retrograde Golgi-to-ER transport of dilysine-tagged proteins. SEC23A, SEC24C, SEC31A, SEC24A, SEC16A, and SEC23IP play roles to transport cargo molecules to the Golgi complex promotes the formation of transport vesicles from the ER. TMED9, TMED7, TMED10 and TMED2, were potential roles in the secretory pathway and translational modifications. COG7, COG4, and COG3 played the main role in ER-Golgi transport.

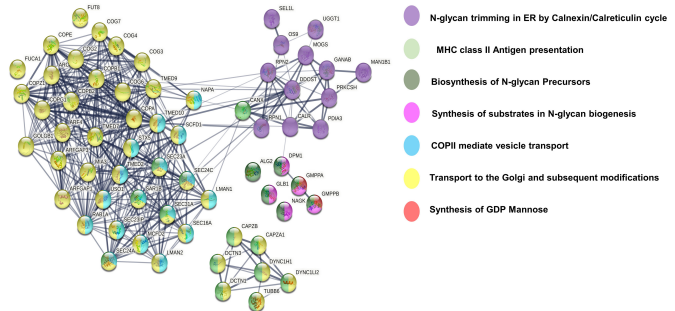
**A**



**B**



**C**



**Figure 10. Comparative proteomics of six medulloblastoma subgroups.** A. The heatmaps show identified proteins associated with “N-Asparagine linked Glycan synthesis” and “extracellular matrix proteins” by GSEA. Each column represents a medulloblastoma patient and each row represents a protein. Moreover, the average abundance of each protein was normalized. The scale bar indicates z-scores of standardized protein values. Red and blue are represented higher or lower expressions, respectively. B. GSEA shows the top 10 up- and downregulated enrichment of biological pathways compared pG3myc to pWNT ( $p < 0.05$ ,  $FDR < 0.25$ ). C. STRING interaction analysis shows the interaction of significant differentially abundant proteins associated with N-glycosylation synthesis.

### 3.5 Comparative Analysis of N-glycans between pWNT and pG3myc group

To an in-depth characterization of N-glycan profiles between pWNT and pG3myc group, 28 statistically differentially expressed N-glycans were further investigated by Pearson's correlation and glycosylation features ( $p < 0.05$  and  $\log_2$  fold change  $> 1.5$ ) (Figure 11A). Hierarchical clustering can be seen with a clear separation of the pWNT and pG3myc group samples ( $n = 3$ ). Compared to pWNT group, four N-glycans were decreased expression, and 24 N-glycans were increased expression in the pG3myc group. All altered N-glycans were classified into several glycosylation traits, such as complex-bi-, tri- and tetra-antennary, bisecting GlcNAc, sialylation, fucosylation, galactosylation and poly-LacNAc modification. Interestingly, all significantly differentially expressed N-glycans were complex-type glycans. Three fucosylated and galactosylated bi- and tetra-antennary complex-type N-glycans were significantly less abundant in the pG3myc group. These N-glycans included: a) bi-fucosylated bi- and tetra-antennary antennary N-glycans with composition N13421 and N05621; b) tri-fucosylated bi-antennary N-glycans with composition N43531. Notably, the most significantly decreased N-glycan was bi-fucosylated and tetra-antennary bisecting glycan with poly-LacNAc in the pG3myc group compared to pWNT group, and the composition was N27901. However, a poly-LacNAc modified tetra-antennary bisecting N-glycan (N07601) and a mono-fucosylated poly-LacNAc modified tetra-antennary bisecting N-glycan (N07611) and a mono-sialylated poly-LacNAc modified tetra-antennary bisecting N-glycan (N17601) were increased abundance in the pG3myc group. Similarly, tri-sialylated and tri-fucosylated tetra-antennary bisecting N-glycan with composition N36631 was more abundant in the pG3myc group. Bi-galactosylated tetra-antennary bisecting N-glycan (N06501) and bi-sialylated and bi-fucosylated bisecting N-glycan (N26621) were increased in the pG3myc group in comparison to pWNT group. Additionally, 16 sialylated tri- and tetra-antennary complex-type N-glycans were also significantly more abundant in the pG3myc group. These N-glycans included: a) mono-sialylated and bi- and tetra-fucosylated tetra-antennary N-glycans with composition N15521 and N15841; b) mono-sialylated and tri- and tetra-fucosylated tri-antennary N-glycans with composition N14731 and N14741; c) bi-sialylated tetra-antennary N-glycan with composition N25701; d) bi-sialylated and bi-fucosylated tetra-antennary N-glycan with composition N25521, N25721 and N25731; e) bi-sialylated and bi- and tri-fucosylated tri-antennary N-glycans with composition N24721 and N24631; f) tri-sialylated tri-antennary N-glycans with composition N34601 and N34901; g) tri-sialylated and mono-fucosylated tri-antennary N-glycan with composition N34611; h) tri-sialylated and bi- and tri-fucosylated tetra-antennary N-glycan with composition N35821 and N35731. Furthermore, mono- and

penta-fucosylated bi-galactosylated tetra-antennary N-glycan with composition N05511 and N05551.

To understand the glyco-synthesis process across all dysregulated N-glycans between pWNT and pG3myc group, we further selected 28 significant expressed N-glycans, 39 backbone N-glycans that 100% detected in the glycan pool and 30 unique N-glycans in pG3myc group. Finally, the representative N-glycan map was established by applying glyco-synthetic rules with 97 N-glycans for the major branching pathway of dysregulated N-glycans between pWNT and pG3myc group. As shown in Figure 11B, after the high-mannose type of N-glycans is formed, hybrid and complex pathways are initiated by adding GlcNAc to mannose. In the N-glycan map, the hybrid-type pathway processed from HexNAc<sub>1</sub>Hex<sub>6</sub>red-HexNAc<sub>1</sub> to Neu5Ac<sub>2</sub>HexNAc<sub>2</sub>Hex<sub>7</sub>red-HexNAc<sub>1</sub> by adding a Gal, a HexNAc and double Neu5Ac. Whereas the complex-type pathway extends from the N-glycan core structure HexNAc<sub>1</sub>Hex<sub>3</sub>red-HexNAc<sub>1</sub>.

To note, the significant downregulated bi-antennary N-glycans were generated from N-glycan composition with HexNAc<sub>3</sub>Hex<sub>4</sub>red-HexNAc<sub>1</sub> (N13421(#54) and N43531(#187)). Firstly, the resulting N13421(#54) were decorated to HexNAc<sub>3</sub>Hex<sub>4</sub>red-HexNAc<sub>1</sub> with two Fuc residues and a sialic acid residue. Next, the resulting N43531(#187) was modified to N13421(#54) with a Fuc residue, a Gal and three sialic acid residues. In addition, the resulting N43531(#187) was also modified to N03521(#45) with a Fuc residue and four sialic acid residues. Regarding to unique expressed bi-antennary N-glycans in the pG3myc group, the resulting N23721(#210) and N33711(#209) were modified to N13601(#59) with a Gal and two Fuc and a sialic acid and with a Gal, a Fuc and two sialic acids. Additionally, the resulting N53531(#229) was generated from N43531(#187) with the addition of sialic acid and Fuc.

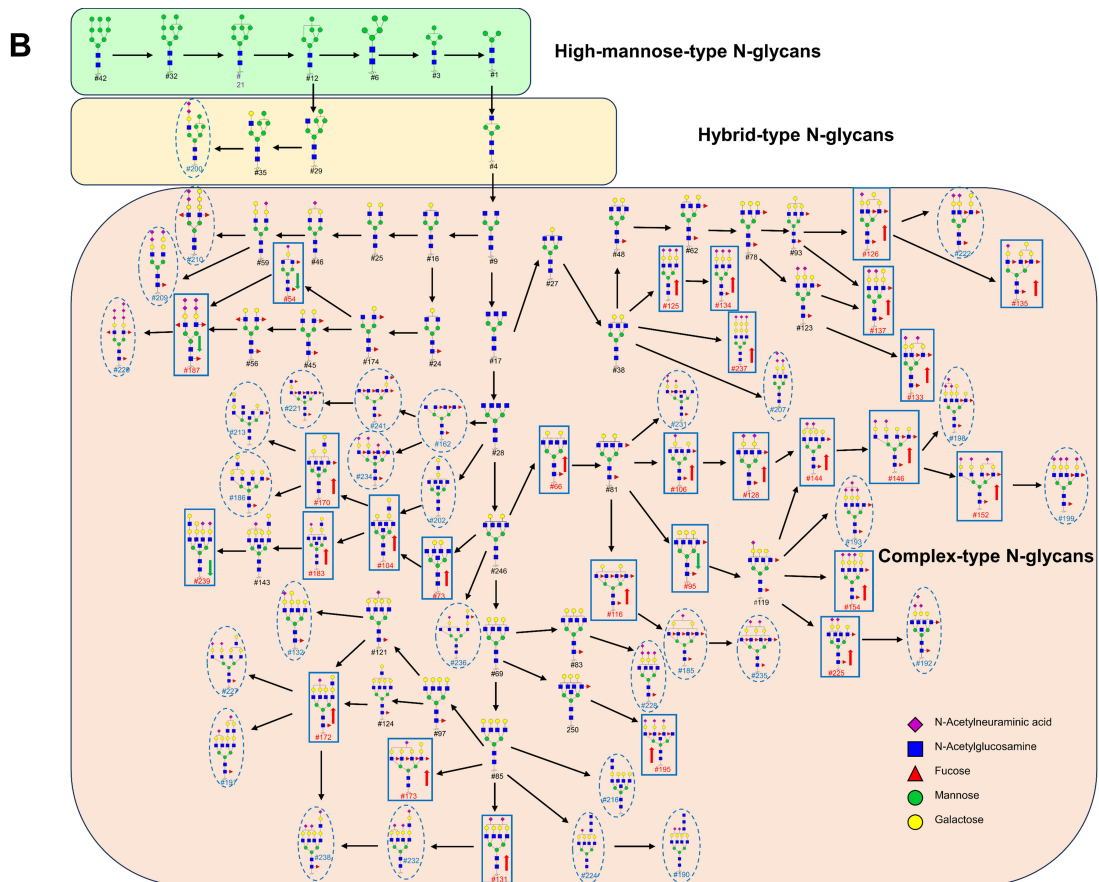
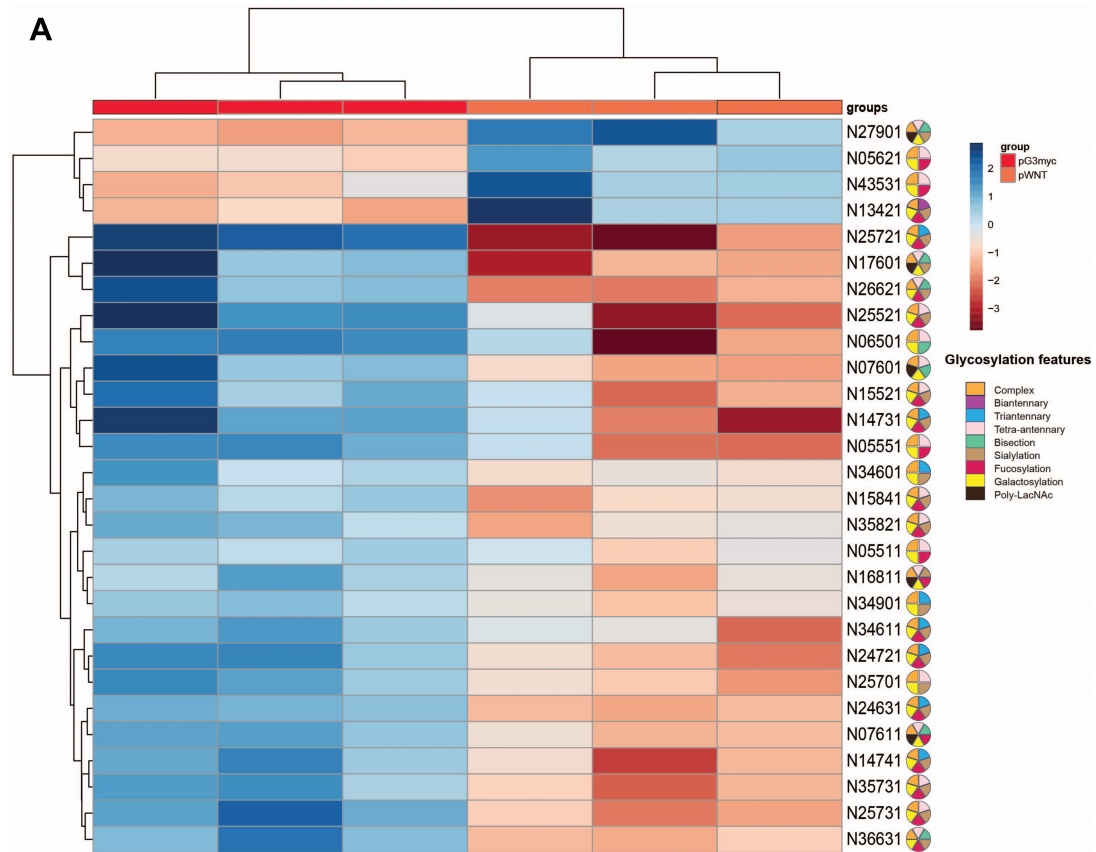
For significant upregulated tri-antennary N-glycans (N34601(#125), N34611(#134), N34901(#237), N14731(#126), N24721(#137), N24631(#133) and N14741(#135)), these glycans were generated from N-glycan composition with HexNAc<sub>4</sub>Hex<sub>4</sub>red-HexNAc<sub>1</sub>. Firstly, the resulting N34601(#125), N34901(#237) and N04621(#78) were decorated to HexNAc<sub>4</sub>Hex<sub>4</sub>red-HexNAc<sub>1</sub> with two Gal and three sialic acid residues and with five Gal and three sialic acid residues and with two Gal and two Fuc residues, respectively. Next, the resulting N34611(#134) was modified to N34601(#125) with a Fuc residue. Then, the resulting N14731(#126), N24721(#137) and N24631(#133) were decorated N04621(#78) with a Gal, a Fuc residue and a sialic acid residue and with a Gal and two sialic acid residues and with a Fuc

and two sialic acid residues, respectively. Finally, N14741(#135) was generated from N14731(#126) with additional Fuc and unique expressed tri-antennary N-glycan (N24741(#222)) was produced from N14731(#126) with addition of sialic acid. Another unique expressed tri-antennary N-glycan, N34501 (#207), was generated from HexNAc<sub>4</sub>Hex<sub>4</sub>red-HexNAc<sub>1</sub> with the addition of a Gal and three sialic acids.

Regrading to downregulated tetra-antennary N-glycans(N05511(#66), N15521(#106), N25521(#128), N25731(#146), N35731(#152), N25721(#144), N35821(#154), N26621(#225), N05551(#116), N36631(#195), N25701(#131), N15841(#173), N16811 (#172), N06501(#73), N07601(#104), N17601(#183) and N07611(#170)), these glycans were from N-glycan composition with HexNAc<sub>5</sub>Hex<sub>3</sub>red-HexNAc<sub>1</sub>. Firstly, the resulting N05511(#66) and N05501(#246) were modified to HexNAc<sub>5</sub>Hex<sub>3</sub>red-HexNAc<sub>1</sub> with two Gal and a Fuc residue and with two Gal, respectively. Secondly, N15521(#106), N05551(#116) and N25721(#119) were modified to N05511(#66) with a Fuc residue and a sialic acid residue and with a Gal and a Fuc residue and with a Gal, a Fuc residue and a sialic acid residues, respectively. Then, N25521(#128) was generated from N15521(#106) with additional sialic acid. N35821(#154) and N26621(#225) were produced from N25721(#119) with the addition of two Gal and two sialic acids with the addition of a GlcNAc and a sialic acid, respectively. N25721(#144) was generated from N25521(#128) with the additional Gal. Finally, N25731(#146) was generated from N25721(#144) with a Fuc residue. N35731(#152) was produced from N25731(#146) with the additional sialic acid residue. Furthermore, N36631(#195) was generated from N05501(#246) with a GlcNAc, a Gal, three Fuc residues and three sialic acid residues. N25701(#131), N15841(#173) and N16811 (#172) were modified to N05501(#246) with two Gal and two sialic acid residues and with three Gal, four Fuc residues and a sialic acid residue and with three Gal, a GlcNAc, a Fuc residue and a sialic acid residue, respectively. For upregulated bisected and poly-LaNAc modified N-glycan in the map, N06501(#73) was produced from N05501(#246) with the additional GlcNAc. Next, the resulting N07601(#104) was modified to N06501(#73) with additional GlcNAc-Gal. Then, N07611(#170) and N17601(#183) were decorated to N07601(#104) with a sialic acid and with a Fuc residue, respectively. On the other hand, two upregulated tetra-antennary N-glycans (N05621(#95) and N27901(#239)), these N-glycans were generated by previous synthesis pathways. In the first, the resulting N05621(#95) was modified to N05511(#66) with a Gal and a Fuc residue. Then, N27901(#239) was produced from N17601(#183) with the addition of two Gal and a sialic acid residue.



Indeed, unique expressed tetra-antennary N-glycans in the pG3myc group are elongated by the addition of monosaccharide derivatives such as Fuc, Gal, GlcNAc, or sialic acid. For instance, the resulting N35731 (#198) was modified to N25731 (#146) with an additional derivative sialic acid. The resulting N36531 (#231) was modified to N05521(#81) with two Fuc residues, a GlcNAc and three sialic acids. The resulting N45621 (#193) and N36621 (#192) were modified to N25721(#119) with three sialic acids and with two sialic acids and a GlcNAc, respectively. The resulting N15551 (#185) and N25551 (#235) were modified to N05551(#116) with a sialic acid and with two sialic acids, respectively. The resulting N08701 (#216) and N18701 (#224) were modified to N05701(#85) with three GlcNAc residues and with three GlcNAc residues and a sialic acid residue, respectively. Next, the resulting N28701 (#190) was decorated to N18701 (#224) with a GlcNAc. The resulting N05341 (#162) and N07501 (#202) were modified to N05301(#28) with four Fuc residues and with two GlcNAc and two Gal, respectively. Next, the resulting N06461 (#241) and N36541 (#234) were modified to N05341 (#162) with two Fuc residues, a GlcNAc and a Gal and with a GlcNAc, two Gal and three sialic acids, respectively. The resulting N08611 (#213) and N07821 (#186) were modified to N07611(#170) with two GlcNAc and with two Gal and a Fuc, respectively. Then, the resulting N07461 (#221) was modified to N07501 (#202) with a GlcNAc. Furthermore, the resulting N16611 (#236) and N45611 (#228) were modified to N45611 (#246) with a Gal, a GlcNAc, a Fuc and a sialic acid and with a Gal, a Fuc and four sialic acids, respectively. Other unique tetra-antennary N-glycans were modified to N16811 (#172) with Gal, GlcNAc, Fuc and sialic acid.



**Figure 11. Comparison of N-glycan profiles between pWNT and pG3myc group.** A. The heat map for the hierarchical clustering of all t-test significant N-glycans with different glycosylation traits ( $p < 0.05$  and  $\log_2$  fold change  $> 1.5$ ). 97 altered N-glycans were classified by biosynthetic class. Each column represents a medulloblastoma patient and each row represents a N-glycan. Each N-glycan is assigned one pie chart depicting glycosylation features in the respective glycan. The scale bar indicates z-scores of standardized N-glycans' abundance. Red columns are represented pG3myc patients and orange column are represented pWNT patients. Red and blue are represented higher or lower expressions, respectively. N-glycan compositions were coded as N- No. Neu5Ac- No. Neu5Ac- No. HexNAc- No. Hex No. red-HexNAc. B. Representative biosynthetic map of dysregulated N-glycans between pWNT and pG3myc group. Significantly changed N-glycans were marked with blue boxes. Unique N-glycans in pG3myc were marked with the dotted ellipse. The red arrow represented upregulated N-glycans, and the green arrow represented downregulated N-glycans.

## 4. Discussion

N-glycosylation is a type of post-translational modification whose dysregulation is a contributing factor to cancer pathogenesis<sup>[209]</sup>. As Archer et al. proposed, six main molecular subgroups, could be verified in the larger cohort<sup>[210]</sup>. Especially since different medulloblastoma subtypes have different clinical outcomes, the current research was conducted to explore and compare the N-glycosylation profile of different proteome subtypes of medulloblastoma at the level of glycosylating enzymes and the resulting N-glycan patterns. To date, this is the first study to use quantitative N-glycomics to establish the N-glycome in medulloblastoma. It was hypothesized that dysregulated N-glycan patterns in different medulloblastoma subtypes give an insight into the glycosylation cues and can help to uncover potential biomarkers and therapeutic targets. To test this hypothesis, nano-LC-MS/MS was employed to analyze the N-glycan profiles of 18 medulloblastoma tissue samples from patients with six subgroups based on medulloblastoma proteomic. The utilized platform facilitated the chromatographic separation of isomeric N-glycans, enabling structural elucidation through the analysis of MS/MS fragmentation patterns in positive ionization mode. To interpret the biological effects of glycosylation in medulloblastoma, N-glycans were characterized in terms of common N-glycan types and derived glycan traits. Moreover, the intensity of the terminal and branching N-glycan patterns and glycosylation-related proteins were integrated as an exceptionally promising approach for the discovery of valuable biomarkers in further investigations.

In this study, the comparison of different subtypes of medulloblastoma patients showed significant changes in N-glycan profiles based on the specific disease subgroups. The relative abundance of bisected and poly-LacNAc modified N-glycans was higher in the worst prognostic non-pWNT/non-pSHH in comparison with low-risk of pWNT/pSHH. Additionally, tetra-antennary N-glycans' relative abundance was more expressed in non-pWNT/non-pSHH. For pG3myc patients, the highest intensity of sialylated and fucosylated N-glycans was found. In pG4 patients, the highest intensity of high-mannose N-glycans was found. Besides, the result shown that N-glycan profiles can distinguish medulloblastoma subtypes. Notably, the expression of dysregulated N-glycans was affected by N-glycan synthesis pathways in pWNT and pG3myc.

These findings carry profound implications for understanding of the progression of medulloblastoma and the difference across six subgroups. The data suggest a potential

regulatory role of N-glycomics modifications in medulloblastoma, and specific N-glycan structures hold a robust potential immunotherapy target. The subsequent sections of this discussion will delve into the mechanistic insights gleaned from the results, the comparison with existing literature, and the broader implications of this study for both basic biology and clinical applications.

#### **4.1 N-glycan profiles detected by HPLC-MS/MS from FFPE**

N-glycan profiling serves as a powerful method for investigating the role of N-glycosylation in diseases [211]. Current techniques for N-glycan profiling utilize fresh frozen tissues or fresh liquid [212]. However, the transportation and preservation of fresh and frozen samples are hard. It was reported that the base peak chromatograms of N-glycans obtained from representative FFPE and frozen tissue specimens displayed remarkable similarity [213]. In this study, heptane and SDC buffer were used to deparaffinize and extract proteins from FFPE sections. HPLC-MS/MS-based N-glycan profiling was used to assess variations in N-glycan patterns in medulloblastoma. 302 different N-glycan compositions were identified across six medulloblastoma subtypes (Supplemental Material S1). Sialylated (~62%), complex tetra-antennary (~49%), and fucosylated structures (~75%) were the most abundant N-glycans, in line with previous results [214-216]. Quantitative alternations in the N-glycome represent a significant parameter investigated in any disease-associated glycomics research [217]. All identified N-glycans were classified into twelve glycosylation features (Figure 8A), and FFPE material proves suitable for conducting differential N-glycomics analyses in medulloblastoma, enabling a distinct differentiation across five subgroups using OPLS-DA modeling (Figure 9A). Interestingly, they correlate with the identified proteome groups. The N-glycan profile of the pG3 and pG4 subgroups cannot be distinguished, because G3 and G4 overlap in genetic characterization, the mutational spectrum, the transcriptional profile, and the DNA-methylation pattern [23]. In summary, this suggests that the FFPE preservation process and the applied methodologies did not introduce any qualitative alternations in the detectable N-glycome.

It is crucial to emphasize that the employed method of analysis exerts a substantial influence on the resultant dataset. Some researchers conducted comprehensive characterization of the entire N-glycome with FFPE tissue samples by MALDI-TOF-MS. However, while MALDI-TOF-MS is proficient in high-throughput glycan profiling, its limitations are evident when it comes to the separation of N-glycan isomers and structural characterization in cases where prior separation is not employed [218]. This study delved deeper into the comprehensive N-

glycome of FFPE tissue, employing structural analysis through nano-LC-ESI-MS/MS. This method allows for the separation of isomeric glycans, providing valuable insights. A total of 302 N-glycans were identified and structurally characterized (Supplemental Material S1). In this case, the isomers were effectively separated, with most structures being observed in multiple peaks, indicative of structural isomerism (Figure 7D). Furthermore, most peaks had >1 glycan structure. In this study, permethylation was used to stabilize sialylated oligosaccharides, which is the most critical type of derivatization used in glycan MS. Herein, 186 N-glycans were contained over one sialic acid residue. Thus, the method of this study could enable efficient identification and quantification of the best-performing N-glycans based on nano-LC-ESI-MS/MS.

## 4.2 N-glycan diversity across different medulloblastoma subtypes

Earlier investigations have indicated that approximately 2% of the mammalian genome encompasses genes indispensable for N-glycan structure biosynthesis<sup>[218]</sup>. N-glycan multiplicity (n), an intrinsic characteristic encoded within glycoprotein gene sequences, is influenced by a multitude of factors, including the expression levels and activity of glycosyltransferases and glycosidases and the availability of nucleotide sugar substrates (e.g., UDP-GlcNAc, GDP-mannose)<sup>[219]</sup>. Additionally, the expression of many cellular parameters, such as regulation at the transcription factors, and epigenetic regulation, have a significant impact on the observed N-glycan structural diversity<sup>[220]</sup>. The number of glycoforms demonstrates a combinatorial relationship concerning the number of N-glycans on a glycoprotein and the diversity of N-glycan configurations<sup>[221]</sup>. In this study, at the protein level, it is evident that a higher abundance of extracellular matrix proteins can be found in WNT-activated medulloblastomas. Likewise, a higher abundance of N-glycan synthesis-associated proteins can be found in the WNT group (Figure 10B, 10C). Notably, pWNT tumors reveal marked N-glycans complexity and diversity but no higher number of different structures across all subtypes (Figure 7B, 7C). In contrast, non-WNT/non-SHH tumors (pG3myc, pG3, and pG4), associated with an unfavorable prognosis<sup>[222]</sup>, exhibit a significantly greater diversity of N-glycans (Figure 7B, 7C). The main reason is that the pG3myc subgroup has a c-Myc amplification or a c-Myc activated proteome profile, most likely the activation of c-Myc in tumors instigates metabolic alterations, notably an increase in UDP-GlcNAc levels, which are essential for N-glycan structural biosynthesis <sup>[127, 223]</sup>. On the other hand, a defining characteristic of non-WNT/non-SHH medulloblastoma lies in the heightened expression

of OTX2, a molecule that is under the regulatory influence of TGF $\beta$  signaling. Its expression increases with UDP-GlcNAc for N-glycosylation [34, 224, 225].

Interestingly, hedgehog-activated medulloblastoma subtypes show the lowest number of N-glycans (Figure 7B, 7C). This is most likely linked to the role of hedgehog signaling in N-glycosylation. Dominique C et al. found that inhibition of hedgehog signaling diminishes flux through the UDP-GlcNAc biosynthesis pathway within M2 macrophages<sup>[226]</sup>. Wei Guo W et al. reported that mutation of glycosyltransferases disrupt hedgehog signaling in vertebrates<sup>[227]</sup>. Compared to WNT/SHH tumors, distinctive N-glycan patterns in the remaining subgroups consisted of sialylated and fucosylated variants arising from almost all branching patterns, indicating that glycosyltransferases (sialyltransferases and fucosyltransferase) as final decorations are a critical factor in medulloblastoma glycosylation multiplicity. Taken together, changes in N-glycan diversity have been associated with medulloblastoma pathogenesis, and the results reveal that N-glycan multiplicity was influenced by dysregulation of genes, enzymes, and metabolic state across different medulloblastoma subtypes.

### **4.3 High-mannose N-glycans are correlated with pG4**

In this study, the relative abundance of high-mannose (paucimannose and oligomannose) was increased in pG4 in accordance with other cancer studies<sup>[95, 102, 228]</sup>. From the perspective of N-glycan biosynthesis, the increase in high-mannose suggests a potential accumulation of precursor and/or an incomplete or restricted N-glycan maturation process, which might be attributed to shorter cell division/replication cycles (reflecting increased cell proliferation) <sup>[229]</sup>. Prior research has indicated that elevated levels of the high-mannose type of N-glycans enhance the adhesion of cancer cells to vascular walls, facilitating extravasation and subsequent invasion into distant tissues <sup>[102]</sup>. The abnormal elevation of high-mannose glycans on malignant cells could serve as a distinctive biomarker for drug development<sup>[230]</sup>. Moreover, compared with other N-glycans, H5N2 N-glycan was more highly expressed in medulloblastoma patients, in line with previous studies<sup>[231]</sup>. Compared with other subgroups, the abundance of H5N2 was the highest in pG4. Tuomas Kaprio et al. reported that increasing the abundance of high-mannose type N-glycan, H5N2, was correlated with poor prognosis in malignant tumors <sup>[232]</sup>. This indicates that high-mannose N-glycans are potential biomarkers in the pG4 group, and H5N2 was associated with high-risk medulloblastoma tumors.

Of note, the relative abundance of the high-mannose type of N-glycans were decreased in pWNT, pG3, and pG3myc compared to all other groups. Specifically, H5N2 exhibited a marked

decrease in pWNT, pG3, and pG3myc, indicating an upsurge in glycosylation processes that reduced H5N2 expression to generate complex and hybrid oligosaccharides in pWNT, pG3, and pG3myc. Reduced levels of the high-mannose type of N-glycans have been discerned in ovarian and gastric cancers<sup>[233, 234]</sup>. Moreover, the modification of high-mannose glycans may be due to a multifaceted biosynthetic process intricately linked to medulloblastoma glycosylation.

#### **4.4 Clinical importance of bisected, poly-LacNAc modified, and tetra-antennary N-glycans in non-WNT/non-SHH medulloblastoma**

In this study, three of the most well-characterized N-glycosylation changes are bisection, poly-LacNAc modification, and the degree of N-glycan branching (tetra-antennary N-linked glycans) in the high risk of non-WNT/non-SHH medulloblastoma patients, in accordance with other studies<sup>[99, 119, 235, 236]</sup>. This study, along with others, has demonstrated that these particular motifs on complex N-glycans play a direct and indirect role in diverse biological processes associated with progression. These functions encompass cancer cell adhesion and metastasis, primarily through their interactions with N-glycans and endogenous lectins such as membrane receptor proteins <sup>[236, 237]</sup>.

Bisecting GlcNAc was  $\beta$ -1,4 GlcNAc branched oligosaccharide structure, the tetra-antennary N-glycan detected at m/z 1153.0975 and found to be more abundant in non-WNT/non-SHH tumors, serves as a prototypical illustration of a branched N-glycan associated with conditions and acts as the precursor for the addition of bisecting GlcNAc residues. Bisecting GlcNAc represents a glycan modification primarily occurring on hybrid or complex N-glycans. It involves the attachment of a  $\beta$ -1,4-linked GlcNAc unit to the trimannosyl core structure, a process catalyzed by  $\beta$ -1,4-N-acetylglucosaminyltransferase III (GnT-III), which is encoded by the MGAT5 gene. The introduction of a bisecting GlcNAc exerts a suppressive effect on the formation of 1,6 GlcNAc branching, an enzymatic process facilitated by GnT-V. Notably, this interaction is strongly linked to cancer metastasis, as GnT-V cannot employ the bisected oligosaccharide as an acceptor substrate<sup>[119]</sup>. MGAT3 is known to exert inhibitory effects on cancer metastasis through a specific mechanism. It involves the addition of bisecting GlcNAc by MGAT3, which impedes the formation of  $\beta$ 1,6 GlcNAc branching catalyzed by MGAT5. The critical aspect of this mechanism is that MGAT3 is unable to employ the bisected oligosaccharide as an acceptor substrate<sup>[238, 239]</sup>. N-glycans bearing GlcNAc branches have been implicated in facilitating cancer cell metastasis. This effect is achieved through the



frequent sialic acid modifications on the distal saccharides of these glycans and their interaction with galectins. This interaction results in the formation of lattices that play a role in regulating the endocytosis of signaling receptors, thereby contributing to the metastatic process<sup>[119]</sup>. Elevated expression of complex N-glycans featuring  $\beta$ 1-6GlcNAc branching has been identified in breast and colorectal carcinomas. Furthermore, the level of this expression is positively associated with the stage of cancer progression<sup>[122]</sup>. In ovarian cancer, N-glycans bearing bisecting GlcNAc provide insights into early detection during peritoneal metastasis, potentially enhancing the prognostic outlook for ovarian cancer patients<sup>[123]</sup>. Consequently, the presence of bisecting GlcNAc may exert an influence on tumor progression and metastasis. Quantitative analysis of N-glycomics data revealed a notable increase in the relative abundance of bisecting N-glycan modification in highly metastatic non-WNT/non-SHH tumors (pG3myc, pG3, and pG4), consistent with observations in various other cancer types. Bisecting GlcNAc significantly influences tumor cell behavior through the modification of membrane or secreted glycoproteins involved in mediating cell-cell and cell-matrix interaction. Key molecules that may be affected by GlcNAc include E-cadherin, EGFR, and integrins, all of which play crucial roles in the malignant transformation of medulloblastoma cells<sup>[240, 241]</sup>. Alterations in their biological function or subcellular localization subsequent to bisecting N-glycan modification may play a contributory role in the metastatic progression of medulloblastoma.

The presence of poly-LacNAc structures correlated with the enzymatic activity of GnT-V ( $\beta$ 1,6 N-acetylglucosaminyltransferase V, encoded by MGAT5), the glycosyltransferase responsible for adding sugars to complex N-glycan precursors with  $\beta$ 1,6 branching<sup>[242]</sup>. The tetra-antennary glycan detected at m/z 1168.0977 and found to be more abundant in non-WNT/non-SHH tumors, serves as a prototypical illustration of a branched N-glycan associated with conditions and acts as the precursor for the addition of poly-LacNAc residues. The structure of poly-LacNAcs is recognized for its pivotal role in mediating cell-cell and cell-matrix interactions, suggesting its potential significance in the context of metastasis<sup>[243]</sup>. Danielle A Scott et al. show that poly-LacNAcs increased in advanced HER2-Positive and metastatic breast cancer tissues<sup>[236]</sup>. It has been reported that the interaction of galectin-3 to poly-LacNAc is thought to be involved in the tumorigenic process<sup>[244]</sup>. In investigations related to lung metastasis, the pivotal involvement of poly-LacNAc structures has been highlighted, particularly in the initial organ endothelium arrest and subsequent extravasation processes. This significance is attributed to the strong affinity of poly-LacNAcs for binding with galectin-3, a lectin abundantly expressed in lung tissue, which is believed to be a pivotal contributor to the

development of lung metastasis [245]. This study showed the high relative abundance of multi poly-LacNAc modifying N-glycan in more aggressive non-WNT/non-SHH tumors compared to WNT/ SHH tumors. Of note, David Cachia et al. reported higher levels of galectin-3 expression in Group 3 and 4 patient-derived tumor tissue, as compared to non-tumor tissue [246]. Therefore, the interaction between galectin-3 and poly-LacNAc leads to the creation of a molecular lattice, which could potentially trigger elevated rates of metastasis in medulloblastoma.

Tetra-antennary N-linked glycans are a product of the enzyme GnT-V, which catalyzes the incorporation of  $\beta$ -1,6-GlcNAc into the developing N-linked glycan, thus forming tri- and tetra-antenna-like oligosaccharides. Enhanced branching has been linked to metastatic processes and has been associated with changes in the hexosamine cycle and activation of the AKT pathway [106, 221, 247]. Furthermore, elevated levels of tetra-antennary complex-type glycans were likewise correlated with a less favorable disease-specific survival outcome for the patients [248]. Tetra-antennary glycans are typically identified on cell surface molecules, including growth factor receptors and adhesion molecules. Research has indicated that these tetra-antennary N-glycans facilitate the binding of membrane receptors (e.g., EGFR or TGF- $\beta$ R) to galectin-3, resulting in enhanced stabilization at the cell surface and heightened signaling [249, 250]. In this study, a high relative abundance of tetra-antennary N-glycans in highly metastatic non-WNT/non-SHH tumors (pG3myc, pG3 and pG4) compared to WNT/ SHH tumors. Taken together, increased branching plays a crucial role in medulloblastoma progression by affecting the formation of a molecular lattice between membrane receptors and galectin.

#### **4.5 Abnormal sialylation and fucosylation are potential medulloblastoma tumor biomarkers**

Dysregulated sialylation and fucosylation of N-glycans emerge as pivotal contributors to the onset and progression of brain cancer [251]. Elevated expression of sialylated and fucosylated N-glycans stands correlated with unfavorable prognoses across diverse human cancers, encompassing breast, colorectal, gastric, urinary bladder carcinoma, and pulmonary adenocarcinoma [252]. The data in this project report a high extent of fucosylation and sialylation in medulloblastoma tumors, in line with previous studies in other cancers [253-256]. Among human organs, the brain exhibits the most abundant sialic acid content [257].

The covalent attachment of sialic acid to the termini of glycoproteins, a process known as sialylation, holds significant biological relevance. This importance stems from the involvement of sialyltransferases and neuraminidases in various physiological processes, including embryonic development, neurodevelopment, reprogramming, oncogenesis and immune responses<sup>[258]</sup>. Sialyltransferases, such as ST6Gal-I and ST6Gal-II, ST3Gal-IV and ST3Gal-VI, participate in the N-glycan modification of mammalian cells<sup>[259]</sup>. Neuraminidases (NEU), also referred to as sialidases, are integral to this process. There are four known mammalian homologs of neuraminidases, NEU1, NEU2, NEU3 and NEU4<sup>[260]</sup>. Sialosides play a vital role in the recycling by sialosides, leading to the regeneration of sialic acid monomers available for reuse. In this study, the number of terminal sialic acids was also taken into consideration in the evaluation process, focusing on the tendency of the relative peak area changes in mono-, bi-, tri-, tetra-, penta-, and hexa-sialylation. Significant differences in the expression of different degrees of sialylation were observed across medulloblastoma subgroups. Specifically, the expression abundance of mono- and bi-sialylation is higher in pWNT, pG3myc, and pG3 compared to other subgroups. Within cancer cells, the proto-oncogene c-Myc upregulates the expression of sialyltransferases, consequently heightening the synthesis of sialylated N-glycans in the Golgi system by these sialyltransferases<sup>[258, 261-263]</sup>. In the current investigation, we have observed an association between NEU4 and the upregulation of the Wnt/ $\beta$ -catenin pathway in a neuroblastoma cell line, resulting in the enhanced proliferation of these cells<sup>[264]</sup>. Within colon cancer cells, NEU3 promotes tumorigenesis by sustaining stemness-like characteristics and self-renewal properties, largely through Wnt signaling<sup>[265]</sup>. This suggests that c-Myc amplification and the activation of the Wnt/ $\beta$ -catenin pathway influence the level of sialyltransferases and neuraminidases, thereby regulating the extent of sialylation.

Research has indicated substantial alterations in sialic acid abundance during the initial phases of tumorigenesis, potentially impacting tumorigenesis by diminishing cell adhesion. The effect could contribute to heightened cell motility and the substantial metastatic capacity of cancer cells<sup>[266, 267]</sup>. Upon binding to sialylated glycans, Siglecs stimulate immunosuppressive signaling, offering a protective advantage to tumor cells<sup>[268-270]</sup>. As an illustration, an extensively sialylated cell-surface protein CD24 interacts with Siglec-10 on macrophages, resulting in the protection of ovarian and breast cancer cells against phagocytotic cell death<sup>[271]</sup>. Furthermore, the relative abundance of N-glycans containing more than two sialic acid residues is higher in non-WNT/non-SHH tumors (pG3myc, pG3, and pG4) in comparison to WNT/SHH tumors (pWNT, pSHHs and pSHHt). This indicates that the high number of sialic acids in N-glycans may be a contributing factor to high-risk medulloblastoma patients.

Fucosylation is the enzymatic process that constructs fucose-containing glycans, utilizing GDP-fucose as a high-energy fucose donor, catalyzed by fucosyltransferases<sup>[272]</sup>. This post-translational modification plays pivotal roles in various biological processes, including the determination of ABO blood group, ontogenesis (involving Notch receptor signaling), and is associated with several pathological conditions, such as atherosclerosis and cancer<sup>[251, 273, 274]</sup>. Notably, Kossowska et al. have reported the prospective efficacy of fucosylation as a biomarker for cancer<sup>[275]</sup>. In this project, the relative abundance of fucosylation is higher in pG3myc and pG3 compared to all other groups. Specifically, mono-, tri-, penta-, and hexa-fucosylation were more abundant in pG3myc. Keiichiro Sakuma et al. reported that c-Myc contributes to fucosylation expression by transcriptional induction of fucosyltransferases in the EGF/bFGF-treated cells<sup>[263]</sup>. Aberrant fucosylation patterns have been documented in numerous cancer types, with the clinical application of specific fucosylated glycan structures serving as a diagnostic and prognostic tool for various cancers<sup>[276-282]</sup>. An illustrative example is the application of  $\alpha$ -1,6-fucosylated  $\alpha$ -fetoprotein as a prevalent biomarker for early hepatocellular carcinoma diagnosis, effectively distinguishing these patients from cirrhosis cases characterized by a moderate elevation of specific fucosylated structures, despite comparable serum  $\alpha$ -fetoprotein levels<sup>[283-285]</sup>. Fucosylation is known to affect cell-cell adhesion, signaling, and immunosuppression in malignant tumors<sup>[286-288]</sup>. Additionally, distinct fucosylated structures are frequently identified in bladder cancer cells, potentially playing a role in tumor invasion and metastasis<sup>[289]</sup>. Taken together, the dysregulation of mono-, tri-, penta- and hexa-fucosylation may be affected by c-myc amplification in pG3myc as a potential biomarker of high-risk medulloblastoma tumors.

#### **4.6 Aberrant N-glycan as malignant progression markers between pWNT and pG3myc**

At the proteome level, surprisingly, the highest similarity can be detected between the best and worst prognostic medulloblastoma subgroups (pWNT and pG3myc)<sup>[26]</sup>. Nonetheless, pWNT tumors exhibited a greater abundance of factors associated with asparagine-linked N-glycosylation compared to pG3myc (Figure 10B). Moreover, these factors are involved in N-glycan biosynthesis (Figure 10C). Based on these observations, it is possible that N-glycosylation plays a key role in diverse clinical behavior between pWNT and pG3myc. N-glycome data shown that significant differences in the upregulated relative levels of three

bisected and ploy-LaNAc modified tetra-antennary N-glycans (N17601, N07601 and N07611) and three bisected tetra-antennary N-glycans (N26621, N06501 and N36631) and a sialylated and fucosylated N-glycan with poly-LaNAc (N16811) in pG3myc compared to pWNT. Moreover, other upregulated N-glycans are sialylated and fucosylated. As discussed above, alterations in the expression profiles of ploy-LaNAc modified and bisected N-glycans have also been linked to enhanced replicative capacity, tissue infiltration, and metastasis, which are pivotal aspects of cancer progression<sup>[237]</sup>. Thus, N17601, N07601, N07611, N26621, N06501, N36631, and N16811 displayed significantly higher levels in pG3myc, indicating that it may be linked to pG3myc progression and metastasis. Additionally, elevating the levels of sialylation and fucosylation affects multiple factors that enhance the metastatic potential of the tumor cells, including reduced cell-cell interactions and heightened invasiveness<sup>[99, 102]</sup>. Based on that, dysregulated sialylated and fucosylated N-glycans may be associated with pG3myc progression and as a target for new therapies in pG3myc. Interestingly, within the pG3myc subgroup, 30 distinct expressed N-glycans featuring sialylation and fucosylation from nearly all branching types, underscoring the significance of terminal modifications in the context of the high-risk pG3myc.

According to a clinical standpoint, the development of an all-encompassing map that integrates glycan structures and their intricate biological associations holds the potential not only to establish a valuable glycol-marker panel and unveil the underlying molecular mechanisms driving cancer <sup>[290]</sup>. Significantly altered N-glycans and unique expression in pG3myc were mapped based on N-glycan biosynthesis (Figure 11B). Essentially, the pathway is assembled based on established glycobiology principles. A total of 97 N-glycans were identified as potential intermediaries linking consecutive glycosylation stages, particularly concerning branching elongation and the formation of terminal N-glycan structures. To elaborate further, the pathway segregates into complex and hybrid types at the pivotal junction point represented by Man3GlcNAc3, GlcNAc, and Hex, which are incrementally appended, leading to the generation of di-, tri, tetra-antennary structures. These are subsequently embellished with sialylation and fucosylation modifications. Note that the glycan map indicates that N-glycans showing differences due to the addition or removal of monosaccharide residues exhibit similar declining or ascending patterns as follows: N13421 and N43531; N06501, N07601, N07611 and N17601; N34601 and N34611; N14731 and N14741; N05511, N15521, N25521, N25731, and N35731; N25721, N35821 and N26621. These findings demonstrate that glycosylation results from a gradual enzymatic process rather than an isolated synthetic event.

Furthermore, among the abnormal N-glycans, multiple fucosylated and sialylated complex-type N-glycans, derived from three distinct antennary backbones (di-, tri-, tetra-), are likely associated with the *in vivo* biosynthesis pathway of SLe<sup>a</sup> or SLe<sup>x</sup>. According to the N-glycan biosynthesis map, the synthesis of SLe<sup>a</sup> or SLe<sup>x</sup> follows a sequential pathway, progressing from branching to sialylation and fucosylation. The sequential addition of Fuc and sialic acid to N-glycans by fucosyltransferase and sialyltransferase finalizes the biosynthesis of SLe<sup>a</sup> or SLe<sup>x</sup>[291]. SLe<sup>a</sup> and SLe<sup>x</sup> are prominent sialylated and fucosylated antigens linked to cancer. They serve as carbohydrate ligands for selectin, mediating cancer cells' extravasation[292]. Elevated levels of SLe<sup>a</sup> and SLe<sup>x</sup> in malignant tumors have been consistently associated with unfavorable prognoses in patients with various cancers, including endometrial cancer, colon cancer, and gastric cancer[290, 293, 294]. Taken together, fucosylation and sialylation by activating fucosyltransferases and sialyltransferases may indicate the final crucial glycosylation step as bad prognostic markers in pG3myc.

## 5. Conclusion

This report represents the pioneering exploration of specific N-glycan structures and variations within medulloblastoma, employing a comprehensive permethylated derivatization approach in conjunction with LC/MS analysis. The study introduces an analytical framework for profiling distinct medulloblastoma subgroups, aiming to identify potential biomarkers and therapeutic targets. This approach seeks to define particular N-glycan structures associated with profound biological implications. The results underscore the significance of augmented branching, bisection, and poly-LaNAc in N-glycans, shedding light on their pivotal role in the unfavorable prognosis of non-WNT/non-SHH tumors, primarily through the facilitation of molecular lattice between membrane receptors and galectins. The results also unveil the potential involvement of fucosylation and fucosylation in pivotal facets of medulloblastoma tumor biology, including cell adhesion and migration. Additionally, the research indicates a surge in high-mannose-type N-glycans, notably associated with high-risk pG4. Furthermore, this investigation underscores the significance of atypical sialylated and fucosylated highly branched N-glycans in driving the malignancy of high-risk pG3myc, thus inviting further exploration into the plausible contributors underlying this delineated glycophenotype.

The current study demonstrates the significant shift observed in N-glycosylation patterns within the dataset, signifying the pivotal roles played by N-glycans in medulloblastoma. To delve deeper into these findings, future investigations will pivot from the current medulloblastoma glycan profiling towards a more targeted glycoprotein profiling approach, thereby markedly enhancing the specificity of potential N-glycosylation biomarkers for this disease. This next phase of analysis will encompass site-specific profiling of glycoproteins, yielding a wealth of biological insights and substantially enriching the pool of potential N-glycan markers.

It is worth noting that this study was conducted with a relatively small sample size of only 18 specimens. To comprehensively unveil the specific roles of bisecting GlcNAc and poly-LaNAc modified N-glycoproteins in medulloblastoma, further investigations employing techniques such as lectin affinity chromatography and mass spectrometry are warranted.

## 6. References

1. Farwell JR, Dohrmann GJ, Flannery JT. Medulloblastoma in childhood: an epidemiological study. *J Neurosurg* 1984; 61(4):657-664.
2. Ostrom QT, Gittleman H, Truitt G, Boscia A, Kruchko C, Barnholtz-Sloan JS. CBTRUS Statistical Report: Primary Brain and Other Central Nervous System Tumors Diagnosed in the United States in 2011-2015. *Neuro Oncol* 2018; 20(suppl\_4):iv1-iv86.
3. Juraschka K, Taylor MD. Medulloblastoma in the age of molecular subgroups: a review. *J Neurosurg Pediatr* 2019; 24(4):353-363.
4. Northcott PA, Robinson GW, Kratz CP, Mabbott DJ, Pomeroy SL, Clifford SC, et al. Medulloblastoma. *Nat Rev Dis Primers* 2019; 5(1):11.
5. Roberts RO, Lynch CF, Jones MP, Hart MN. Medulloblastoma: a population-based study of 532 cases. *J Neuropathol Exp Neurol* 1991; 50(2):134-144.
6. Merchant TE, Pollack IF, Loeffler JS. Brain tumors across the age spectrum: biology, therapy, and late effects. *Semin Radiat Oncol* 2010; 20(1):58-66.
7. King AA, Seidel K, Di C, Leisenring WM, Perkins SM, Krull KR, et al. Long-term neurologic health and psychosocial function of adult survivors of childhood medulloblastoma/PNET: a report from the Childhood Cancer Survivor Study. *Neuro Oncol* 2017; 19(5):689-698.
8. Olivier TW, Bass JK, Ashford JM, Beaulieu R, Scott SM, Schreiber JE, et al. Cognitive Implications of Ototoxicity in Pediatric Patients With Embryonal Brain Tumors. *J Clin Oncol* 2019; 37(18):1566-1575.
9. Mulhern RK, Palmer SL, Merchant TE, Wallace D, Kocak M, Brouwers P, et al. Neurocognitive consequences of risk-adapted therapy for childhood medulloblastoma. *J Clin Oncol* 2005; 23(24):5511-5519.
10. Salloum R, Chen Y, Yasui Y, Packer R, Leisenring W, Wells E, et al. Late Morbidity and Mortality Among Medulloblastoma Survivors Diagnosed Across Three Decades: A Report From the Childhood Cancer Survivor Study. *J Clin Oncol* 2019; 37(9):731-740.
11. Majd N, Penas-Prado M. Updates on Management of Adult Medulloblastoma. *Curr Treat Options Oncol* 2019; 20(8):64.
12. Khanna V, Achey RL, Ostrom QT, Block-Beach H, Kruchko C, Barnholtz-Sloan JS, et al. Incidence and survival trends for medulloblastomas in the United States from 2001 to 2013. *J Neurooncol* 2017; 135(3):433-441.
13. Johnston DL, Keene D, Kostova M, Strother D, Lafay-Cousin L, Fryer C, et al. Incidence of medulloblastoma in Canadian children. *J Neurooncol* 2014; 120(3):575-579.
14. Waszak SM, Northcott PA, Buchhalter I, Robinson GW, Sutter C, Groebner S, et al. Spectrum and prevalence of genetic predisposition in medulloblastoma: a retrospective genetic study and prospective validation in a clinical trial cohort. *Lancet Oncol* 2018; 19(6):785-798.
15. Ezzat S, Kamal M, El-Khateeb N, El-Beltagy M, Taha H, Refaat A, et al. Pediatric brain tumors in a low/middle income country: does it differ from that in developed world? *J Neurooncol* 2016; 126(2):371-376.
16. Makino K, Nakamura H, Yano S, Kuratsu J. Population-based epidemiological study of primary intracranial tumors in childhood. *Childs Nerv Syst* 2010; 26(8):1029-1034.
17. Pomeroy SL, Tamayo P, Gaasenbeek M, Sturla LM, Angelo M, McLaughlin ME, et al. Prediction of central nervous system embryonal tumour outcome based on gene expression. *Nature* 2002; 415(6870):436-442.
18. Cho YJ, Tsherniak A, Tamayo P, Santagata S, Ligon A, Greulich H, et al. Integrative genomic analysis of medulloblastoma identifies a molecular subgroup that drives poor clinical outcome. *J Clin Oncol* 2011; 29(11):1424-1430.



19. Kool M, Koster J, Bunt J, Hasselt NE, Lakeman A, van Sluis P, et al. Integrated genomics identifies five medulloblastoma subtypes with distinct genetic profiles, pathway signatures and clinicopathological features. *PLoS One* 2008; 3(8):e3088.
20. Thompson MC, Fuller C, Hogg TL, Dalton J, Finkelstein D, Lau CC, et al. Genomics identifies medulloblastoma subgroups that are enriched for specific genetic alterations. *J Clin Oncol* 2006; 24(12):1924-1931.
21. Remke M, Hielscher T, Northcott PA, Witt H, Ryzhova M, Wittmann A, et al. Adult medulloblastoma comprises three major molecular variants. *J Clin Oncol* 2011; 29(19):2717-2723.
22. Taylor MD, Northcott PA, Korshunov A, Remke M, Cho YJ, Clifford SC, et al. Molecular subgroups of medulloblastoma: the current consensus. *Acta Neuropathol* 2012; 123(4):465-472.
23. Louis DN, Perry A, Wesseling P, Brat DJ, Cree IA, Figarella-Branger D, et al. The 2021 WHO Classification of Tumors of the Central Nervous System: a summary. *Neuro Oncol* 2021; 23(8):1231-1251.
24. Horbinski C, Berger T, Packer RJ, Wen PY. Clinical implications of the 2021 edition of the WHO classification of central nervous system tumours. *Nat Rev Neurol* 2022; 18(9):515-529.
25. Archer TC, Ehrenberger T, Mundt F, Gold MP, Krug K, Mah CK, et al. Proteomics, Post-translational Modifications, and Integrative Analyses Reveal Molecular Heterogeneity within Medulloblastoma Subgroups. *Cancer Cell* 2018; 34(3):396-410.e398.
26. Voß H, Godbole S, Schlumbohm S, Schumann Y, Peng B, Mynarek M, et al. Multiomic profiling of medulloblastoma reveals subtype-specific targetable alterations at the proteome and N-glycan level. *bioRxiv* 2023:2023.2001.2009.523234.
27. Cavalli FMG, Remke M, Rampasek L, Peacock J, Shih DJH, Luu B, et al. Intertumoral Heterogeneity within Medulloblastoma Subgroups. *Cancer Cell* 2017; 31(6):737-754.e736.
28. Gajjar A, Chintagumpala M, Ashley D, Kellie S, Kun LE, Merchant TE, et al. Risk-adapted craniospinal radiotherapy followed by high-dose chemotherapy and stem-cell rescue in children with newly diagnosed medulloblastoma (St Jude Medulloblastoma-96): long-term results from a prospective, multicentre trial. *Lancet Oncol* 2006; 7(10):813-820.
29. Menyhárt O, Györffy B. Molecular stratifications, biomarker candidates and new therapeutic options in current medulloblastoma treatment approaches. *Cancer Metastasis Rev* 2020; 39(1):211-233.
30. Clifford SC, Lannering B, Schwalbe EC, Hicks D, O'Toole K, Nicholson SL, et al. Biomarker-driven stratification of disease-risk in non-metastatic medulloblastoma: Results from the multi-center HIT-SIOP-PNET4 clinical trial. *Oncotarget* 2015; 6(36):38827-38839.
31. Clifford SC, Lusher ME, Lindsey JC, Langdon JA, Gilbertson RJ, Straughton D, et al. Wnt/Wingless pathway activation and chromosome 6 loss characterize a distinct molecular sub-group of medulloblastomas associated with a favorable prognosis. *Cell Cycle* 2006; 5(22):2666-2670.
32. Ellison DW, Onilude OE, Lindsey JC, Lusher ME, Weston CL, Taylor RE, et al. beta-Catenin status predicts a favorable outcome in childhood medulloblastoma: the United Kingdom Children's Cancer Study Group Brain Tumour Committee. *J Clin Oncol* 2005; 23(31):7951-7957.
33. Zurawel RH, Chiappa SA, Allen C, Raffel C. Sporadic medulloblastomas contain oncogenic beta-catenin mutations. *Cancer Res* 1998; 58(5):896-899.
34. Northcott PA, Buchhalter I, Morrissy AS, Hovestadt V, Weischenfeldt J, Ehrenberger T, et al. The whole-genome landscape of medulloblastoma subtypes. *Nature* 2017; 547(7663):311-317.
35. Eberhart CG, Tihan T, Burger PC. Nuclear localization and mutation of beta-catenin in medulloblastomas. *J Neuropathol Exp Neurol* 2000; 59(4):333-337.

36. He TC, Sparks AB, Rago C, Hermeking H, Zawel L, da Costa LT, et al. Identification of c-MYC as a target of the APC pathway. *Science* 1998; 281(5382):1509-1512.
37. Kool M, Korshunov A, Remke M, Jones DT, Schlanstein M, Northcott PA, et al. Molecular subgroups of medulloblastoma: an international meta-analysis of transcriptome, genetic aberrations, and clinical data of WNT, SHH, Group 3, and Group 4 medulloblastomas. *Acta Neuropathol* 2012; 123(4):473-484.
38. Zou H, Poore B, Broniscer A, Pollack IF, Hu B. Molecular Heterogeneity and Cellular Diversity: Implications for Precision Treatment in Medulloblastoma. *Cancers (Basel)* 2020; 12(3).
39. Schwalbe EC, Lindsey JC, Nakjang S, Crosier S, Smith AJ, Hicks D, et al. Novel molecular subgroups for clinical classification and outcome prediction in childhood medulloblastoma: a cohort study. *Lancet Oncol* 2017; 18(7):958-971.
40. Shih DJ, Northcott PA, Remke M, Korshunov A, Ramaswamy V, Kool M, et al. Cytogenetic prognostication within medulloblastoma subgroups. *J Clin Oncol* 2014; 32(9):886-896.
41. Wallace VA. Purkinje-cell-derived Sonic hedgehog regulates granule neuron precursor cell proliferation in the developing mouse cerebellum. *Curr Biol* 1999; 9(8):445-448.
42. Vaillant C, Monard D. SHH pathway and cerebellar development. *Cerebellum* 2009; 8(3):291-301.
43. Brown NJ, Wilson B, Shahrestani S, Choi EH, Lien BV, Paladugu A, et al. The 100 Most Influential Publications on Medulloblastoma: Areas of Past, Current, and Future Focus. *World Neurosurg* 2021; 146:119-139.
44. Kool M, Jones DT, Jäger N, Northcott PA, Pugh TJ, Hovestadt V, et al. Genome sequencing of SHH medulloblastoma predicts genotype-related response to smoothed inhibition. *Cancer Cell* 2014; 25(3):393-405.
45. Ray S, Chaturvedi NK, Bhakat KK, Rizzino A, Mahapatra S. Subgroup-Specific Diagnostic, Prognostic, and Predictive Markers Influencing Pediatric Medulloblastoma Treatment. *Diagnostics (Basel)* 2021; 12(1).
46. Fang FY, Rosenblum JS, Ho WS, Heiss JD. New Developments in the Pathogenesis, Therapeutic Targeting, and Treatment of Pediatric Medulloblastoma. *Cancers (Basel)* 2022; 14(9).
47. Taylor MD, Liu L, Raffel C, Hui CC, Mainprize TG, Zhang X, et al. Mutations in SUFU predispose to medulloblastoma. *Nat Genet* 2002; 31(3):306-310.
48. Northcott PA, Hielscher T, Dubuc A, Mack S, Shih D, Remke M, et al. Pediatric and adult sonic hedgehog medulloblastomas are clinically and molecularly distinct. *Acta Neuropathol* 2011; 122(2):231-240.
49. Horvath S, Mah V, Lu AT, Woo JS, Choi OW, Jasinska AJ, et al. The cerebellum ages slowly according to the epigenetic clock. *Aging (Albany NY)* 2015; 7(5):294-306.
50. Lu AT, Hannon E, Levine ME, Hao K, Crimmins EM, Lunnon K, et al. Genetic variants near MLST8 and DHX57 affect the epigenetic age of the cerebellum. *Nat Commun* 2016; 7:10561.
51. Northcott PA, Jones DT, Kool M, Robinson GW, Gilbertson RJ, Cho YJ, et al. Medulloblastomics: the end of the beginning. *Nat Rev Cancer* 2012; 12(12):818-834.
52. Goschzik T, Zur Mühlen A, Kristiansen G, Haberler C, Stefanits H, Friedrich C, et al. Molecular stratification of medulloblastoma: comparison of histological and genetic methods to detect Wnt activated tumours. *Neuropathol Appl Neurobiol* 2015; 41(2):135-144.
53. Orr BA. Pathology, diagnostics, and classification of medulloblastoma. *Brain Pathol* 2020; 30(3):664-678.
54. Kijima N, Kanemura Y. Molecular Classification of Medulloblastoma. *Neurol Med Chir (Tokyo)* 2016; 56(11):687-697.

55. Kaur K, Kakkar A, Kumar A, Mallick S, Julka PK, Gupta D, et al. Integrating Molecular Subclassification of Medulloblastomas into Routine Clinical Practice: A Simplified Approach. *Brain Pathol* 2016; 26(3):334-343.
56. Ellison DW, Dalton J, Kocak M, Nicholson SL, Fraga C, Neale G, et al. Medulloblastoma: clinicopathological correlates of SHH, WNT, and non-SHH/WNT molecular subgroups. *Acta Neuropathol* 2011; 121(3):381-396.
57. Eid AM, Heabah NAE. Medulloblastoma: clinicopathological parameters, risk stratification, and survival analysis of immunohistochemically validated molecular subgroups. *J Egypt Natl Canc Inst* 2021; 33(1):6.
58. Roussel MF, Robinson GW. Role of MYC in Medulloblastoma. *Cold Spring Harb Perspect Med* 2013; 3(11).
59. Van Ommeren R, Garzia L, Holgado BL, Ramaswamy V, Taylor MD. The molecular biology of medulloblastoma metastasis. *Brain Pathol* 2020; 30(3):691-702.
60. Tao R, Murad N, Xu Z, Zhang P, Okonechnikov K, Kool M, et al. MYC Drives Group 3 Medulloblastoma through Transformation of Sox2(+) Astrocyte Progenitor Cells. *Cancer Res* 2019; 79(8):1967-1980.
61. Northcott PA, Lee C, Zichner T, Stütz AM, Erkek S, Kawauchi D, et al. Enhancer hijacking activates GFII family oncogenes in medulloblastoma. *Nature* 2014; 511(7510):428-434.
62. Northcott PA, Korshunov A, Witt H, Hielscher T, Eberhart CG, Mack S, et al. Medulloblastoma comprises four distinct molecular variants. *J Clin Oncol* 2011; 29(11):1408-1414.
63. Mastronuzzi A, Miele E, Po A, Antonelli M, Buttarelli FR, Colafati GS, et al. Large cell anaplastic medulloblastoma metastatic to the scalp: tumor and derived stem-like cells features. *BMC Cancer* 2014; 14:262.
64. Robinson G, Parker M, Kranenburg TA, Lu C, Chen X, Ding L, et al. Novel mutations target distinct subgroups of medulloblastoma. *Nature* 2012; 488(7409):43-48.
65. Gajjar AJ, Robinson GW. Medulloblastoma-translating discoveries from the bench to the bedside. *Nat Rev Clin Oncol* 2014; 11(12):714-722.
66. Ning MS, Perkins SM, Dewees T, Shinohara ET. Evidence of high mortality in long term survivors of childhood medulloblastoma. *J Neurooncol* 2015; 122(2):321-327.
67. Kocakaya S, Beier CP, Beier D. Chemotherapy increases long-term survival in patients with adult medulloblastoma--a literature-based meta-analysis. *Neuro Oncol* 2016; 18(3):408-416.
68. Rutkowski S, Cohen B, Finlay J, Luksch R, Ridola V, Valteau-Couanet D, et al. Medulloblastoma in young children. *Pediatr Blood Cancer* 2010; 54(4):635-637.
69. Michiels EM, Schouten-Van Meeteren AY, Doz F, Janssens GO, van Dalen EC. Chemotherapy for children with medulloblastoma. *Cochrane Database Syst Rev* 2015; 1:Cd006678.
70. Ohtsubo K, Marth JD. Glycosylation in cellular mechanisms of health and disease. *Cell* 2006; 126(5):855-867.
71. Berois N, Pittini A, Osinaga E. Targeting Tumor Glycans for Cancer Therapy: Successes, Limitations, and Perspectives. *Cancers (Basel)* 2022; 14(3).
72. Pinho SS, Reis CA. Glycosylation in cancer: mechanisms and clinical implications. *Nat Rev Cancer* 2015; 15(9):540-555.
73. Groux-Degroote S, Guérardel Y, Delannoy P. Gangliosides: Structures, Biosynthesis, Analysis, and Roles in Cancer. *Chembiochem* 2017; 18(13):1146-1154.
74. Thomas D, Rathinavel AK, Radhakrishnan P. Altered glycosylation in cancer: A promising target for biomarkers and therapeutics. *Biochim Biophys Acta Rev Cancer* 2021; 1875(1):188464.

75. Wang Y, Chen H. Protein glycosylation alterations in hepatocellular carcinoma: function and clinical implications. *Oncogene* 2023; 42(24):1970-1979.
76. Fuster MM, Esko JD. The sweet and sour of cancer: glycans as novel therapeutic targets. *Nat Rev Cancer* 2005; 5(7):526-542.
77. Critcher M, Hassan AA, Huang ML. Seeing the forest through the trees: characterizing the glycoproteome. *Trends Biochem Sci* 2022; 47(6):492-505.
78. Yoo J, Mashalidis EH, Kuk ACY, Yamamoto K, Kaeser B, Ichikawa S, et al. GlcNAc-1-P-transferase-tunicamycin complex structure reveals basis for inhibition of N-glycosylation. *Nat Struct Mol Biol* 2018; 25(3):217-224.
79. Gao N, Shang J, Lehrman MA. Unexpected basis for impaired Glc3Man9GlcNAc2-P-P-dolichol biosynthesis by elevated expression of GlcNAc-1-P transferase. *Glycobiology* 2008; 18(1):125-134.
80. Aebi M. N-linked protein glycosylation in the ER. *Biochim Biophys Acta* 2013; 1833(11):2430-2437.
81. Shrimal S, Gilmore R. Oligosaccharyltransferase structures provide novel insight into the mechanism of asparagine-linked glycosylation in prokaryotic and eukaryotic cells. *Glycobiology* 2019; 29(4):288-297.
82. Huang S, Haga Y, Li J, Zhang J, Kweon HK, Seino J, et al. Mitotic phosphorylation inhibits the Golgi mannosidase MAN1A1. *Cell Rep* 2022; 41(8):111679.
83. Vliegenthart JF. The complexity of glycoprotein-derived glycans. *Proc Jpn Acad Ser B Phys Biol Sci* 2017; 93(2):64-86.
84. Chen Q, Tan Z, Guan F, Ren Y. The Essential Functions and Detection of Bisecting GlcNAc in Cell Biology. *Front Chem* 2020; 8:511.
85. Krasnova L, Wong CH. Oligosaccharide Synthesis and Translational Innovation. *J Am Chem Soc* 2019; 141(9):3735-3754.
86. Wang SH, Wu TJ, Lee CW, Yu J. Dissecting the conformation of glycans and their interactions with proteins. *J Biomed Sci* 2020; 27(1):93.
87. Nakano M, Mishra SK, Tokoro Y, Sato K, Nakajima K, Yamaguchi Y, et al. Bisecting GlcNAc Is a General Suppressor of Terminal Modification of N-glycan. *Mol Cell Proteomics* 2019; 18(10):2044-2057.
88. Vasconcelos-Dos-Santos A, Oliveira IA, Lucena MC, Mantuano NR, Whelan SA, Dias WB, et al. Biosynthetic Machinery Involved in Aberrant Glycosylation: Promising Targets for Developing of Drugs Against Cancer. *Front Oncol* 2015; 5:138.
89. Zhong Q, Xiao X, Qiu Y, Xu Z, Chen C, Chong B, et al. Protein posttranslational modifications in health and diseases: Functions, regulatory mechanisms, and therapeutic implications. *MedComm (2020)* 2023; 4(3):e261.
90. Wang M, Zhu J, Lubman DM, Gao C. Aberrant glycosylation and cancer biomarker discovery: a promising and thorny journey. *Clin Chem Lab Med* 2019; 57(4):407-416.
91. Legler K, Rosprim R, Karius T, Eylmann K, Rossberg M, Wirtz RM, et al. Reduced mannosidase MAN1A1 expression leads to aberrant N-glycosylation and impaired survival in breast cancer. *Br J Cancer* 2018; 118(6):847-856.
92. Helenius A, Aebi M. Roles of N-linked glycans in the endoplasmic reticulum. *Annu Rev Biochem* 2004; 73:1019-1049.
93. Phoomak C, Silsirivanit A, Park D, Sawanyawisuth K, Vaeteewoottacharn K, Wongkham C, et al. O-GlcNAcylation mediates metastasis of cholangiocarcinoma through FOXO3 and MAN1A1. *Oncogene* 2018; 37(42):5648-5665.
94. Park DD, Phoomak C, Xu G, Olney LP, Tran KA, Park SS, et al. Metastasis of cholangiocarcinoma is promoted by extended high-mannose glycans. *Proc Natl Acad Sci U S A* 2020; 117(14):7633-7644.

95. de Leoz ML, Young LJ, An HJ, Kronewitter SR, Kim J, Miyamoto S, et al. High-mannose glycans are elevated during breast cancer progression. *Mol Cell Proteomics* 2011; 10(1):M110.002717.
96. Takayama H, Ohta M, Iwashita Y, Uchida H, Shitomi Y, Yada K, et al. Altered glycosylation associated with dedifferentiation of hepatocellular carcinoma: a lectin microarray-based study. *BMC Cancer* 2020; 20(1):192.
97. Li S, Mo C, Peng Q, Kang X, Sun C, Jiang K, et al. Cell surface glycan alterations in epithelial mesenchymal transition process of Huh7 hepatocellular carcinoma cell. *PLoS One* 2013; 8(8):e71273.
98. Balog CI, Stavenhagen K, Fung WL, Koeleman CA, McDonnell LA, Verhoeven A, et al. N-glycosylation of colorectal cancer tissues: a liquid chromatography and mass spectrometry-based investigation. *Mol Cell Proteomics* 2012; 11(9):571-585.
99. Sethi MK, Thaysen-Andersen M, Smith JT, Baker MS, Packer NH, Hancock WS, et al. Comparative N-glycan profiling of colorectal cancer cell lines reveals unique bisecting GlcNAc and  $\alpha$ -2,3-linked sialic acid determinants are associated with membrane proteins of the more metastatic/aggressive cell lines. *J Proteome Res* 2014; 13(1):277-288.
100. Alonso-Garcia V, Chaboya C, Li Q, Le B, Congleton TJ, Florez J, et al. High Mannose N-Glycans Promote Migration of Bone-Marrow-Derived Mesenchymal Stromal Cells. *Int J Mol Sci* 2020; 21(19).
101. Wei Y, Chen Q, Huang S, Liu Y, Li Y, Xing Y, et al. The Interaction between DNMT1 and High-Mannose CD133 Maintains the Slow-Cycling State and Tumorigenic Potential of Glioma Stem Cell. *Adv Sci (Weinh)* 2022; 9(26):e2202216.
102. Ščupáková K, Adelaja OT, Balluff B, Ayyappan V, Tressler CM, Jenkinson NM, et al. Clinical importance of high-mannose, fucosylated, and complex N-glycans in breast cancer metastasis. *JCI Insight* 2021; 6(24).
103. Dennis JW, Granovsky M, Warren CE. Glycoprotein glycosylation and cancer progression. *Biochim Biophys Acta* 1999; 1473(1):21-34.
104. Taniguchi N, Korekane H. Branched N-glycans and their implications for cell adhesion, signaling and clinical applications for cancer biomarkers and in therapeutics. *BMB Rep* 2011; 44(12):772-781.
105. de Freitas Junior JC, Morgado-Díaz JA. The role of N-glycans in colorectal cancer progression: potential biomarkers and therapeutic applications. *Oncotarget* 2016; 7(15):19395-19413.
106. Dennis JW, Laferté S, Waghorne C, Breitman ML, Kerbel RS. Beta 1-6 branching of Asn-linked oligosaccharides is directly associated with metastasis. *Science* 1987; 236(4801):582-585.
107. Ogata SI, Muramatsu T, Kobata A. New structural characteristic of the large glycopeptides from transformed cells. *Nature* 1976; 259(5544):580-582.
108. Yamashita K, Ohkura T, Tachibana Y, Takasaki S, Kobata A. Comparative study of the oligosaccharides released from baby hamster kidney cells and their polyoma transformant by hydrazinolysis. *J Biol Chem* 1984; 259(17):10834-10840.
109. Seelentag WK, Li WP, Schmitz SF, Metzger U, Aeberhard P, Heitz PU, et al. Prognostic value of beta1,6-branched oligosaccharides in human colorectal carcinoma. *Cancer Res* 1998; 58(23):5559-5564.
110. Hanzawa K, Tanaka-Okamoto M, Murakami H, Suzuki N, Mukai M, Takahashi H, et al. Increased levels of acidic free-N-glycans, including multi-antennary and fucosylated structures, in the urine of cancer patients. *PLoS One* 2022; 17(4):e0266927.
111. Vagin O, Tokhtaeva E, Yakubov I, Shevchenko E, Sachs G. Inverse correlation between the extent of N-glycan branching and intercellular adhesion in epithelia. Contribution of the Na,K-ATPase beta1 subunit. *J Biol Chem* 2008; 283(4):2192-2202.

112. Sasai K, Ikeda Y, Fujii T, Tsuda T, Taniguchi N. UDP-GlcNAc concentration is an important factor in the biosynthesis of beta1,6-branched oligosaccharides: regulation based on the kinetic properties of N-acetylglucosaminyltransferase V. *Glycobiology* 2002; 12(2):119-127.
113. Thiery JP, Sleeman JP. Complex networks orchestrate epithelial-mesenchymal transitions. *Nat Rev Mol Cell Biol* 2006; 7(2):131-142.
114. Pinho SS, Reis CA, Paredes J, Magalhães AM, Ferreira AC, Figueiredo J, et al. The role of N-acetylglucosaminyltransferase III and V in the post-transcriptional modifications of E-cadherin. *Hum Mol Genet* 2009; 18(14):2599-2608.
115. Pinho SS, Osório H, Nita-Lazar M, Gomes J, Lopes C, Gärtner F, et al. Role of E-cadherin N-glycosylation profile in a mammary tumor model. *Biochem Biophys Res Commun* 2009; 379(4):1091-1096.
116. Pinho SS, Figueiredo J, Cabral J, Carvalho S, Dourado J, Magalhães A, et al. E-cadherin and adherens-junctions stability in gastric carcinoma: functional implications of glycosyltransferases involving N-glycan branching biosynthesis, N-acetylglucosaminyltransferases III and V. *Biochim Biophys Acta* 2013; 1830(3):2690-2700.
117. Tang L, Chen X, Zhang X, Guo Y, Su J, Zhang J, et al. N-Glycosylation in progression of skin cancer. *Med Oncol* 2019; 36(6):50.
118. Narasimhan S. Control of glycoprotein synthesis. UDP-GlcNAc:glycopeptide beta 4-N-acetylglucosaminyltransferase III, an enzyme in hen oviduct which adds GlcNAc in beta 1-4 linkage to the beta-linked mannose of the trimannosyl core of N-glycosyl oligosaccharides. *J Biol Chem* 1982; 257(17):10235-10242.
119. Miwa HE, Song Y, Alvarez R, Cummings RD, Stanley P. The bisecting GlcNAc in cell growth control and tumor progression. *Glycoconj J* 2012; 29(8-9):609-618.
120. Yoshimura M, Nishikawa A, Ihara Y, Taniguchi S, Taniguchi N. Suppression of lung metastasis of B16 mouse melanoma by N-acetylglucosaminyltransferase III gene transfection. *Proc Natl Acad Sci U S A* 1995; 92(19):8754-8758.
121. Sheng Y, Yoshimura M, Inoue S, Oritani K, Nishiura T, Yoshida H, et al. Remodeling of glycoconjugates on CD44 enhances cell adhesion to hyaluronate, tumor growth and metastasis in B16 melanoma cells expressing beta1,4-N-acetylglucosaminyltransferase III. *Int J Cancer* 1997; 73(6):850-858.
122. Fernandes B, Sagman U, Auger M, Demetrio M, Dennis JW. Beta 1-6 branched oligosaccharides as a marker of tumor progression in human breast and colon neoplasia. *Cancer Res* 1991; 51(2):718-723.
123. Zhang X, Wang Y, Qian Y, Wu X, Zhang Z, Liu X, et al. Discovery of specific metastasis-related N-glycan alterations in epithelial ovarian cancer based on quantitative glycomics. *PLoS One* 2014; 9(2):e87978.
124. Rebbaa A, Yamamoto H, Saito T, Meuillet E, Kim P, Kersey DS, et al. Gene transfection-mediated overexpression of beta1,4-N-acetylglucosamine bisecting oligosaccharides in glioma cell line U373 MG inhibits epidermal growth factor receptor function. *J Biol Chem* 1997; 272(14):9275-9279.
125. Gu J, Zhao Y, Isaji T, Shibukawa Y, Ihara H, Takahashi M, et al. Beta1,4-N-Acetylglucosaminyltransferase III down-regulates neurite outgrowth induced by costimulation of epidermal growth factor and integrins through the Ras/ERK signaling pathway in PC12 cells. *Glycobiology* 2004; 14(2):177-186.
126. North SJ, Huang HH, Sundaram S, Jang-Lee J, Etienne AT, Trollope A, et al. Glycomics profiling of Chinese hamster ovary cell glycosylation mutants reveals N-glycans of a novel size and complexity. *J Biol Chem* 2010; 285(8):5759-5775.
127. Dennis JW, Lau KS, Demetriou M, Nabi IR. Adaptive regulation at the cell surface by N-glycosylation. *Traffic* 2009; 10(11):1569-1578.

128. de-Freitas-Junior JC, Carvalho S, Dias AM, Oliveira P, Cabral J, Seruca R, et al. Insulin/IGF-I signaling pathways enhances tumor cell invasion through bisecting GlcNAc N-glycans modulation. an interplay with E-cadherin. *PLoS One* 2013; 8(11):e81579.
129. Padmanaban V, Krol I, Suhail Y, Szczerba BM, Aceto N, Bader JS, et al. E-cadherin is required for metastasis in multiple models of breast cancer. *Nature* 2019; 573(7774):439-444.
130. Takahashi M, Kuroki Y, Ohtsubo K, Taniguchi N. Core fucose and bisecting GlcNAc, the direct modifiers of the N-glycan core: their functions and target proteins. *Carbohydr Res* 2009; 344(12):1387-1390.
131. Shoreibah M, Perng GS, Adler B, Weinstein J, Basu R, Cupples R, et al. Isolation, characterization, and expression of a cDNA encoding N-acetylglucosaminyltransferase V. *J Biol Chem* 1993; 268(21):15381-15385.
132. Lucena MC, Carvalho-Cruz P, Donadio JL, Oliveira IA, de Queiroz RM, Marinho-Carvalho MM, et al. Epithelial Mesenchymal Transition Induces Aberrant Glycosylation through Hexosamine Biosynthetic Pathway Activation. *J Biol Chem* 2016; 291(25):12917-12929.
133. Holst S, Wuhler M, Rombouts Y. Glycosylation characteristics of colorectal cancer. *Adv Cancer Res* 2015; 126:203-256.
134. Zhang T, Wu X, Ke C, Yin M, Li Z, Fan L, et al. Identification of potential biomarkers for ovarian cancer by urinary metabolomic profiling. *J Proteome Res* 2013; 12(1):505-512.
135. Tsuboi S, Hatakeyama S, Ohyama C, Fukuda M. Two opposing roles of O-glycans in tumor metastasis. *Trends Mol Med* 2012; 18(4):224-232.
136. Tsuboi S, Sutoh M, Hatakeyama S, Hiraoka N, Habuchi T, Horikawa Y, et al. A novel strategy for evasion of NK cell immunity by tumours expressing core2 O-glycans. *Embo j* 2011; 30(15):3173-3185.
137. He XJ, Tao HQ, Hu ZM, Ma YY, Xu J, Wang HJ, et al. Expression of galectin-1 in carcinoma-associated fibroblasts promotes gastric cancer cell invasion through upregulation of integrin  $\beta$ 1. *Cancer Sci* 2014; 105(11):1402-1410.
138. Chong Y, Tang D, Xiong Q, Jiang X, Xu C, Huang Y, et al. Galectin-1 from cancer-associated fibroblasts induces epithelial-mesenchymal transition through  $\beta$ 1 integrin-mediated upregulation of Gli1 in gastric cancer. *J Exp Clin Cancer Res* 2016; 35(1):175.
139. Chen X, Varki A. Advances in the biology and chemistry of sialic acids. *ACS Chem Biol* 2010; 5(2):163-176.
140. Eylar EH, Madoff MA, Brody OV, Oncley JL. The contribution of sialic acid to the surface charge of the erythrocyte. *J Biol Chem* 1962; 237:1992-2000.
141. Deng L, Chen X, Varki A. Exploration of sialic acid diversity and biology using sialoglycan microarrays. *Biopolymers* 2013; 99(10):650-665.
142. Liu Y, Pan D, Bellis SL, Song Y. Effect of altered glycosylation on the structure of the I-like domain of beta1 integrin: a molecular dynamics study. *Proteins* 2008; 73(4):989-1000.
143. Jian Y, Xu Z, Xu C, Zhang L, Sun X, Yang D, et al. The Roles of Glycans in Bladder Cancer. *Front Oncol* 2020; 10:957.
144. Swindall AF, Bellis SL. Sialylation of the Fas death receptor by ST6Gal-I provides protection against Fas-mediated apoptosis in colon carcinoma cells. *J Biol Chem* 2011; 286(26):22982-22990.
145. Gupta R, Leon F, Thompson CM, Nimmakayala R, Karmakar S, Nallasamy P, et al. Global analysis of human glycosyltransferases reveals novel targets for pancreatic cancer pathogenesis. *Br J Cancer* 2020; 122(11):1661-1672.
146. Takahashi S, Oda T, Hasebe T, Sasaki S, Kinoshita T, Konishi M, et al. Overexpression of sialyl Lewis x antigen is associated with formation of extratumoral venous invasion and predicts postoperative development of massive hepatic metastasis in cases with pancreatic ductal adenocarcinoma. *Pathobiology* 2001; 69(3):127-135.

147. Balmaña M, Sarrats A, Llop E, Barrabés S, Saldova R, Ferri MJ, et al. Identification of potential pancreatic cancer serum markers: Increased sialyl-Lewis X on ceruloplasmin. *Clin Chim Acta* 2015; 442:56-62.
148. Almaraz RT, Tian Y, Bhattacharya R, Tan E, Chen SH, Dallas MR, et al. Metabolic flux increases glycoprotein sialylation: implications for cell adhesion and cancer metastasis. *Mol Cell Proteomics* 2012; 11(7):M112.017558.
149. Tonetti M, Sturla L, Bisso A, Benatti U, De Flora A. Synthesis of GDP-L-fucose by the human FX protein. *J Biol Chem* 1996; 271(44):27274-27279.
150. Li J, Hsu HC, Mountz JD, Allen JG. Unmasking Fucosylation: from Cell Adhesion to Immune System Regulation and Diseases. *Cell Chem Biol* 2018; 25(5):499-512.
151. Scharberg EA, Olsen C, Bugert P. An update on the H blood group system. *Immunohematology* 2019; 35(2):67-68.
152. Shao K, Chen ZY, Gautam S, Deng NH, Zhou Y, Wu XZ. Posttranslational modification of E-cadherin by core fucosylation regulates Src activation and induces epithelial-mesenchymal transition-like process in lung cancer cells. *Glycobiology* 2016; 26(2):142-154.
153. Merlotti A, Malizia AL, Michea P, Bonte PE, Goudot C, Carregal MS, et al. Aberrant fucosylation enables breast cancer clusterin to interact with dendritic cell-specific ICAM-grabbing non-integrin (DC-SIGN). *Oncoimmunology* 2019; 8(9):e1629257.
154. Jassam SA, Maherally Z, Ashkan K, Pilkington GJ, Fillmore HL. Fucosyltransferase 4 and 7 mediates adhesion of non-small cell lung cancer cells to brain-derived endothelial cells and results in modification of the blood-brain-barrier: in vitro investigation of CD15 and CD15s in lung-to-brain metastasis. *J Neurooncol* 2019; 143(3):405-415.
155. Seeberger PH, Freedberg DI, Cummings RD. Glycans in Biotechnology and the Pharmaceutical Industry. In: *Essentials of Glycobiology*. Varki A, Cummings RD, Esko JD, et al. (editors). Cold Spring Harbor (NY): Cold Spring Harbor Laboratory Press Copyright © 2022 The Consortium of Glycobiology Editors, La Jolla, California; published by Cold Spring Harbor Laboratory Press; doi:10.1101/glycobiology.4e.57. All rights reserved.; 2022. pp. 771-784.
156. Fernandes E, Sores J, Cotton S, Peixoto A, Ferreira D, Freitas R, et al. Esophageal, gastric and colorectal cancers: Looking beyond classical serological biomarkers towards glycoproteomics-assisted precision oncology. *Theranostics* 2020; 10(11):4903-4928.
157. Peixoto A, Relvas-Santos M, Azevedo R, Santos LL, Ferreira JA. Protein Glycosylation and Tumor Microenvironment Alterations Driving Cancer Hallmarks. *Front Oncol* 2019; 9:380.
158. Saxena M, van der Burg SH, Melief CJM, Bhardwaj N. Therapeutic cancer vaccines. *Nat Rev Cancer* 2021; 21(6):360-378.
159. Slovin SF, Ragupathi G, Adluri S, Ungers G, Terry K, Kim S, et al. Carbohydrate vaccines in cancer: immunogenicity of a fully synthetic globo H hexasaccharide conjugate in man. *Proc Natl Acad Sci U S A* 1999; 96(10):5710-5715.
160. Danishefsky SJ, Shue YK, Chang MN, Wong CH. Development of Globo-H cancer vaccine. *Acc Chem Res* 2015; 48(3):643-652.
161. Azevedo R, Ferreira JA, Peixoto A, Neves M, Sousa N, Lima A, et al. Emerging antibody-based therapeutic strategies for bladder cancer: A systematic review. *J Control Release* 2015; 214:40-61.
162. Fernandes E, Ferreira JA, Andreia P, Luís L, Barroso S, Sarmiento B, et al. New trends in guided nanotherapies for digestive cancers: A systematic review. *J Control Release* 2015; 209:288-307.
163. Posey AD, Jr., Schwab RD, Boesteanu AC, Steentoft C, Mandel U, Engels B, et al. Engineered CAR T Cells Targeting the Cancer-Associated Tn-Glycoform of the Membrane Mucin MUC1 Control Adenocarcinoma. *Immunity* 2016; 44(6):1444-1454.



164. Pace A, Scirocchi F, Napoletano C, Zizzari IG, D'Angelo L, Santoro A, et al. Glycan-Lectin Interactions as Novel Immunosuppression Drivers in Glioblastoma. *Int J Mol Sci* 2022; 23(11).
165. Marciscano AE, Anandasabapathy N. The role of dendritic cells in cancer and anti-tumor immunity. *Semin Immunol* 2021; 52:101481.
166. Lakshminarayanan V, Thompson P, Wolfert MA, Buskas T, Bradley JM, Pathangey LB, et al. Immune recognition of tumor-associated mucin MUC1 is achieved by a fully synthetic aberrantly glycosylated MUC1 tripartite vaccine. *Proc Natl Acad Sci U S A* 2012; 109(1):261-266.
167. Abdel-Aal AB, Lakshminarayanan V, Thompson P, Supekar N, Bradley JM, Wolfert MA, et al. Immune and anticancer responses elicited by fully synthetic aberrantly glycosylated MUC1 tripartite vaccines modified by a TLR2 or TLR9 agonist. *ChemBiochem* 2014; 15(10):1508-1513.
168. In: *Essentials of Glycobiology*. Varki A, Cummings RD, Esko JD, et al. (editors). Cold Spring Harbor (NY): Cold Spring Harbor Laboratory Press Copyright © 2022 by the Consortium of Glycobiology Editors, La Jolla, California. Published by Cold Spring Harbor Laboratory Press, Cold Spring Harbor, New York. All rights reserved.; 2022.
169. Morelle W, Faid V, Chirat F, Michalski JC. Analysis of N- and O-linked glycans from glycoproteins using MALDI-TOF mass spectrometry. *Methods Mol Biol* 2009; 534:5-21.
170. Shajahan A, Heiss C, Ishihara M, Azadi P. Glycomic and glycoproteomic analysis of glycoproteins-a tutorial. *Anal Bioanal Chem* 2017; 409(19):4483-4505.
171. Yang S, Toghi Eshghi S, Chiu H, DeVoe DL, Zhang H. Glycomic analysis by glycoprotein immobilization for glycan extraction and liquid chromatography on microfluidic chip. *Anal Chem* 2013; 85(21):10117-10125.
172. Burock R, Cajic S, Hennig R, Buettner FFR, Reichl U, Rapp E. Reliable N-Glycan Analysis-Removal of Frequently Occurring Oligosaccharide Impurities by Enzymatic Degradation. *Molecules* 2023; 28(4).
173. Sun S, Shah P, Eshghi ST, Yang W, Trikannad N, Yang S, et al. Comprehensive analysis of protein glycosylation by solid-phase extraction of N-linked glycans and glycosite-containing peptides. *Nat Biotechnol* 2016; 34(1):84-88.
174. Veillon L, Zhou S, Mechref Y. Quantitative Glycomics: A Combined Analytical and Bioinformatics Approach. *Methods Enzymol* 2017; 585:431-477.
175. Rudd PM, Karlsson NG, Khoo KH, Thaysen-Andersen M, Wells L, Packer NH. Glycomics and Glycoproteomics. In: *Essentials of Glycobiology*. Varki A, Cummings RD, Esko JD, et al. (editors). Cold Spring Harbor (NY): Cold Spring Harbor Laboratory Press Copyright © 2022 The Consortium of Glycobiology Editors, La Jolla, California; published by Cold Spring Harbor Laboratory Press; doi:10.1101/glycobiology.4e.51. All rights reserved.; 2022. pp. 689-704.
176. Harvey DJ. Collision-induced fragmentation of underivatized N-linked carbohydrates ionized by electrospray. *J Mass Spectrom* 2000; 35(10):1178-1190.
177. Huang Y, Dodds ED. Ion mobility studies of carbohydrates as group I adducts: isomer specific collisional cross section dependence on metal ion radius. *Anal Chem* 2013; 85(20):9728-9735.
178. Zaia J. Mass spectrometry and glycomics. *Omics* 2010; 14(4):401-418.
179. Zaia J. Mass spectrometry and the emerging field of glycomics. *Chem Biol* 2008; 15(9):881-892.
180. Zhou S, Veillon L, Dong X, Huang Y, Mechref Y. Direct comparison of derivatization strategies for LC-MS/MS analysis of N-glycans. *Analyst* 2017; 142(23):4446-4455.

181. Kang P, Mechref Y, Novotny MV. High-throughput solid-phase permethylation of glycans prior to mass spectrometry. *Rapid Commun Mass Spectrom* 2008; 22(5):721-734.
182. Alley WR, Jr., Madera M, Mechref Y, Novotny MV. Chip-based reversed-phase liquid chromatography-mass spectrometry of permethylated N-linked glycans: a potential methodology for cancer-biomarker discovery. *Anal Chem* 2010; 82(12):5095-5106.
183. Donohoo KB, Wang J, Goli M, Yu A, Peng W, Hakim MA, et al. Advances in mass spectrometry-based glycomics-An update covering the period 2017-2021. *Electrophoresis* 2022; 43(1-2):119-142.
184. Cho BG, Gutierrez Reyes CD, Mechref Y. N-Glycomics of Cerebrospinal Fluid: Method Comparison. *Molecules* 2021; 26(6).
185. Vreeker GC, Wuhrer M. Reversed-phase separation methods for glycan analysis. *Anal Bioanal Chem* 2017; 409(2):359-378.
186. Liu Z, Xu M, Zhang W, Miao X, Wang PG, Li S, et al. Recent development in hydrophilic interaction liquid chromatography stationary materials for glycopeptide analysis. *Anal Methods* 2022; 14(44):4437-4448.
187. Abrahams JL, Campbell MP, Packer NH. Building a PGC-LC-MS N-glycan retention library and elution mapping resource. *Glycoconj J* 2018; 35(1):15-29.
188. Gautam S, Banazadeh A, Cho BG, Goli M, Zhong J, Mechref Y. Mesoporous Graphitized Carbon Column for Efficient Isomeric Separation of Permethylated Glycans. *Anal Chem* 2021; 93(12):5061-5070.
189. Veillon L, Huang Y, Peng W, Dong X, Cho BG, Mechref Y. Characterization of isomeric glycan structures by LC-MS/MS. *Electrophoresis* 2017; 38(17):2100-2114.
190. Schmid D, Behnke B, Metzger J, Kuhn R. Nano-HPLC-mass spectrometry and MEKC for the analysis of oligosaccharides from human milk. *Biomed Chromatogr* 2002; 16(2):151-156.
191. Wuhrer M, Deelder AM, Hokke CH. Protein glycosylation analysis by liquid chromatography-mass spectrometry. *J Chromatogr B Analyt Technol Biomed Life Sci* 2005; 825(2):124-133.
192. Kurz S, Sheikh MO, Lu S, Wells L, Tiemeyer M. Separation and Identification of Permethylated Glycan Isomers by Reversed Phase NanoLC-NSI-MS(n). *Mol Cell Proteomics* 2021; 20:100045.
193. Zhou S, Hu Y, Mechref Y. High-temperature LC-MS/MS of permethylated glycans derived from glycoproteins. *Electrophoresis* 2016; 37(11):1506-1513.
194. Porfirio S, Archer-Hartmann S, Moreau GB, Ramakrishnan G, Haque R, Kirkpatrick BD, et al. New strategies for profiling and characterization of human milk oligosaccharides. *Glycobiology* 2020; 30(10):774-786.
195. Wada Y, Azadi P, Costello CE, Dell A, Dwek RA, Geyer H, et al. Comparison of the methods for profiling glycoprotein glycans--HUPO Human Disease Glycomics/Proteome Initiative multi-institutional study. *Glycobiology* 2007; 17(4):411-422.
196. Costello CE, Contado-Miller JM, Cipollo JF. A glycomics platform for the analysis of permethylated oligosaccharide alditols. *J Am Soc Mass Spectrom* 2007; 18(10):1799-1812.
197. Banazadeh A, Veillon L, Wooding KM, Zabet-Moghaddam M, Mechref Y. Recent advances in mass spectrometric analysis of glycoproteins. *Electrophoresis* 2017; 38(1):162-189.
198. Ashwood C, Lin CH, Thaysen-Andersen M, Packer NH. Discrimination of Isomers of Released N- and O-Glycans Using Diagnostic Product Ions in Negative Ion PGC-LC-ESI-MS/MS. *J Am Soc Mass Spectrom* 2018; 29(6):1194-1209.
199. Marie AL, Ray S, Ivanov AR. Highly-sensitive label-free deep profiling of N-glycans released from biomedically-relevant samples. *Nat Commun* 2023; 14(1):1618.

200. Morelle W, Michalski JC. Analysis of protein glycosylation by mass spectrometry. *Nat Protoc* 2007; 2(7):1585-1602.
201. Guan Y, Zhang M, Gaikwad M, Voss H, Fazel R, Ansari S, et al. Correction to An Integrated Strategy Reveals Complex Glycosylation of Erythropoietin Using Mass Spectrometry. *J Proteome Res* 2022; 21(10):2552.
202. Neelamegham S, Aoki-Kinoshita K, Bolton E, Frank M, Lisacek F, Lütteke T, et al. Updates to the Symbol Nomenclature for Glycans guidelines. *Glycobiology* 2019; 29(9):620-624.
203. Mehta AY, Cummings RD. GlycoGlyph: a glycan visualizing, drawing and naming application. *Bioinformatics* 2020; 36(11):3613-3614.
204. Subramanian A, Tamayo P, Mootha VK, Mukherjee S, Ebert BL, Gillette MA, et al. Gene set enrichment analysis: a knowledge-based approach for interpreting genome-wide expression profiles. *Proc Natl Acad Sci U S A* 2005; 102(43):15545-15550.
205. Shannon P, Markiel A, Ozier O, Baliga NS, Wang JT, Ramage D, et al. Cytoscape: a software environment for integrated models of biomolecular interaction networks. *Genome Res* 2003; 13(11):2498-2504.
206. Merico D, Isserlin R, Stueker O, Emili A, Bader GD. Enrichment map: a network-based method for gene-set enrichment visualization and interpretation. *PLoS One* 2010; 5(11):e13984.
207. Kucera M, Isserlin R, Arkhangorodsky A, Bader GD. AutoAnnotate: A Cytoscape app for summarizing networks with semantic annotations. *F1000Res* 2016; 5:1717.
208. Colley KJ, Varki A, Haltiwanger RS, Kinoshita T. Cellular Organization of Glycosylation. In: *Essentials of Glycobiology*. Varki A, Cummings RD, Esko JD, et al. (editors). Cold Spring Harbor (NY): Cold Spring Harbor Laboratory Press Copyright © 2022 The Consortium of Glycobiology Editors, La Jolla, California; published by Cold Spring Harbor Laboratory Press; doi:10.1101/glycobiology.4e.4. All rights reserved.; 2022. pp. 43-52.
209. Esmail S, Manolson MF. Advances in understanding N-glycosylation structure, function, and regulation in health and disease. *Eur J Cell Biol* 2021; 100(7-8):151186.
210. Archer TC, Ehrenberger T, Mundt F, Gold MP, Krug K, Mah CK, et al. Proteomics, Post-translational Modifications, and Integrative Analyses Reveal Molecular Heterogeneity within Medulloblastoma Subgroups. *Cancer Cell* 2018; 34(3):396-410.e398.
211. Etxebarria J, Reichardt NC. Methods for the absolute quantification of N-glycan biomarkers. *Biochim Biophys Acta* 2016; 1860(8):1676-1687.
212. Szigeti M, Guttman A. Sample Preparation Scale-Up for Deep N-glycomic Analysis of Human Serum by Capillary Electrophoresis and CE-ESI-MS. *Mol Cell Proteomics* 2019; 18(12):2524-2531.
213. Wang X, Deng Z, Huang C, Zhu T, Lou J, Wang L, et al. Differential N-glycan patterns identified in lung adenocarcinoma by N-glycan profiling of formalin-fixed paraffin-embedded (FFPE) tissue sections. *J Proteomics* 2018; 172:1-10.
214. Hinneburg H, Korać P, Schirmeister F, Gasparov S, Seeberger PH, Zoldoš V, et al. Unlocking Cancer Glycomes from Histopathological Formalin-fixed and Paraffin-embedded (FFPE) Tissue Microdissections. *Mol Cell Proteomics* 2017; 16(4):524-536.
215. Gizaw ST, Ohashi T, Tanaka M, Hinou H, Nishimura S. Glycoblotting method allows for rapid and efficient glycome profiling of human Alzheimer's disease brain, serum and cerebrospinal fluid towards potential biomarker discovery. *Biochim Biophys Acta* 2016; 1860(8):1716-1727.
216. Barone R, Sturiale L, Palmigiano A, Zappia M, Garozzo D. Glycomics of pediatric and adulthood diseases of the central nervous system. *J Proteomics* 2012; 75(17):5123-5139.
217. Moh ES, Thaysen-Andersen M, Packer NH. Relative versus absolute quantitation in disease glycomics. *Proteomics Clin Appl* 2015; 9(3-4):368-382.

218. Everest-Dass AV, Abrahams JL, Kolarich D, Packer NH, Campbell MP. Structural features for distinguishing N- and O-linked glycan isomers by LC-ESI-IT MS/MS. *J Am Soc Mass Spectrom* 2013; 24(6):895-906.
219. Lau KS, Dennis JW. N-Glycans in cancer progression. *Glycobiology* 2008; 18(10):750-760.
220. Toustou C, Walet-Balieu ML, Kiefer-Meyer MC, Houdou M, Lerouge P, Foulquier F, et al. Towards understanding the extensive diversity of protein N-glycan structures in eukaryotes. *Biol Rev Camb Philos Soc* 2022; 97(2):732-748.
221. Lau KS, Partridge EA, Grigorian A, Silvescu CI, Reinhold VN, Demetriou M, et al. Complex N-glycan number and degree of branching cooperate to regulate cell proliferation and differentiation. *Cell* 2007; 129(1):123-134.
222. Williamson D, Schwalbe EC, Hicks D, Aldinger KA, Lindsey JC, Crosier S, et al. Medulloblastoma group 3 and 4 tumors comprise a clinically and biologically significant expression continuum reflecting human cerebellar development. *Cell Rep* 2022; 40(5):111162.
223. Morrish F, Isern N, Sadilek M, Jeffrey M, Hockenbery DM. c-Myc activates multiple metabolic networks to generate substrates for cell-cycle entry. *Oncogene* 2009; 28(27):2485-2491.
224. Northcott PA, Shih DJ, Remke M, Cho YJ, Kool M, Hawkins C, et al. Rapid, reliable, and reproducible molecular sub-grouping of clinical medulloblastoma samples. *Acta Neuropathol* 2012; 123(4):615-626.
225. Münger K, Pietenpol JA, Pittelkow MR, Holt JT, Moses HL. Transforming growth factor beta 1 regulation of c-myc expression, pRB phosphorylation, and cell cycle progression in keratinocytes. *Cell Growth Differ* 1992; 3(5):291-298.
226. Hinshaw DC, Hanna A, Lama-Sherpa T, Metge B, Kammerud SC, Benavides GA, et al. Hedgehog Signaling Regulates Metabolism and Polarization of Mammary Tumor-Associated Macrophages. *Cancer Res* 2021; 81(21):5425-5437.
227. Guo W, Roelink H. Loss of the Heparan Sulfate Proteoglycan Glypican5 Facilitates Long-Range Sonic Hedgehog Signaling. *Stem Cells* 2019; 37(7):899-909.
228. Boyaval F, Dalebout H, Van Zeijl R, Wang W, Fariña-Sarasqueta A, Lageveen-Kammeijer GSM, et al. High-Mannose N-Glycans as Malignant Progression Markers in Early-Stage Colorectal Cancer. *Cancers (Basel)* 2022; 14(6).
229. Varki A, Lowe JB. Biological Roles of Glycans. In: *Essentials of Glycobiology*. Varki A, Cummings RD, Esko JD, et al. (editors). Cold Spring Harbor (NY): Cold Spring Harbor Laboratory Press Copyright © 2009, The Consortium of Glycobiology Editors, La Jolla, California.; 2009.
230. Oh YJ, Dent MW, Freels AR, Zhou Q, Lebrilla CB, Merchant ML, et al. Antitumor activity of a lectin targeting cancer-associated high-mannose glycans. *Mol Ther* 2022; 30(4):1523-1535.
231. Liu Y, Han Y, Zhu W, Luo Q, Yuan J, Liu X. Characterization of N-glycome profile in mouse brain tissue regions by MALDI-TOF/MS. *Anal Bioanal Chem* 2023.
232. Kaprio T, Satomaa T, Heiskanen A, Hokke CH, Deelder AM, Mustonen H, et al. N-glycomic profiling as a tool to separate rectal adenomas from carcinomas. *Mol Cell Proteomics* 2015; 14(2):277-288.
233. Liu DR, Guan QL, Gao MT, Jiang L, Kang HX. Mannose receptor as a potential biomarker for gastric cancer: a pilot study. *Int J Biol Markers* 2017; 32(3):e278-e283.
234. Chen H, Deng Z, Huang C, Wu H, Zhao X, Li Y. Mass spectrometric profiling reveals association of N-glycan patterns with epithelial ovarian cancer progression. *Tumour Biol* 2017; 39(7):1010428317716249.

235. Gaunitz S, Tjernberg LO, Schedin-Weiss S. The N-glycan profile in cortex and hippocampus is altered in Alzheimer disease. *J Neurochem* 2021; 159(2):292-304.
236. Scott DA, Casadonte R, Cardinali B, Spruill L, Mehta AS, Carli F, et al. Increases in Tumor N-Glycan Polylactosamines Associated with Advanced HER2-Positive and Triple-Negative Breast Cancer Tissues. *Proteomics Clin Appl* 2019; 13(1):e1800014.
237. Hanahan D, Weinberg RA. Hallmarks of cancer: the next generation. *Cell* 2011; 144(5):646-674.
238. Gu J, Nishikawa A, Tsuruoka N, Ohno M, Yamaguchi N, Kangawa K, et al. Purification and characterization of UDP-N-acetylglucosamine: alpha-6-D-mannoside beta 1-6N-acetylglucosaminyltransferase (N-acetylglucosaminyltransferase V) from a human lung cancer cell line. *J Biochem* 1993; 113(5):614-619.
239. Schachter H. Biosynthetic controls that determine the branching and microheterogeneity of protein-bound oligosaccharides. *Biochem Cell Biol* 1986; 64(3):163-181.
240. van Bree N, Wilhelm M. The Tumor Microenvironment of Medulloblastoma: An Intricate Multicellular Network with Therapeutic Potential. *Cancers (Basel)* 2022; 14(20).
241. Fiorilli P, Partridge D, Staniszewska I, Wang JY, Grabacka M, So K, et al. Integrins mediate adhesion of medulloblastoma cells to tenascin and activate pathways associated with survival and proliferation. *Lab Invest* 2008; 88(11):1143-1156.
242. Chen C, Wang S, Gadi MR, Zhu H, Liu F, Liu CC, et al. Enzymatic modular synthesis and microarray assay of poly-N-acetylglucosamine derivatives. *Chem Commun (Camb)* 2020; 56(55):7549-7552.
243. Lu CH, Wu WY, Lai YJ, Yang CM, Yu LC. Suppression of B3GNT7 gene expression in colon adenocarcinoma and its potential effect in the metastasis of colon cancer cells. *Glycobiology* 2014; 24(4):359-367.
244. Oliveira-Ferrer L, Legler K, Milde-Langosch K. Role of protein glycosylation in cancer metastasis. *Semin Cancer Biol* 2017; 44:141-152.
245. Krishnan V, Bane SM, Kawle PD, Naresh KN, Kalraiya RD. Altered melanoma cell surface glycosylation mediates organ specific adhesion and metastasis via lectin receptors on the lung vascular endothelium. *Clin Exp Metastasis* 2005; 22(1):11-24.
246. Cachia D, Eskandari R, McDonald DG, Infinger LK, III WAV, Varma AK, et al. Low-dose radiation followed by on-target inhibition of Galectin-3 in combination with anti-4-1BB monoclonal antibody regulates immune responses in Group 3 and Group 4 medulloblastoma mouse model (P11-13.001). *Neurology* 2023; 100(17 Supplement 2):3857.
247. Guo HB, Johnson H, Randolph M, Nagy T, Blalock R, Pierce M. Specific posttranslational modification regulates early events in mammary carcinoma formation. *Proc Natl Acad Sci U S A* 2010; 107(49):21116-21121.
248. Heijs B, Holst-Bernal S, de Graaff MA, Briaire-de Bruijn IH, Rodriguez-Girondo M, van de Sande MAJ, et al. Molecular signatures of tumor progression in myxoid liposarcoma identified by N-glycan mass spectrometry imaging. *Lab Invest* 2020; 100(9):1252-1261.
249. Partridge EA, Le Roy C, Di Guglielmo GM, Pawling J, Cheung P, Granovsky M, et al. Regulation of cytokine receptors by Golgi N-glycan processing and endocytosis. *Science* 2004; 306(5693):120-124.
250. Hirabayashi J, Hashidate T, Arata Y, Nishi N, Nakamura T, Hirashima M, et al. Oligosaccharide specificity of galectins: a search by frontal affinity chromatography. *Biochim Biophys Acta* 2002; 1572(2-3):232-254.
251. Veillon L, Fakih C, Abou-El-Hassan H, Kobeissy F, Mechref Y. Glycosylation Changes in Brain Cancer. *ACS Chem Neurosci* 2018; 9(1):51-72.
252. Nangia-Makker P, Conklin J, Hogan V, Raz A. Carbohydrate-binding proteins in cancer, and their ligands as therapeutic agents. *Trends Mol Med* 2002; 8(4):187-192.

253. Liu YC, Yen HY, Chen CY, Chen CH, Cheng PF, Juan YH, et al. Sialylation and fucosylation of epidermal growth factor receptor suppress its dimerization and activation in lung cancer cells. *Proc Natl Acad Sci U S A* 2011; 108(28):11332-11337.
254. De Vellis C, Pietrobono S, Stecca B. The Role of Glycosylation in Melanoma Progression. *Cells* 2021; 10(8).
255. Gao Z, Xu M, Yue S, Shan H, Xia J, Jiang J, et al. Abnormal sialylation and fucosylation of saliva glycoproteins: Characteristics of lung cancer-specific biomarkers. *Curr Res Pharmacol Drug Discov* 2022; 3:100079.
256. Saldova R, Fan Y, Fitzpatrick JM, Watson RW, Rudd PM. Core fucosylation and alpha2-3 sialylation in serum N-glycome is significantly increased in prostate cancer comparing to benign prostate hyperplasia. *Glycobiology* 2011; 21(2):195-205.
257. Schnaar RL, Gerardy-Schahn R, Hildebrandt H. Sialic acids in the brain: gangliosides and polysialic acid in nervous system development, stability, disease, and regeneration. *Physiol Rev* 2014; 94(2):461-518.
258. Li F, Ding J. Sialylation is involved in cell fate decision during development, reprogramming and cancer progression. *Protein Cell* 2019; 10(8):550-565.
259. Bhide GP, Colley KJ. Sialylation of N-glycans: mechanism, cellular compartmentalization and function. *Histochem Cell Biol* 2017; 147(2):149-174.
260. Miyagi T, Takahashi K, Hata K, Shiozaki K, Yamaguchi K. Sialidase significance for cancer progression. *Glycoconj J* 2012; 29(8-9):567-577.
261. Büll C, Stoel MA, den Brok MH, Adema GJ. Sialic acids sweeten a tumor's life. *Cancer Res* 2014; 74(12):3199-3204.
262. Seales EC, Jurado GA, Singhal A, Bellis SL. Ras oncogene directs expression of a differentially sialylated, functionally altered beta1 integrin. *Oncogene* 2003; 22(46):7137-7145.
263. Sakuma K, Aoki M, Kannagi R. Transcription factors c-Myc and CDX2 mediate E-selectin ligand expression in colon cancer cells undergoing EGF/bFGF-induced epithelial-mesenchymal transition. *Proc Natl Acad Sci U S A* 2012; 109(20):7776-7781.
264. Okun S, Peek A, Igdoura SA. Neuraminidase 4 (NEU4): new biological and physiological player. *Glycobiology* 2023; 33(3):182-187.
265. Yoshizumi S, Suzuki S, Hirai M, Hinokio Y, Yamada T, Yamada T, et al. Increased hepatic expression of ganglioside-specific sialidase, NEU3, improves insulin sensitivity and glucose tolerance in mice. *Metabolism* 2007; 56(3):420-429.
266. Yang H, Lu L, Chen X. An overview and future prospects of sialic acids. *Biotechnol Adv* 2021; 46:107678.
267. Dobie C, Skropeta D. Insights into the role of sialylation in cancer progression and metastasis. *Br J Cancer* 2021; 124(1):76-90.
268. Macauley MS, Crocker PR, Paulson JC. Siglec-mediated regulation of immune cell function in disease. *Nat Rev Immunol* 2014; 14(10):653-666.
269. Rambaruth ND, Dwek MV. Cell surface glycan-lectin interactions in tumor metastasis. *Acta Histochem* 2011; 113(6):591-600.
270. van de Wall S, Santegoets KCM, van Houtum EJH, Büll C, Adema GJ. Sialoglycans and Siglecs Can Shape the Tumor Immune Microenvironment. *Trends Immunol* 2020; 41(4):274-285.
271. Barkal AA, Brewer RE, Markovic M, Kowarsky M, Barkal SA, Zaro BW, et al. CD24 signalling through macrophage Siglec-10 is a target for cancer immunotherapy. *Nature* 2019; 572(7769):392-396.
272. Jia L, Zhang J, Ma T, Guo Y, Yu Y, Cui J. The Function of Fucosylation in Progression of Lung Cancer. *Front Oncol* 2018; 8:565.
273. Becker DJ, Lowe JB. Fucose: biosynthesis and biological function in mammals. *Glycobiology* 2003; 13(7):41r-53r.

274. Vestweber D, Blanks JE. Mechanisms that regulate the function of the selectins and their ligands. *Physiol Rev* 1999; 79(1):181-213.
275. Kossowska B, Ferens-Sieczkowska M, Gancarz R, Passowicz-Muszyńska E, Jankowska R. Fucosylation of serum glycoproteins in lung cancer patients. *Clin Chem Lab Med* 2005; 43(4):361-369.
276. Shan M, Yang D, Dou H, Zhang L. Fucosylation in cancer biology and its clinical applications. *Prog Mol Biol Transl Sci* 2019; 162:93-119.
277. Christiansen MN, Chik J, Lee L, Anugraham M, Abrahams JL, Packer NH. Cell surface protein glycosylation in cancer. *Proteomics* 2014; 14(4-5):525-546.
278. Nakagoe T, Sawai T, Tsuji T, Jibiki M, Nanashima A, Yamaguchi H, et al. Circulating sialyl Lewis(x), sialyl Lewis(a), and sialyl Tn antigens in colorectal cancer patients: multivariate analysis of predictive factors for serum antigen levels. *J Gastroenterol* 2001; 36(3):166-172.
279. Konno A, Hoshino Y, Terashima S, Motoki R, Kawaguchi T. Carbohydrate expression profile of colorectal cancer cells is relevant to metastatic pattern and prognosis. *Clin Exp Metastasis* 2002; 19(1):61-70.
280. Albuquerque APB, Balmaña M, Mereiter S, Pinto F, Reis CA, Beltrão EIC. Hypoxia and serum deprivation induces glycan alterations in triple negative breast cancer cells. *Biol Chem* 2018; 399(7):661-672.
281. Vajaria BN, Patel PS. Glycosylation: a hallmark of cancer? *Glycoconj J* 2017; 34(2):147-156.
282. Li D, Mallory T, Satomura S. AFP-L3: a new generation of tumor marker for hepatocellular carcinoma. *Clin Chim Acta* 2001; 313(1-2):15-19.
283. Aoyagi Y, Isemura M, Yosizawa Z, Suzuki Y, Sekine C, Ono T, et al. Fucosylation of serum alpha-fetoprotein in patients with primary hepatocellular carcinoma. *Biochim Biophys Acta* 1985; 830(3):217-223.
284. Miyoshi E, Noda K, Yamaguchi Y, Inoue S, Ikeda Y, Wang W, et al. The alpha1-6-fucosyltransferase gene and its biological significance. *Biochim Biophys Acta* 1999; 1473(1):9-20.
285. Aoyagi Y, Saitoh A, Suzuki Y, Igarashi K, Oguro M, Yokota T, et al. Fucosylation index of alpha-fetoprotein, a possible aid in the early recognition of hepatocellular carcinoma in patients with cirrhosis. *Hepatology* 1993; 17(1):50-52.
286. Wang W, Okajima T, Takeuchi H. Significant Roles of Notch O-Glycosylation in Cancer. *Molecules* 2022; 27(6).
287. Huang Y, Zhang HL, Li ZL, Du T, Chen YH, Wang Y, et al. FUT8-mediated aberrant N-glycosylation of B7H3 suppresses the immune response in triple-negative breast cancer. *Nat Commun* 2021; 12(1):2672.
288. Fujita K, Hatano K, Hashimoto M, Tomiyama E, Miyoshi E, Nonomura N, et al. Fucosylation in Urological Cancers. *Int J Mol Sci* 2021; 22(24).
289. Kajiwara H, Yasuda M, Kumaki N, Shibayama T, Osamura Y. Expression of carbohydrate antigens (SSEA-1, sialyl-Lewis X, DU-PAN-2 and CA19-9) and E-selectin in urothelial carcinoma of the renal pelvis, ureter, and urinary bladder. *Tokai J Exp Clin Med* 2005; 30(3):177-182.
290. Lee SH, Jeong S, Lee J, Yeo IS, Oh MJ, Kim U, et al. Glycomic profiling of targeted serum haptoglobin for gastric cancer using nano LC/MS and LC/MS/MS. *Mol Biosyst* 2016; 12(12):3611-3621.
291. Magnani JL. The discovery, biology, and drug development of sialyl Lea and sialyl Lex. *Arch Biochem Biophys* 2004; 426(2):122-131.
292. Kannagi R, Izawa M, Koike T, Miyazaki K, Kimura N. Carbohydrate-mediated cell adhesion in cancer metastasis and angiogenesis. *Cancer Sci* 2004; 95(5):377-384.

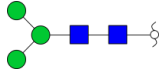
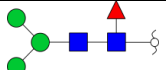
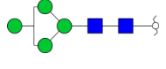
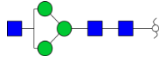
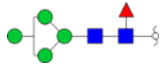
293. Kolben T, Müller L, Meister S, Keilmann L, Buschmann C, Trillsch F, et al. Blood group antigens SLeX, SLeA, and LeY as prognostic markers in endometrial cancer. *J Cancer Res Clin Oncol* 2022; 148(12):3323-3335.
294. Zwenger A, Rabassa M, Demichelis S, Grossman G, Segal-Eiras A, Croce MV. High expression of sLex associated with poor survival in Argentinian colorectal cancer patients. *Int J Biol Markers* 2014; 29(1):e30-39.



## 7. Supplemental material

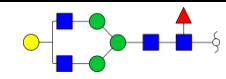
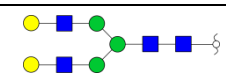

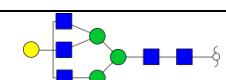



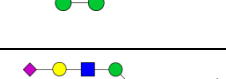


### S1 The identified 302 N-glycans from medulloblastoma patients at MS1 and MS2 levels.

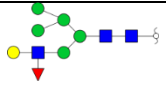
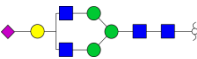
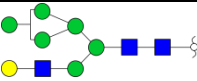
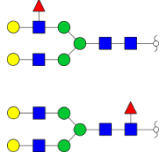
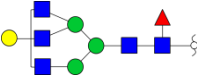
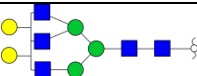
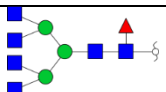
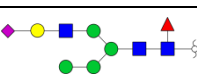
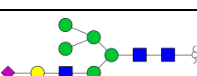
N-glycan composition is abbreviated as Neu5AcHexNAcHexFucNeuAc, Neu5Ac is an N-Acetylneuraminic acid monosaccharide, HexNAc is an N-Acetylglucosamine monosaccharide, Hex is mannose and galactose monosaccharides, Fuc is a fucose monosaccharide and Red-HexNAc is reduced N-Acetylglucosamine. Sugar code: Neu5Ac\_HexNAc\_Hex\_Fuc\_red-HexNAc.

No.	N-glycan composition	Preferred N-glycan structures	Permethylation monoisotopic Mw		Deviation(ppm)	m/z	Charge
			Experiment	Theory			
1	HexNAc <sub>1</sub> Hex <sub>3</sub> Red-HexNAc <sub>1</sub>		1164.6243	1164.6251	0.70	1165.6316	1
2	HexNAc <sub>1</sub> Hex <sub>3</sub> Fuc <sub>1</sub> Red-HexNAc <sub>1</sub>		1338.7142	1338.7143	0.1	1339.7214	1
3	HexNAc <sub>1</sub> Hex <sub>4</sub> Red-HexNAc <sub>1</sub>		1368.727	1368.7249	1.54	1369.7343	1
4	HexNAc <sub>2</sub> Hex <sub>3</sub> Red-HexNAc <sub>1</sub>		1409.7503	1409.7515	0.81	705.88245	2
5	HexNAc <sub>1</sub> Hex <sub>4</sub> Fuc <sub>1</sub> Red-HexNAc <sub>1</sub>		1542.8125	1542.8141	1.04	772.41355	2

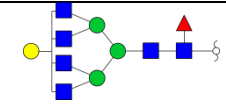
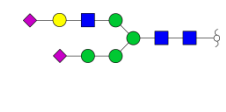
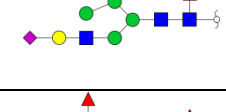
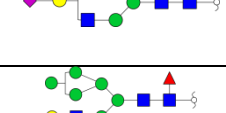
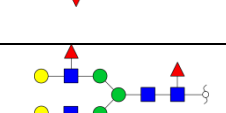
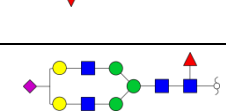
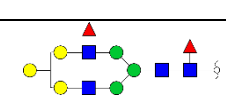
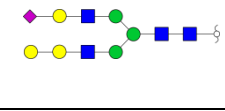

6	HexNAc <sub>1</sub> Hex <sub>5</sub> Red-HexNAc <sub>1</sub>		1572.8258	1572.8247	0.72	787.42018	2
7	HexNAc <sub>2</sub> Hex <sub>3</sub> Fuc <sub>1</sub> Red-HexNAc <sub>1</sub>		1583.8393	1583.8392	0.85	792.92694	2
8	HexNAc <sub>2</sub> Hex <sub>4</sub> Red-HexNAc <sub>1</sub>		1613.8499	1613.8505	0.81	807.93224	2
9	HexNAc <sub>3</sub> Hex <sub>3</sub> Red-HexNAc <sub>1</sub>		1654.8772	1654.8778	0.34	828.44587	2
10	HexNAc <sub>1</sub> Hex <sub>5</sub> Fuc <sub>1</sub> Red-HexNAc <sub>1</sub>		1746.9132	1746.9136	0.38	874.46388	2
11	Neu5Ac <sub>1</sub> HexNAc <sub>2</sub> Hex <sub>3</sub> Red-HexNAc <sub>1</sub>		1770.9241	1770.9251	0.56	886.46933	2
12	HexNAc <sub>1</sub> Hex <sub>6</sub> Red-HexNAc <sub>1</sub>		1776.9227	1776.9245	0.97	889.46861	2
13	HexNAc <sub>2</sub> Hex <sub>4</sub> Fuc <sub>1</sub> Red-HexNAc <sub>1</sub>		1787.9389	1787.9404	0.85	894.97674	2
14	HexNAc <sub>2</sub> Hex <sub>5</sub> Red-HexNAc <sub>1</sub>		1817.9498	1817.9510	0.65	909.98215	2
15	HexNAc <sub>3</sub> Hex <sub>3</sub> Fuc <sub>1</sub> Red-HexNAc <sub>1</sub>		1828.9671	1828.9670	0.07	915.49083	2

16	HexNAc <sub>3</sub> Hex <sub>4</sub> Red-HexNAc <sub>1</sub>		1858.9734	1858.9776	0.82	930.49399	2
17	HexNAc <sub>4</sub> Hex <sub>3</sub> Red-HexNAc <sub>1</sub>		1900.0019	1900.0041	1.15	951.00823	2
18	Neu5Ac <sub>1</sub> HexNAc <sub>2</sub> Hex <sub>3</sub> Fuc <sub>1</sub> Red-HexNAc <sub>1</sub>		1945.0127	1945.0143	0.83	973.51364	2
19	HexNAc <sub>1</sub> Hex <sub>6</sub> Fuc <sub>1</sub> Red-HexNAc <sub>1</sub>		1951.0126	1951.0137	0.53	976.51359	2
20	Neu5Ac <sub>1</sub> HexNAc <sub>2</sub> Hex <sub>4</sub> Red-HeNAc <sub>1</sub>		1975.0232	1975.0249	0.84	988.51886	2
21	HexNAc <sub>1</sub> Hex <sub>7</sub> Red-HexNAc <sub>1</sub>		1981.024	1981.0242	0.10	991.5193	2
22	HexNAc <sub>2</sub> Hex <sub>5</sub> Fuc <sub>1</sub> Red-HexNAc <sub>1</sub>		1992.0391	1992.0402	0.55	997.0268	2
23	HexNAc <sub>2</sub> Hex <sub>6</sub> Red-HexNAc <sub>1</sub>		2022.0477	2022.0508	1.5	1012.0311	2

24	HexNAc <sub>3</sub> Hex <sub>4</sub> Fuc <sub>1</sub> Red-HexNAc <sub>1</sub>		2033.0652	2033.0668	0.76	1017.5399	2
25	HexNAc <sub>3</sub> Hex <sub>5</sub> Red-HexNAc <sub>1</sub>		2063.0787	2063.0773	0.68	1032.5466	2
26	HexNAc <sub>4</sub> Hex <sub>3</sub> Fuc <sub>1</sub> Red-HexNAc <sub>1</sub>		2074.0933	2074.0933	0.00	1038.0539	2
27	HexNAc <sub>4</sub> Hex <sub>4</sub> Red-HexNAc <sub>1</sub>		2104.1018	2104.1039	0.97	1053.0582	2
28	HexNAc <sub>5</sub> Hex <sub>3</sub> Red-HexNAc <sub>1</sub>		2145.1269	2145.1304	1.63	1073.5707	2
29	Neu5Ac <sub>1</sub> HexNAc <sub>2</sub> Hex <sub>4</sub> Fuc <sub>1</sub> Red-HexNAc <sub>1</sub>		2149.1109	2149.1141	1.48	1075.5627	2
30	HexNAc <sub>2</sub> Hex <sub>5</sub> Fuc <sub>2</sub> Red-HexNAc <sub>1</sub>		2166.1369	2166.1294	2.35	1084.0757	2
31	Neu5Ac <sub>1</sub> HexNAc <sub>2</sub> Hex <sub>5</sub> Red-HexNAc <sub>1</sub>		2179.1231	2179.1247	0.71	1090.5688	2
32	HexNAc <sub>1</sub> Hex <sub>8</sub> Red-HexNAc <sub>1</sub>		2185.1217	2185.1240	1.04	1093.5681	2
33	HexNAc <sub>2</sub> Hex <sub>6</sub> Fuc <sub>1</sub> Red-HexNAc <sub>1</sub>		2196.1378	2196.1400	0.98	1099.0762	2

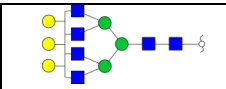
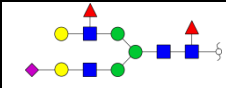
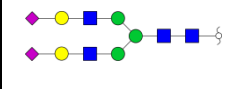
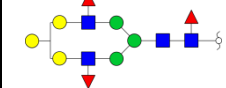
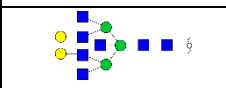
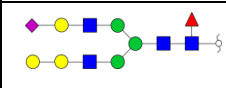
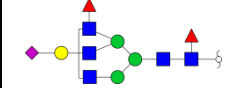
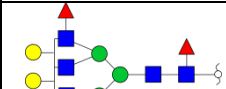

							
34	Neu5Ac <sub>1</sub> HexNAc <sub>3</sub> Hex <sub>4</sub> Red-HexNAc <sub>1</sub>		2220.1502	2220.1512	0.40	1111.0824	2
35	HexNAc <sub>2</sub> Hex <sub>7</sub> Red-HexNAc <sub>1</sub>		2226.1481	2226.1505	1.09	1114.0813	2
36	HexNAc <sub>3</sub> Hex <sub>5</sub> Fuc <sub>1</sub> Red-HexNAc <sub>1</sub>		2237.1616	2237.1665	0.14	1119.5904	2
37	HexNAc <sub>4</sub> Hex <sub>4</sub> Fuc <sub>1</sub> Red-HexNAc <sub>1</sub>		2278.1929	2278.1931	0.07	1140.1037	2
38	HexNAc <sub>4</sub> Hex <sub>5</sub> Red-HexNAc <sub>1</sub>		2308.2016	2308.2036	0.87	1155.1081	2
39	HexNAc <sub>5</sub> Hex <sub>3</sub> Fuc <sub>1</sub> Red-HexNAc <sub>1</sub>		2319.218	2319.2196	0.69	774.07995	3
40	Neu5Ac <sub>1</sub> HexNAc <sub>2</sub> Hex <sub>5</sub> Fuc <sub>1</sub> Red-HexNAc <sub>1</sub>		2353.2121	2353.2139	0.74	1177.6133	2
41	Neu5Ac <sub>1</sub> HexNAc <sub>2</sub> Hex <sub>6</sub> Red-HexNAc <sub>1</sub>		2383.2231	2383.2244	0.55	1192.6188	2

42	HexNAc <sub>1</sub> Hex <sub>9</sub> Red-HexNAc <sub>1</sub>		2389.2216	2389.2238	0.89	1195.6181	2
43	Neu5Ac <sub>1</sub> HexNAc <sub>3</sub> Hex <sub>4</sub> Fuc <sub>1</sub> Red-HexNAc <sub>1</sub>		2394.2378	2394.2404	1.08	799.08655	3
44	HexNAc <sub>2</sub> Hex <sub>7</sub> Fuc <sub>1</sub> Red-HexNAc <sub>1</sub>		2400.2488	2400.2398	3.78	1201.1317	2
45	HexNAc <sub>3</sub> Hex <sub>5</sub> Fuc <sub>2</sub> Red-HexNAc <sub>1</sub>		2411.2511	2411.2557	1.92	1206.6328	2
46	Neu5Ac <sub>1</sub> HexNAc <sub>3</sub> Hex <sub>5</sub> Red-HexNAc <sub>1</sub>		2424.2486	2424.2510	0.97	809.09016	3
47	HexNAc <sub>3</sub> Hex <sub>6</sub> Fuc <sub>1</sub> Red-HexNAc <sub>1</sub>		2441.2664	2441.2663	0.05	814.76565	3
48	HexNAc <sub>4</sub> Hex <sub>5</sub> Fuc <sub>1</sub> Red-HexNAc <sub>1</sub>		2482.2909	2482.2929	0.78	828.43757	3
49	HexNAc <sub>5</sub> Hex <sub>3</sub> Fuc <sub>2</sub> Red-HexNAc <sub>1</sub>		2493.2706	2493.3088	0.73	1247.6426	2
50	Neu5Ac <sub>2</sub> HexNAc <sub>2</sub> Hex <sub>4</sub> Fuc <sub>1</sub> Red-HexNAc <sub>1</sub>		2510.2953	2510.2878	3.01	837.77237	3

51	HexNAc <sub>5</sub> Hex <sub>4</sub> Fuc <sub>1</sub> Red-HexNAc <sub>1</sub>		2523.3185	2523.3194	0.35	842.11294	3
52	Neu5Ac <sub>2</sub> HexNAc <sub>2</sub> Hex <sub>5</sub> Red-HexNAc <sub>1</sub>		2540.2973	2540.2983	0.39	847.77304	3
53	Neu5Ac <sub>1</sub> HexNAc <sub>2</sub> Hex <sub>6</sub> Fuc <sub>1</sub> Red-HexNAc <sub>1</sub>		2557.3137	2557.3137	0.03	1279.6641	2
54	Neu5Ac <sub>1</sub> HexNAc <sub>3</sub> Hex <sub>4</sub> Fuc <sub>2</sub> Red-HexNAc <sub>1</sub>		2568.3253	2568.3296	1.68	857.11572	3
55	HexNAc <sub>2</sub> Hex <sub>7</sub> Fuc <sub>2</sub> Red-HexNAc <sub>1</sub>		2574.3376	2574.329	3.36	859.11983	3
56	HexNAc <sub>3</sub> Hex <sub>5</sub> Fuc <sub>3</sub> Red-HexNAc <sub>1</sub>		2585.3322	2585.3450	2.33	1293.6734	2
57	Neu5Ac <sub>1</sub> HexNAc <sub>3</sub> Hex <sub>5</sub> Fuc <sub>1</sub> Red-HexNAc <sub>1</sub>		2598.3399	2598.3402	0.10	867.12059	3
58	HexNAc <sub>3</sub> Hex <sub>6</sub> Fuc <sub>2</sub> Red-HexNAc <sub>1</sub>		2615.3633	2615.3555	2.98	872.79504	3
59	Neu5Ac <sub>1</sub> HexNAc <sub>3</sub> Hex <sub>6</sub> Red-HexNAc <sub>1</sub>		2628.3506	2628.3508	0.049	877.12356	3

60	HexNAc <sub>7</sub> Hex <sub>3</sub> Red-HexNAc <sub>1</sub>		2635.3777	2635.3831	2.03	879.46651	3
61	Neu5Ac <sub>1</sub> HexNAc <sub>4</sub> Hex <sub>4</sub> Fuc <sub>1</sub> Red-HexNAc <sub>1</sub>		2639.3667	2639.3667	0.01	880.7955	3
62	HexNAc <sub>4</sub> Hex <sub>5</sub> Fuc <sub>2</sub> Red-HexNAc <sub>1</sub>		2656.3821	2656.3821	0.02	886.46745	3
63	Neu5Ac <sub>1</sub> HexNAc <sub>4</sub> Hex <sub>5</sub> Red-HexNAc <sub>1</sub>		2669.3764	2669.3773	0.33	890.79941	3
64	HexNAc <sub>5</sub> Hex <sub>4</sub> Fuc <sub>2</sub> Red-HexNAc <sub>1</sub>		2697.3719	2697.4086	0.11	1349.6932	2
65	Neu5Ac <sub>2</sub> HexNAc <sub>2</sub> Hex <sub>5</sub> Fuc <sub>1</sub> Red-HexNAc <sub>1</sub>		2714.3946	2714.3875	2.61	905.80548	3
66	HexNAc <sub>5</sub> Hex <sub>5</sub> Fuc <sub>1</sub> Red-HexNAc <sub>1</sub>		2727.4189	2727.4192	0.09	910.14692	3
67	Neu5Ac <sub>1</sub> HexNAc <sub>2</sub> Hex <sub>6</sub> Fuc <sub>2</sub> Red-HexNAc <sub>1</sub>		2731.4046	2731.4029	0.65	911.47547	3
68	Neu5Ac <sub>2</sub> HexNAc <sub>3</sub> Hex <sub>4</sub> Fuc <sub>1</sub> Red-HexNAc <sub>1</sub>		2755.4105	2755.4141	1.29	919.47745	3



69	HexNAc <sub>5</sub> Hex <sub>6</sub> Red-HexNAc <sub>1</sub>		2757.4289	2757.4297	0.29	920.15025	3
70	Neu5Ac <sub>1</sub> HexNAc <sub>3</sub> Hex <sub>5</sub> Fuc <sub>2</sub> Red-HexNAc <sub>1</sub>		2772.426	2772.4294	1.22	925.14927	3
71	Neu5Ac <sub>2</sub> HexNAc <sub>3</sub> Hex <sub>5</sub> Red-HexNAc <sub>1</sub>		2785.4237	2785.4247	0.33	929.48184	3
72	HexNAc <sub>3</sub> Hex <sub>6</sub> Fuc <sub>3</sub> Red-HexNAc <sub>1</sub>		2789.4367	2789.4447	2.87	930.81952	3
73	HexNAc <sub>6</sub> Hex <sub>5</sub> Red-HexNAc <sub>1</sub>		2798.4564	2798.4563	0.05	933.82608	3
74	Neu5Ac <sub>1</sub> HexNAc <sub>3</sub> Hex <sub>6</sub> Fuc <sub>1</sub> Red-HexNAc <sub>1</sub>		2802.4449	2802.4400	1.77	935.15557	3
75	Neu5Ac <sub>1</sub> HexNAc <sub>4</sub> Hex <sub>4</sub> Fuc <sub>2</sub> Red-HexNAc <sub>1</sub>		2813.46	2813.4560	1.45	938.82729	3
76	HexNAc <sub>4</sub> Hex <sub>5</sub> Fuc <sub>3</sub> Red-HexNAc <sub>1</sub>		2830.47	2830.4713	0.44	944.49727	3
77	Neu5Ac <sub>1</sub> HexNAc <sub>4</sub> Hex <sub>5</sub> Fuc <sub>1</sub> Red-HexNAc <sub>1</sub>		2843.4649	2843.4665	0.56	948.8289	3

78	HexNAc <sub>4</sub> Hex <sub>6</sub> Fuc <sub>2</sub> Red-HexNAc <sub>1</sub>		2860.4877	2860.4818	2.06	954.50318	3
79	Neu5Ac <sub>1</sub> HexNAc <sub>4</sub> Hex <sub>6</sub> Red-HexNAc <sub>1</sub>		2873.4742	2873.4763	0.99	958.83202	3
80	Neu5Ac <sub>1</sub> HexNAc <sub>5</sub> Hex <sub>4</sub> Fuc <sub>1</sub> Red-HexNAc <sub>1</sub>		2884.4936	2884.4904	0.19	962.50516	3
81	HexNAc <sub>5</sub> Hex <sub>5</sub> Fuc <sub>2</sub> Red-HexNAc <sub>1</sub>		2901.505	2901.5084	1.16	968.1756	3
82	Neu5Ac <sub>2</sub> HexNAc <sub>3</sub> Hex <sub>4</sub> Fuc <sub>2</sub> Red-HexNAc <sub>1</sub>		2929.5021	2929.5033	0.40	977.50797	3
83	HexNAc <sub>5</sub> Hex <sub>6</sub> Fuc <sub>1</sub> Red-HexNAc <sub>1</sub>		2931.5154	2931.5190	1.20	978.17909	3
84	Neu5Ac <sub>2</sub> HexNAc <sub>3</sub> Hex <sub>5</sub> Fuc <sub>1</sub> Red-HexNAc <sub>1</sub>		2959.5127	2959.5139	0.38	987.5115	3
85	HexNAc <sub>5</sub> Hex <sub>7</sub> Red-HexNAc <sub>1</sub>		2961.5216	2961.5295	2.66	988.18113	3

86	HexNAc <sub>6</sub> Hex <sub>5</sub> Fuc <sub>1</sub> Red-HexNAc <sub>1</sub>		2972.5456	2972.5455	0.04	991.85581	3
87	Neu5Ac <sub>1</sub> HexNAc <sub>3</sub> Hex <sub>6</sub> Fuc <sub>2</sub> Red-HexNAc <sub>1</sub>		2976.532	2976.5292	0.96	993.1846	3
88	Neu5Ac <sub>2</sub> HexNAc <sub>3</sub> Hex <sub>6</sub> Red-HexNAc <sub>1</sub>		2989.521	2989.5244	1.13	997.51429	3
89	Neu5Ac <sub>2</sub> HexNAc <sub>4</sub> Hex <sub>4</sub> Fuc <sub>1</sub> Red-HexNAc <sub>1</sub>		3000.5371	3000.5404	1.09	1001.1863	3
90	Neu5Ac <sub>1</sub> HexNAc <sub>4</sub> Hex <sub>5</sub> Fuc <sub>2</sub> Red-HexNAc <sub>1</sub>		3017.5516	3017.5557	1.36	1006.8578	3
91	HexNAc <sub>4</sub> Hex <sub>6</sub> Fuc <sub>3</sub> Red-HexNAc <sub>1</sub>		3034.5641	3034.5710	2.28	1012.5287	3
92	Neu5Ac <sub>1</sub> HexNAc <sub>4</sub> Hex <sub>6</sub> Fuc <sub>1</sub> Red-HexNAc <sub>1</sub>		3047.5665	3047.5663	0.08	1016.8628	3
93	HexNAc <sub>4</sub> Hex <sub>7</sub> Fuc <sub>2</sub> Red-HexNAc <sub>1</sub>		3064.5889	3064.5816	2.39	1022.5369	3
94	Neu5Ac <sub>1</sub> HexNAc <sub>5</sub> Hex <sub>5</sub> Fuc <sub>1</sub> Red-HexNAc <sub>1</sub>		3088.5914	3088.5928	0.46	1030.5377	3

95	HexNAc <sub>5</sub> Hex <sub>6</sub> Fuc <sub>2</sub> Red-HexNAc <sub>1</sub>		3105.6159	3105.6082	2.50	1036.2126	3
96	Neu5Ac <sub>2</sub> HexNAc <sub>3</sub> Hex <sub>5</sub> Fuc <sub>2</sub> Red-HexNAc <sub>1</sub>		3133.6027	3133.6031	0.11	1045.5415	3
97	HexNAc <sub>5</sub> Hex <sub>7</sub> Fuc <sub>1</sub> Red-HexNAc <sub>1</sub>		3135.6216	3135.6187	0.93	1046.2145	3
98	Neu5Ac <sub>1</sub> HexNAc <sub>3</sub> Hex <sub>6</sub> Fuc <sub>3</sub> Red-HexNAc <sub>1</sub>		3150.6247	3150.6184	2.01	1051.2155	3
99	Neu5Ac <sub>2</sub> HexNAc <sub>3</sub> Hex <sub>6</sub> Fuc <sub>1</sub> Red-HexNAc <sub>1</sub>		3163.6094	3163.6136	1.33	1055.5437	3
100	Neu5Ac <sub>2</sub> HexNAc <sub>4</sub> Hex <sub>5</sub> Fuc <sub>1</sub> Red-HexNAc <sub>1</sub>		3204.6364	3204.6402	1.17	1069.2194	3
101	Neu5Ac <sub>1</sub> HexNAc <sub>4</sub> Hex <sub>6</sub> Fuc <sub>2</sub> Red-HexNAc <sub>1</sub>		3221.653	3221.6555	0.77	1074.8916	3
102	Neu5Ac <sub>2</sub> HexNAc <sub>4</sub> Hex <sub>6</sub> Red-HexNAc <sub>1</sub>		3234.6525	3234.6508	0.55	1079.2248	3
103	HexNAc <sub>4</sub> Hex <sub>7</sub> Fuc <sub>3</sub> Red-HexNAc <sub>1</sub>		3238.6762	3238.6708	1.67	1080.566	3

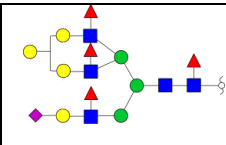
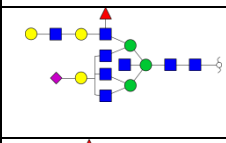
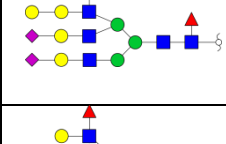
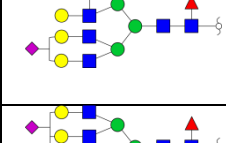
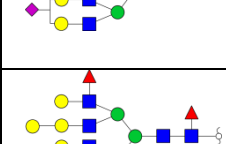
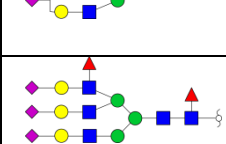
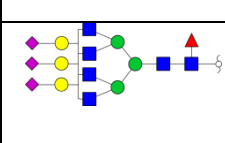

104	HexNAc <sub>7</sub> Hex <sub>6</sub> Red-HexNAc <sub>1</sub>		3247.6825	3247.6824	0.045	1083.5681	3
105	Neu5Ac <sub>1</sub> HexNAc <sub>4</sub> Hex <sub>7</sub> Fuc <sub>1</sub> Red-HexNAc <sub>1</sub>		3251.6758	3251.6661	3.00	1084.8992	3
106	Neu5Ac <sub>1</sub> HexNAc <sub>5</sub> Hex <sub>5</sub> Fuc <sub>2</sub> Red-HexNAc <sub>1</sub>		3262.6794	3262.6821	0.80	1088.5671	3
107	Neu5Ac <sub>1</sub> HexNAc <sub>5</sub> Hex <sub>6</sub> Fuc <sub>1</sub> Red-HexNAc <sub>1</sub>		3292.6897	3292.6926	0.87	1098.5705	3
108	Neu5Ac <sub>2</sub> HexNAc <sub>3</sub> Hex <sub>5</sub> Fuc <sub>3</sub> Red-HexNAc <sub>1</sub>		3307.6862	3307.6923	1.83	1103.5693	3
109	HexNAc <sub>5</sub> Hex <sub>7</sub> Fuc <sub>2</sub> Red-HexNAc <sub>1</sub>		3309.7109	3309.7079	0.91	1104.2443	3
110	Neu5Ac <sub>3</sub> HexNAc <sub>3</sub> Hex <sub>5</sub> Fuc <sub>1</sub> Red-HexNAc <sub>1</sub>		3320.687	3320.6875	0.15	1107.9029	3
111	Neu5Ac <sub>1</sub> HexNAc <sub>5</sub> Hex <sub>7</sub> Red-HexNAc <sub>1</sub>		3322.7007	3322.7032	0.73	1108.5742	3
112	Neu5Ac <sub>2</sub> HexNAc <sub>4</sub> Hex <sub>5</sub> Fuc <sub>2</sub> Red-HexNAc <sub>1</sub>		3378.7292	3378.7294	0.05	1127.2503	3

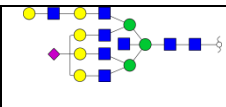
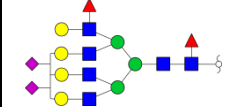
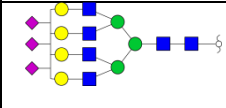
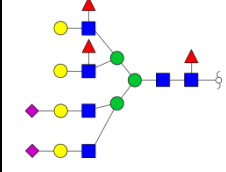
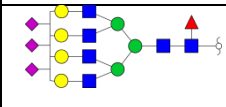
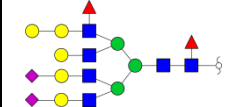
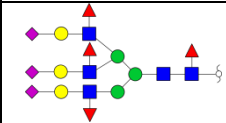
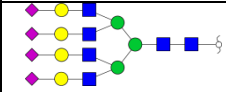
113	Neu5Ac <sub>1</sub> HexNAc <sub>4</sub> Hex <sub>6</sub> Fuc <sub>3</sub> Red-HexNAc <sub>1</sub>		3395.7425	3395.7447	0.64	1132.9215	3
114	Neu5Ac <sub>2</sub> HexNAc <sub>4</sub> Hex <sub>6</sub> Fuc <sub>1</sub> Red-HexNAc <sub>1</sub>		3408.7397	3408.7400	0.06	1137.2539	3
115	HexNAc <sub>4</sub> Hex <sub>7</sub> Fuc <sub>4</sub> Red-HexNAc <sub>1</sub>		3412.7642	3412.7600	1.23	1138.5953	3
116	HexNAc <sub>5</sub> Hex <sub>5</sub> Fuc <sub>5</sub> Red-HexNAc <sub>1</sub>		3423.78	3423.7760	1.17	1142.2673	3
117	Neu5Ac <sub>1</sub> HexNAc <sub>4</sub> Hex <sub>7</sub> Fuc <sub>2</sub> Red-HexNAc <sub>1</sub>		3425.76	3425.7553	1.39	1142.9273	3
118	Neu5Ac <sub>2</sub> HexNAc <sub>5</sub> Hex <sub>5</sub> Fuc <sub>1</sub> Red-HexNAc <sub>1</sub>		3449.7629	3449.7665	1.03	1150.9282	3
119	Neu5Ac <sub>1</sub> HexNAc <sub>5</sub> Hex <sub>6</sub> Fuc <sub>2</sub> Red-HexNAc <sub>1</sub>		3466.7814	3466.7818	0.11	1156.6011	3

120	HexNAc <sub>5</sub> Hex <sub>7</sub> Fuc <sub>3</sub> Red-HexNAc <sub>1</sub>		3483.789	3483.7971	2.33	1162.2703	3
121	Neu5Ac <sub>1</sub> HexNAc <sub>5</sub> Hex <sub>7</sub> Fuc <sub>1</sub> Red-HexNAc <sub>1</sub>		3496.7905	3496.7924	0.53	1166.6041	3
122	HexNAc <sub>5</sub> Hex <sub>8</sub> Fuc <sub>2</sub> Red-HexNAc <sub>1</sub>		3513.8156	3513.8077	2.26	1172.2792	3
123	Neu5Ac <sub>2</sub> HexNAc <sub>4</sub> Hex <sub>6</sub> Fuc <sub>2</sub> Red-HexNAc <sub>1</sub>		3582.8257	3582.8292	0.96	1195.2825	3
124	HexNAc <sub>6</sub> Hex <sub>8</sub> Fuc <sub>1</sub> Red-HexNAc <sub>1</sub>		3584.8372	3584.8448	2.11	1195.953	3
125	Neu5Ac <sub>3</sub> HexNAc <sub>4</sub> Hex <sub>6</sub> Red-HexNAc <sub>1</sub>		3595.8267	3595.8244	0.65	899.96395	4
126	Neu5Ac <sub>1</sub> HexNAc <sub>4</sub> Hex <sub>7</sub> Fuc <sub>3</sub> Red-HexNAc <sub>1</sub>		3599.8478	3599.8445	0.93	1200.9566	3
127	Neu5Ac <sub>2</sub> HexNAc <sub>4</sub> Hex <sub>7</sub> Fuc <sub>1</sub> Red-HexNAc <sub>1</sub>		3612.848	3612.8397	2.30	904.21927	4

128	Neu5Ac <sub>2</sub> HexNAc <sub>5</sub> Hex <sub>5</sub> Fuc <sub>2</sub> Red-HexNAc <sub>1</sub>		3623.8713	3623.8557	3.98	906.97511	4
129	Neu5Ac <sub>2</sub> HexNAc <sub>5</sub> Hex <sub>6</sub> Fuc <sub>1</sub> Red-HexNAc <sub>1</sub>		3653.8666	3653.8663	0.1	1218.9628	3
130	Neu5Ac <sub>1</sub> HexNAc <sub>5</sub> Hex <sub>7</sub> Fuc <sub>2</sub> Red-HexNAc <sub>1</sub>		3670.8736	3670.8816	2.17	1224.6318	3
131	Neu5Ac <sub>2</sub> HexNAc <sub>5</sub> Hex <sub>7</sub> Red-HexNAc <sub>1</sub>		3683.8777	3683.8769	0.24	1228.9665	3
132	Neu5Ac <sub>1</sub> HexNAc <sub>5</sub> Hex <sub>8</sub> Fuc <sub>1</sub> Red-HexNAc <sub>1</sub>		3700.8988	3700.8922	1.80	1234.6402	3
133	Neu5Ac <sub>2</sub> HexNAc <sub>4</sub> Hex <sub>6</sub> Fuc <sub>3</sub> Red-HexNAc <sub>1</sub>		3756.9164	3756.9184	0.52	1253.3127	3
134	Neu5Ac <sub>3</sub> HexNAc <sub>4</sub> Hex <sub>6</sub> Fuc <sub>1</sub> Red-HexNAc <sub>1</sub>		3769.9101	3769.9136	0.92	943.48481	4



135	Neu5Ac <sub>1</sub> HexNAc <sub>4</sub> Hex <sub>7</sub> Fuc <sub>4</sub> Red-HexNAc <sub>1</sub>		3773.9328	3773.9337	0.23	1258.9849	3
136	Neu5Ac <sub>1</sub> HexNAc <sub>7</sub> Hex <sub>6</sub> Fuc <sub>1</sub> Red-HexNAc <sub>1</sub>		3782.9396	3782.9453	1.48	946.74217	4
137	Neu5Ac <sub>2</sub> HexNAc <sub>4</sub> Hex <sub>7</sub> Fuc <sub>2</sub> Red-HexNAc <sub>1</sub>		3786.9354	3786.9289	1.72	947.74114	4
138	Neu5Ac <sub>1</sub> HexNAc <sub>5</sub> Hex <sub>7</sub> Fuc <sub>3</sub> Red-HexNAc <sub>1</sub>		3844.9634	3844.9708	1.92	1282.6617	3
139	Neu5Ac <sub>2</sub> HexNAc <sub>5</sub> Hex <sub>7</sub> Fuc <sub>1</sub> Red-HexNAc <sub>1</sub>		3857.9613	3857.9607	1.22	965.49761	4
140	Neu5Ac <sub>1</sub> HexNAc <sub>5</sub> Hex <sub>8</sub> Fuc <sub>2</sub> Red-HexNAc <sub>1</sub>		3874.9927	3874.9814	2.93	969.75544	4
141	Neu5Ac <sub>3</sub> HexNAc <sub>4</sub> Hex <sub>6</sub> Fuc <sub>2</sub> Red-HexNAc <sub>1</sub>		3944.0025	3944.0028	0.07	987.0075	4
142	Neu5Ac <sub>3</sub> HexNAc <sub>5</sub> Hex <sub>6</sub> Fuc <sub>1</sub> Red-HexNAc <sub>1</sub>		4015.0376	4015.0400	0.57	1004.7667	4

143	Neu5Ac <sub>1</sub> HexNAc <sub>7</sub> Hex <sub>8</sub> Red-HexNAc <sub>1</sub>		4017.0375	4017.0556	1.70	1340.0198	3
144	Neu5Ac <sub>2</sub> HexNAc <sub>5</sub> Hex <sub>7</sub> Fuc <sub>2</sub> Red-HexNAc <sub>1</sub>		4032.0579	4032.0553	0.66	1009.0217	4
145	Neu5Ac <sub>3</sub> HexNAc <sub>5</sub> Hex <sub>7</sub> Red-HexNAc <sub>1</sub>		4045.0484	4045.0505	0.51	1012.2694	4
146	Neu5Ac <sub>2</sub> HexNAc <sub>5</sub> Hex <sub>7</sub> Fuc <sub>3</sub> Red-HexNAc <sub>1</sub>		4206.1423	4206.1445	0.51	1052.5428	4
147	Neu5Ac <sub>3</sub> HexNAc <sub>5</sub> Hex <sub>7</sub> Fuc <sub>1</sub> Red-HexNAc <sub>1</sub>		4219.1413	4219.1397	0.38	1055.7926	4
148	Neu5Ac <sub>2</sub> HexNAc <sub>5</sub> Hex <sub>8</sub> Fuc <sub>2</sub> Red-HexNAc <sub>1</sub>		4236.1644	4236.1550	2.22	1060.0484	4
149	Neu5Ac <sub>3</sub> HexNAc <sub>4</sub> Hex <sub>6</sub> Fuc <sub>4</sub> Red-HexNAc <sub>1</sub>		4292.1745	4292.1813	1.56	1074.0509	4
150	Neu5Ac <sub>4</sub> HexNAc <sub>5</sub> Hex <sub>7</sub> Red-HexNAc <sub>1</sub>		4406.2216	4406.2242	0.57	1102.5627	4

151	Neu5Ac <sub>3</sub> HexNAc <sub>5</sub> Hex <sub>8</sub> Fuc <sub>1</sub> Red-HexNAc <sub>1</sub>		4423.2441	4423.2395	1.05	1106.8183	4
152	Neu5Ac <sub>3</sub> HexNAc <sub>5</sub> Hex <sub>7</sub> Fuc <sub>3</sub> Red-HexNAc <sub>1</sub>		4567.3062	4567.3181	2.60	1142.8338	4
153	Neu5Ac <sub>4</sub> HexNAc <sub>5</sub> Hex <sub>7</sub> Fuc <sub>1</sub> Red-HexNAc <sub>1</sub>		4580.3139	4580.3134	0.12	1146.0858	4
154	Neu5Ac <sub>3</sub> HexNAc <sub>5</sub> Hex <sub>8</sub> Fuc <sub>2</sub> Red-HexNAc <sub>1</sub>		4597.3349	4597.3287	1.36	1150.341	4
155	HexNAc <sub>2</sub> Hex <sub>4</sub> Fuc <sub>2</sub> Red-HexNAc <sub>1</sub>		1962.0335	1962.0296	1.97	982.02402	2
156	HexNAc <sub>4</sub> Hex <sub>3</sub> Fuc <sub>3</sub> Red-HexNAc <sub>1</sub>		2422.2681	2422.2717	1.49	1212.1228	2
157	Neu5Ac <sub>1</sub> HexNAc <sub>4</sub> Hex <sub>4</sub> Red-HexNAc <sub>1</sub>		2465.2769	2465.2775	0.25	822.76623	3
158	HexNAc <sub>4</sub> Hex <sub>4</sub> Fuc <sub>3</sub> Red-HexNAc <sub>1</sub>		2626.3721	2626.3715	0.24	876.46464	3

159	HexNAc <sub>6</sub> Hex <sub>3</sub> Fuc <sub>2</sub> Red-HexNAc <sub>1</sub>		2738.4322	2738.4352	1.07	913.81802	3
160	Neu5Ac <sub>1</sub> HexNAc <sub>4</sub> Hex <sub>3</sub> Fuc <sub>3</sub> Red-HexNAc <sub>1</sub>		2783.4157	2783.4454	2.42	928.81252	3
161	HexNAc <sub>4</sub> Hex <sub>4</sub> Fuc <sub>4</sub> Red-HexNAc <sub>1</sub>		2800.4605	2800.4607	0.07	934.49412	3
162	HexNAc <sub>5</sub> Hex <sub>3</sub> Fuc <sub>4</sub> Red-HexNAc <sub>1</sub>		2841.4791	2841.4873	2.86	948.16697	3
163	Neu5Ac <sub>1</sub> HexNAc <sub>4</sub> Hex <sub>3</sub> Fuc <sub>4</sub> Red-HexNAc <sub>1</sub>		2957.53	2957.5346	1.55	986.8506	3
164	HexNAc <sub>5</sub> Hex <sub>4</sub> Fuc <sub>4</sub> Red-HexNAc <sub>1</sub>		3045.5954	3045.5870	2.75	1016.2057	3
165	HexNAc <sub>7</sub> Hex <sub>5</sub> Fuc <sub>1</sub> Red-HexNAc <sub>1</sub>		3217.6692	3217.6718	0.80	1073.5637	3

166	Neu5Ac <sub>1</sub> HexNAc <sub>5</sub> Hex <sub>4</sub> Fuc <sub>3</sub> Red-HexNAc <sub>1</sub>		3232.6778	3232.6715	1.96	1078.5666	3
167	HexNAc <sub>5</sub> Hex <sub>5</sub> Fuc <sub>4</sub> Red-HexNAc <sub>1</sub>		3249.6924	3249.6868	1.73	1084.2381	3
168	Neu5Ac <sub>3</sub> HexNAc <sub>2</sub> Hex <sub>6</sub> Fuc <sub>1</sub> Red-HexNAc <sub>1</sub>		3279.694	3279.6610	1.02	1094.2386	3
169	Neu5Ac <sub>2</sub> HexNAc <sub>3</sub> Hex <sub>8</sub> Red-HexNAc <sub>1</sub>		3397.7335	3397.7240	2.82	1133.5851	3
170	HexNAc <sub>7</sub> Hex <sub>6</sub> Fuc <sub>1</sub> Red-HexNAc <sub>1</sub>		3421.771	3421.7716	0.16	1141.5976	3
171	Neu5Ac <sub>1</sub> HexNAc <sub>6</sub> Hex <sub>8</sub> Red-HexNAc <sub>1</sub>		3771.924	3771.9293	1.39	1258.3153	3
172	Neu5Ac <sub>1</sub> HexNAc <sub>6</sub> Hex <sub>8</sub> Fuc <sub>1</sub> Red-HexNAc <sub>1</sub>		3946.0151	3946.0185	0.85	1316.3456	3
173	Neu5Ac <sub>1</sub> HexNAc <sub>5</sub> Hex <sub>8</sub> Fuc <sub>4</sub> Red-HexNAc <sub>1</sub>		4223.1718	4223.1598	2.85	1408.7312	3
174	HexNAc <sub>3</sub> Hex <sub>4</sub> Fuc <sub>2</sub> Red-HexNAc <sub>1</sub>		2207.1523	2207.1560	1.65	1104.5834	3

175	HexNAc <sub>4</sub> Hex <sub>4</sub> Fuc <sub>2</sub> Red-HexNAc <sub>1</sub>		2452.2813	2452.2823	0.39	1227.1479	2
176	HexNAc <sub>5</sub> Hex <sub>8</sub> Fuc <sub>1</sub> Red-HexNAc <sub>1</sub>		3339.728	3339.7185	2.86	1114.2499	3
177	Neu5Ac <sub>6</sub> HexNAc <sub>3</sub> Hex <sub>5</sub> Fuc <sub>2</sub> Red-HexNAc <sub>1</sub>		4578.2998	4578.2977	0.46	1145.5822	4
178	HexNAc <sub>4</sub> Hex <sub>7</sub> Fuc <sub>1</sub> Red-HexNAc <sub>1</sub>		2890.4979	2890.4924	1.91	964.50659	3
179	Neu5Ac <sub>3</sub> HexNAc <sub>4</sub> Hex <sub>5</sub> Fuc <sub>1</sub> Red-HexNAc <sub>1</sub>		3565.812	3565.8139	0.51	1189.6113	3
180	HexNAc <sub>4</sub> Hex <sub>6</sub> Fuc <sub>1</sub> Red-HexNAc <sub>1</sub>		2686.3911	2686.3926	0.56	896.47096	3
181	Neu5Ac <sub>1</sub> HexNAc <sub>3</sub> Hex <sub>7</sub> Fuc <sub>2</sub> Red-HexNAc <sub>1</sub>		3180.6364	3180.6290	2.35	1061.2194	3
182	Neu5Ac <sub>1</sub> HexNAc <sub>7</sub> Hex <sub>4</sub> Fuc <sub>2</sub> Red-HexNAc <sub>1</sub>		3548.8361	3548.8349	0.34	888.2163	4
183	Neu5Ac <sub>1</sub> HexNAc <sub>7</sub> Hex <sub>6</sub> Red-HexNAc <sub>1</sub>		3608.8548	3608.8561	0.33	1203.9589	3

184	Neu5Ac <sub>1</sub> HexNAc <sub>5</sub> Hex <sub>5</sub> Fuc <sub>4</sub> Red-HexNAc <sub>1</sub>		3610.8563	3610.8605	1.15	903.72136	4
185	Neu5Ac <sub>1</sub> HexNAc <sub>5</sub> Hex <sub>5</sub> Fuc <sub>5</sub> Red-HexNAc <sub>1</sub>		3784.951	3784.9497	0.35	1262.6576	3
186	HexNAc <sub>7</sub> Hex <sub>7</sub> Fuc <sub>2</sub> Red-HexNAc <sub>1</sub>		3799.9644	3799.9606	1.02	1267.6621	3
187	Neu5Ac <sub>4</sub> HexNAc <sub>3</sub> Hex <sub>5</sub> Fuc <sub>3</sub> Red-HexNAc <sub>1</sub>		4030.036	4030.0396	0.88	1008.5148	4
188	Neu5Ac <sub>2</sub> HexNAc <sub>5</sub> Hex <sub>8</sub> Fuc <sub>1</sub> Red-HexNAc <sub>1</sub>		4062.0726	4062.0658	1.68	1016.5254	4
189	Neu5Ac <sub>3</sub> HexNAc <sub>5</sub> Hex <sub>7</sub> Fuc <sub>2</sub> Red-HexNAc <sub>1</sub>		4393.2277	4393.2289	0.27	1099.3142	4
190	Neu5Ac <sub>2</sub> HexNAc <sub>8</sub> Hex <sub>7</sub> Red-HexNAc <sub>1</sub>		4419.2546	4419.2558	0.26	1105.8209	4

191	Neu5Ac <sub>2</sub> HexNAc <sub>7</sub> Hex <sub>4</sub> Fuc <sub>5</sub> Red-HexNAc <sub>1</sub>		4432.2623	4432.2762	3.13	1109.0659	4
192	Neu5Ac <sub>3</sub> HexNAc <sub>6</sub> Hex <sub>6</sub> Fuc <sub>2</sub> Red-HexNAc <sub>1</sub>		4434.2685	4434.2555	2.95	1109.5744	4
193	Neu5Ac <sub>4</sub> HexNAc <sub>5</sub> Hex <sub>6</sub> Fuc <sub>2</sub> Red-HexNAc <sub>1</sub>		4550.2997	4550.3028	0.67	1138.5822	4
194	Neu5Ac <sub>2</sub> HexNAc <sub>8</sub> Hex <sub>7</sub> Fuc <sub>1</sub> Red-HexNAc <sub>1</sub>		4593.3412	4593.3450	0.82	1149.3426	4
195	Neu5Ac <sub>3</sub> HexNAc <sub>6</sub> Hex <sub>6</sub> Fuc <sub>3</sub> Red-HexNAc <sub>1</sub>		4608.3608	4608.3447	3.51	1153.0975	4
196	Neu5Ac <sub>4</sub> HexNAc <sub>5</sub> Hex <sub>7</sub> Fuc <sub>2</sub> Red-HexNAc <sub>1</sub>		4754.3994	4754.4026	0.66	1189.6071	4



197	Neu5Ac <sub>2</sub> HexNAc <sub>7</sub> Hex <sub>9</sub> Fuc <sub>1</sub> Red-HexNAc <sub>1</sub>		4756.4135	4756.4183	0.98	1190.1107	4
198	Neu5Ac <sub>3</sub> HexNAc <sub>5</sub> Hex <sub>8</sub> Fuc <sub>3</sub> Red-HexNAc <sub>1</sub>		4771.4217	4771.4179	0.80	1193.8627	4
199	Neu5Ac <sub>4</sub> HexNAc <sub>5</sub> Hex <sub>7</sub> Fuc <sub>3</sub> Red-HexNAc <sub>1</sub>		4928.4973	4928.4918	1.13	1233.1316	4
200	Neu5Ac <sub>2</sub> HexNAc <sub>2</sub> Hex <sub>7</sub> Red-HexNAc <sub>1</sub>		2948.5071	2948.4949	3.14	983.84297	3
201	Neu5Ac <sub>2</sub> HexNAc <sub>4</sub> Hex <sub>5</sub> Red-HexNAc <sub>1</sub>		3030.5521	3030.5510	0.38	1011.1913	3
202	HexNAc <sub>7</sub> Hex <sub>5</sub> Red-HexNAc <sub>1</sub>		3043.5837	3043.5826	0.37	1015.5352	3
203	HexNAc <sub>5</sub> Hex <sub>5</sub> Fuc <sub>3</sub> Red-HexNAc <sub>1</sub>		3075.5934	3075.5976	1.35	1026.2051	3
204	Neu5Ac <sub>3</sub> HexNAc <sub>3</sub> Hex <sub>5</sub> Red-HexNAc <sub>1</sub>		3146.5963	3146.5983	0.63	1049.8727	3

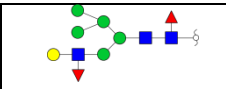
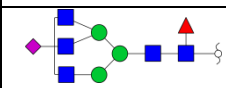
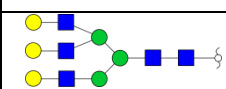
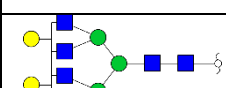
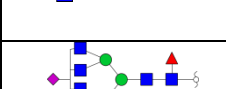

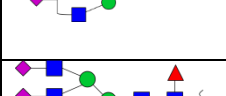
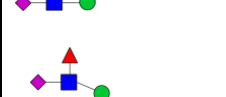
205	Neu5Ac <sub>3</sub> HexNAc <sub>3</sub> Hex <sub>6</sub> Red-HexNAc <sub>1</sub>		3350.6957	3350.6981	0.70	1117.9058	3
206	Neu5Ac <sub>2</sub> HexNAc <sub>3</sub> Hex <sub>7</sub> Fuc <sub>1</sub> Red-HexNAc <sub>1</sub>		3367.7121	3367.7134	0.38	1123.578	3
207	Neu5Ac <sub>3</sub> HexNAc <sub>4</sub> Hex <sub>5</sub> Red-HexNAc <sub>1</sub>		3391.7242	3391.7246	0.12	1131.582	3
208	Neu5Ac <sub>1</sub> HexNAc <sub>5</sub> Hex <sub>4</sub> Fuc <sub>4</sub> Red-HexNAc <sub>1</sub>		3406.7544	3406.7607	1.84	1136.5921	3
209	Neu5Ac <sub>3</sub> HexNAc <sub>3</sub> Hex <sub>6</sub> Fuc <sub>1</sub> Red-HexNAc <sub>1</sub>		3524.7869	3524.8237	0.10	1175.9363	3
210	Neu5Ac <sub>2</sub> HexNAc <sub>3</sub> Hex <sub>7</sub> Fuc <sub>2</sub> Red-HexNAc <sub>1</sub>		3541.8043	3541.8026	0.48	1181.6087	3
211	Neu5Ac <sub>2</sub> HexNAc <sub>5</sub> Hex <sub>4</sub> Fuc <sub>3</sub> Red-HexNAc <sub>1</sub>		3593.839	3593.8452	1.70	1198.9536	3

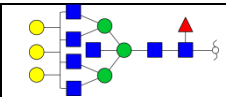
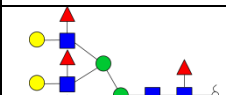
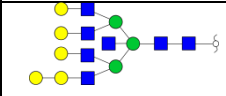
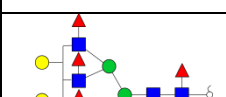
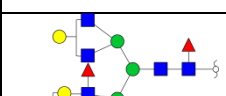
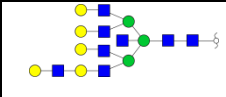
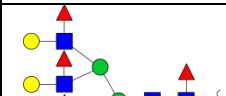
212	HexNAc <sub>7</sub> Hex <sub>7</sub> Fuc <sub>1</sub> Red-HexNAc <sub>1</sub>		3625.8767	3625.8714	1.48	1209.6328	3
213	HexNAc <sub>8</sub> Hex <sub>6</sub> Fuc <sub>1</sub> Red-HexNAc <sub>1</sub>		3666.902	3666.8979	1.12	1223.3079	3
214	Neu5Ac <sub>1</sub> HexNAc <sub>6</sub> Hex <sub>5</sub> Fuc <sub>3</sub> Red-HexNAc <sub>1</sub>		3681.8977	3681.8976	0.04	1228.3118	3
215	HexNAc <sub>5</sub> Hex <sub>8</sub> Fuc <sub>3</sub> Red-HexNAc <sub>1</sub>		3687.8882	3687.8969	2.35	1230.3033	3
216	HexNAc <sub>8</sub> Hex <sub>7</sub> Red-HexNAc <sub>1</sub>		3696.9095	3696.9085	0.29	1233.3104	3
217	Neu5Ac <sub>3</sub> HexNAc <sub>4</sub> Hex <sub>5</sub> Fuc <sub>2</sub> Red-HexNAc <sub>1</sub>		3739.9007	3739.9031	0.62	1247.6409	3
218	Neu5Ac <sub>2</sub> HexNAc <sub>5</sub> Hex <sub>4</sub> Fuc <sub>4</sub> Red-HexNAc <sub>1</sub>		3767.925	3767.9344	2.48	942.98853	4

219	Neu5Ac <sub>3</sub> HexNAc <sub>5</sub> Hex <sub>5</sub> Fuc <sub>1</sub> Red-HexNAc <sub>1</sub>		3810.9368	3810.9402	0.87	953.75039	4
220	HexNAc <sub>8</sub> Hex <sub>7</sub> Fuc <sub>1</sub> Red-HexNAc <sub>1</sub>		3870.998	3870.9977	0.09	1291.34	3
221	HexNAc <sub>7</sub> Hex <sub>4</sub> Fuc <sub>6</sub> Red-HexNAc <sub>1</sub>		3884.0094	3884.0181	2.23	1295.6771	3
222	Neu5Ac <sub>2</sub> HexNAc <sub>4</sub> Hex <sub>7</sub> Fuc <sub>3</sub> Red-HexNAc <sub>1</sub>		3961.0226	3961.0182	1.13	1321.3481	3
223	HexNAc <sub>7</sub> Hex <sub>9</sub> Fuc <sub>1</sub> Red-HexNAc <sub>1</sub>		4034.0699	4034.0709	0.24	1345.6972	3
224	Neu5Ac <sub>1</sub> HexNAc <sub>8</sub> Hex <sub>7</sub> Red-HexNAc <sub>1</sub>		4058.0841	4058.0822	0.49	1015.5283	4
225	Neu5Ac <sub>2</sub> HexNAc <sub>6</sub> Hex <sub>6</sub> Fuc <sub>2</sub> Red-HexNAc <sub>1</sub>		4073.0964	4073.0818	3.59	1019.2814	4

226	Neu5Ac <sub>3</sub> HexNAc <sub>5</sub> Hex <sub>6</sub> Fuc <sub>2</sub> Red-HexNAc <sub>1</sub>		4189.1246	4189.1292	1.07	1048.2884	4
227	Neu5Ac <sub>2</sub> HexNAc <sub>6</sub> Hex <sub>8</sub> Fuc <sub>1</sub> Red-HexNAc <sub>1</sub>		4307.1903	4307.1922	0.42	1077.8049	4
228	Neu5Ac <sub>4</sub> HexNAc <sub>5</sub> Hex <sub>6</sub> Fuc <sub>1</sub> Red-HexNAc <sub>1</sub>		4376.2154	4376.2136	0.42	1095.0611	4
229	Neu5Ac <sub>5</sub> HexNAc <sub>3</sub> Hex <sub>5</sub> Fuc <sub>3</sub> Red-HexNAc <sub>1</sub>		4391.2111	4391.2133	0.48	1464.7443	3
230	Neu5Ac <sub>1</sub> HexNAc <sub>7</sub> Hex <sub>9</sub> Fuc <sub>1</sub> Red-HexNAc <sub>1</sub>		4395.2465	4395.2446	0.45	1099.8189	4
231	Neu5Ac <sub>3</sub> HexNAc <sub>6</sub> Hex <sub>5</sub> Fuc <sub>3</sub> Red-HexNAc <sub>1</sub>		4404.2453	4404.2449	0.1	1102.0686	4
232	Neu5Ac <sub>3</sub> HexNAc <sub>6</sub> Hex <sub>8</sub> Red-HexNAc <sub>1</sub>		4494.2725	4494.2766	0.90	1124.5754	4
233	Neu5Ac <sub>3</sub> HexNAc <sub>6</sub> Hex <sub>5</sub> Fuc <sub>4</sub> Red-HexNAc <sub>1</sub>		4578.3284	4578.3341	1.24	1145.5894	4

234	Neu5Ac <sub>2</sub> HexNAc <sub>6</sub> Hex <sub>6</sub> Fuc <sub>3</sub> Red-HexNAc <sub>1</sub>		4595.3492	4595.3494	0.04	1149.8446	4
235	Neu5Ac <sub>1</sub> HexNAc <sub>6</sub> Hex <sub>6</sub> Fuc <sub>1</sub> Red-HexNAc <sub>1</sub>		3537.8215	3537.8189	0.73	1180.2811	3
236	Neu5Ac <sub>3</sub> HexNAc <sub>4</sub> Hex <sub>9</sub> Red-HexNAc <sub>1</sub>		4208.1246	4208.1237	0.22	1053.0384	4
237	Neu5Ac <sub>3</sub> HexNAc <sub>6</sub> Hex <sub>8</sub> Fuc <sub>1</sub> Red-HexNAc <sub>1</sub>		4668.3615	4668.3658	0.91	1168.0977	4
238	Neu5Ac <sub>2</sub> HexNAc <sub>7</sub> Hex <sub>9</sub> Red-HexNAc <sub>1</sub>		4582.3159	4582.3290	2.85	1146.5862	4
239	Neu5Ac <sub>4</sub> HexNAc <sub>4</sub> Hex <sub>9</sub> Red-HexNAc <sub>1</sub>		4569.3007	4569.2974	0.73	1143.3324	4
240	HexNAc <sub>6</sub> Hex <sub>4</sub> Fuc <sub>6</sub> Red-HexNAc <sub>1</sub>		3638.8921	3638.8918	0.10	1213.9563	3
241	Neu5Ac <sub>2</sub> HexNAc <sub>3</sub> Hex <sub>3</sub> Fuc <sub>3</sub> Red-HexNAc <sub>1</sub>		2899.5025	2899.4927	3.38	967.50725	3

242	HexNAc <sub>2</sub> Hex <sub>6</sub> Fuc <sub>2</sub> Red-HexNAc <sub>1</sub>		2370.224	2370.2292	2.18	1186.1193	2
243	Neu5Ac <sub>1</sub> HexNAc <sub>4</sub> Hex <sub>3</sub> Fuc <sub>1</sub> Red-HexNAc <sub>1</sub>		2435.2668	2435.2670	0.06	1218.6417	2
244	HexNAc <sub>4</sub> Hex <sub>6</sub> Red-HexNAc <sub>1</sub>		2512.3031	2512.3034	0.11	838.44087	3
245	HexNAc <sub>5</sub> Hex <sub>5</sub> Red-HexNAc <sub>1</sub>		2553.3302	2553.3300	0.10	852.11733	3
246	Neu5Ac <sub>1</sub> HexNAc <sub>5</sub> Hex <sub>3</sub> Fuc <sub>1</sub> Red-HexNAc <sub>1</sub>		2680.3901	2680.3933	1.18	894.47064	3
247	Neu5Ac <sub>2</sub> HexNAc <sub>5</sub> Hex <sub>3</sub> Fuc <sub>1</sub> Red-HexNAc <sub>1</sub>		3041.5643	3041.5670	0.86	1014.862	3
248	Neu5Ac <sub>3</sub> HexNAc <sub>4</sub> Hex <sub>3</sub> Fuc <sub>1</sub> Red-HexNAc <sub>1</sub>		3157.6138	3157.6143	0.15	1053.5452	3
249	HexNAc <sub>6</sub> Hex <sub>6</sub> Fuc <sub>1</sub> Red-HexNAc <sub>1</sub>		3176.6449	3176.6453	0.11	1059.8885	3

							
250	HexNAc <sub>4</sub> Hex <sub>6</sub> Fuc <sub>4</sub> Red-HexNAc <sub>1</sub>		3208.6556	3208.6603	1.44	1070.5592	3
251	HexNAc <sub>6</sub> Hex <sub>8</sub> Red-HexNAc <sub>1</sub>		3410.7489	3410.7556	1.95	1137.9236	3
252	HexNAc <sub>5</sub> Hex <sub>6</sub> Fuc <sub>4</sub> Red-HexNAc <sub>1</sub>		3453.7822	3453.7866	1.26	1152.268	3
253	Neu5Ac <sub>1</sub> HexNAc <sub>5</sub> Hex <sub>6</sub> Fuc <sub>3</sub> Red-HexNAc <sub>1</sub>		3640.8685	3640.8710	0.68	1214.6301	3
254	HexNAc <sub>7</sub> Hex <sub>8</sub> Red-HexNAc <sub>1</sub>		3655.8726	3655.8819	2.54	1219.6315	3
255	HexNAc <sub>5</sub> Hex <sub>7</sub> Fuc <sub>4</sub> Red-HexNAc <sub>1</sub>		3657.8918	3657.8864	1.50	1220.3045	3



256	HexNAc <sub>6</sub> Hex <sub>6</sub> Fuc <sub>4</sub> Red-HexNAc <sub>1</sub>		3698.9098	3698.9129	0.83	1233.9772	3
257	Neu5Ac <sub>1</sub> HexNAc <sub>6</sub> Hex <sub>7</sub> Fuc <sub>1</sub> Red-HexNAc <sub>1</sub>		3741.9093	3741.9187	2.50	1248.3104	3
258	Neu5Ac <sub>2</sub> HexNAc <sub>5</sub> Hex <sub>6</sub> Fuc <sub>2</sub> Red-HexNAc <sub>1</sub>		3827.9522	3827.9555	0.85	1276.9913	3
259	HexNAc <sub>7</sub> Hex <sub>8</sub> Fuc <sub>1</sub> Red-HexNAc <sub>1</sub>		3829.9644	3829.9711	1.80	1277.6621	3
260	HexNAc <sub>7</sub> Hex <sub>9</sub> Red-HexNAc <sub>1</sub>		3859.9725	3859.9817	2.37	965.99886	4
261	Neu5Ac <sub>1</sub> HexNAc <sub>6</sub> Hex <sub>6</sub> Fuc <sub>3</sub> Red-HexNAc <sub>1</sub>		3885.9973	3885.9974	0.01	1296.3397	3
262	HexNAc <sub>6</sub> Hex <sub>7</sub> Fuc <sub>4</sub> Red-HexNAc <sub>1</sub>		3903.0199	3903.0127	1.86	1302.0139	3

263	Neu5Ac <sub>1</sub> HexNAc <sub>5</sub> Hex <sub>7</sub> Fuc <sub>4</sub> Red-HexNAc <sub>1</sub>		4019.0581	4019.06	0.48	1340.6933	3
264	HexNAc <sub>5</sub> Hex <sub>8</sub> Fuc <sub>5</sub> Red-HexNAc <sub>1</sub>		4036.0848	4036.0753	2.35	1010.0285	4
265	Neu5Ac <sub>1</sub> HexNAc <sub>7</sub> Hex <sub>9</sub> Red-HexNAc <sub>1</sub>		4221.1469	4221.1554	1.99	1056.294	4
266	Neu5Ac <sub>2</sub> HexNAc <sub>5</sub> Hex <sub>8</sub> Fuc <sub>4</sub> Red-HexNAc <sub>1</sub>		4584.3262	4584.3335	1.57	1147.0888	4
267	Neu5Ac <sub>5</sub> HexNAc <sub>5</sub> Hex <sub>7</sub> Fuc <sub>1</sub> Red-HexNAc <sub>1</sub>		4941.4855	4941.4871	0.30	1236.3787	4
268	Neu5Ac <sub>3</sub> HexNAc <sub>7</sub> Hex <sub>9</sub> Red-HexNAc <sub>1</sub>		4943.493	4943.5027	1.95	1236.8805	4
269	Neu5Ac <sub>3</sub> HexNAc <sub>4</sub> Hex <sub>4</sub> Fuc <sub>1</sub> Red-HexNAc <sub>1</sub>		3361.7124	3361.7141	0.49	1121.5793	3
270	HexNAc <sub>6</sub> Hex <sub>4</sub> Fuc <sub>1</sub> Red-HexNAc <sub>1</sub>		2768.4424	2768.4457	1.19	923.82141	3

271	Neu5Ac <sub>1</sub> HexNAc <sub>5</sub> Hex <sub>6</sub> Red-HexNAc <sub>1</sub>		3118.5986	3118.6034	1.53	1040.5401	3
272	Neu5Ac <sub>1</sub> HexNAc <sub>6</sub> Hex <sub>4</sub> Fuc <sub>1</sub> Red-HexNAc <sub>1</sub>		3129.616	3129.6194	1.07	1044.2126	3
273	Neu5Ac <sub>1</sub> HexNAc <sub>6</sub> Hex <sub>5</sub> Fuc <sub>1</sub> Red-HexNAc <sub>1</sub>		3333.7162	3333.7192	0.88	1112.246	3
274	Neu5Ac <sub>1</sub> HexNAc <sub>3</sub> Hex <sub>3</sub> Red-HexNAc <sub>1</sub>		2016.0514	2016.0514	0.01	1009.033	2
275	HexNAc <sub>4</sub> Hex <sub>3</sub> Fuc <sub>2</sub> Red-HexNAc <sub>1</sub>		2248.1812	2248.1825	0.58	1125.0979	2
276	Neu5Ac <sub>2</sub> HexNAc <sub>4</sub> Hex <sub>3</sub> Red-HexNAc <sub>1</sub>		2622.3497	2622.3514	0.65	875.12385	3
277	Neu5Ac <sub>1</sub> HexNAc <sub>4</sub> Hex <sub>4</sub> Fuc <sub>4</sub> Red-HexNAc <sub>1</sub>		3161.6434	3161.6344	2.86	1054.8884	3
278	Neu5Ac <sub>2</sub> HexNAc <sub>4</sub> Hex <sub>4</sub> Fuc <sub>2</sub> Red-HexNAc <sub>1</sub>		3174.6312	3174.6296	0.51	1059.2177	3

279	Neu5Ac <sub>2</sub> HexNAc <sub>3</sub> Hex <sub>7</sub> Red-HexNAc <sub>1</sub>		3193.6263	3193.6242	0.67	1065.5494	3
280	Neu5Ac <sub>2</sub> HexNAc <sub>3</sub> Hex <sub>6</sub> Fuc <sub>2</sub> Red-HexNAc <sub>1</sub>		3337.7064	3337.7028	1.07	1113.5761	3
281	Neu5Ac <sub>1</sub> HexNAc <sub>6</sub> Hex <sub>5</sub> Fuc <sub>2</sub> Red-HexNAc <sub>1</sub>		3507.8064	3507.8084	0.55	1170.2761	3
282	Neu5Ac <sub>1</sub> HexNAc <sub>6</sub> Hex <sub>7</sub> Red-HexNAc <sub>1</sub>		3567.8357	3567.8295	1.75	1190.2859	3
283	Neu5Ac <sub>2</sub> HexNAc <sub>6</sub> Hex <sub>6</sub> Fuc <sub>1</sub> Red-HexNAc <sub>1</sub>		3898.9921	3898.9926	0.12	975.75531	4
284	Neu5Ac <sub>2</sub> HexNAc <sub>6</sub> Hex <sub>7</sub> Fuc <sub>1</sub> Red-HexNAc <sub>1</sub>		4103.0918	4103.0924	0.13	1026.7802	4
285	Neu5Ac <sub>3</sub> HexNAc <sub>4</sub> Hex <sub>6</sub> Fuc <sub>3</sub> Red-HexNAc <sub>1</sub>		4118.0934	4118.0920	0.34	1030.5306	4
286	Neu5Ac <sub>1</sub> HexNAc <sub>6</sub> Hex <sub>8</sub> Fuc <sub>2</sub> Red-HexNAc <sub>1</sub>		4120.0848	4120.1077	0.59	1033.7785	4
287	Neu5Ac <sub>1</sub> HexNAc <sub>7</sub> Hex <sub>8</sub> Fuc <sub>1</sub> Red-HexNAc <sub>1</sub>		4191.1379	4191.1448	1.63	1048.7917	4

288	Neu5Ac <sub>1</sub> HexNAc <sub>8</sub> Hex <sub>7</sub> Fuc <sub>1</sub> Red-HexNAc <sub>1</sub>		4232.1766	4232.1714	1.25	1411.7328	3
289	Neu5Ac <sub>3</sub> HexNAc <sub>6</sub> Hex <sub>6</sub> Fuc <sub>1</sub> Red-HexNAc <sub>1</sub>		4260.1642	4260.1663	0.47	1066.0483	4
290	Neu5Ac <sub>1</sub> HexNAc <sub>6</sub> Hex <sub>9</sub> Fuc <sub>2</sub> Red-HexNAc <sub>1</sub>		4324.2097	4324.2075	0.53	1082.0597	4
291	Neu5Ac <sub>3</sub> HexNAc <sub>6</sub> Hex <sub>7</sub> Fuc <sub>1</sub> Red-HexNAc <sub>1</sub>		4464.2661	4464.2660	0.02	1117.0738	4
292	Neu5Ac <sub>2</sub> HexNAc <sub>6</sub> Hex <sub>8</sub> Fuc <sub>3</sub> Red-HexNAc <sub>1</sub>		4655.3657	4655.3706	1.03	1164.8487	4
293	Neu5Ac <sub>2</sub> HexNAc <sub>6</sub> Hex <sub>9</sub> Fuc <sub>2</sub> Red-HexNAc <sub>1</sub>		4685.3924	4685.3811	2.42	1172.3554	4
294	Neu5Ac <sub>4</sub> HexNAc <sub>6</sub> Hex <sub>7</sub> Fuc <sub>1</sub> Red-HexNAc <sub>1</sub>		4825.4323	4825.4397	1.52	1207.3654	4
295	Neu5Ac <sub>4</sub> HexNAc <sub>6</sub> Hex <sub>8</sub> Fuc <sub>1</sub> Red-HexNAc <sub>1</sub>		5029.5417	5029.5395	0.45	1258.3927	4
296	Neu5Ac <sub>6</sub> HexNAc <sub>5</sub> Hex <sub>7</sub> Fuc <sub>1</sub> Red-HexNAc <sub>1</sub>		5302.6635	5302.6607	0.54	1326.6734	4

297	Neu5Ac <sub>2</sub> HexNAc <sub>3</sub> Hex <sub>3</sub> Red-HexNAc <sub>1</sub>		2377.2278	2377.3351	1.14	1189.6182	2
298	HexNAc <sub>6</sub> Hex <sub>3</sub> Fuc <sub>1</sub> Red-HexNAc <sub>1</sub>		2564.3451	2564.3460	0.32	1283.1798	2
299	HexNAc <sub>6</sub> Hex <sub>4</sub> Fuc <sub>2</sub> Red-HexNAc <sub>1</sub>		2942.5323	2942.5422	0.88	981.85138	3
300	Neu5Ac <sub>1</sub> HexNAc <sub>3</sub> Hex <sub>3</sub> Fuc <sub>1</sub> Red-HexNAc <sub>1</sub>		2190.1376	2190.1407	1.38	1096.0761	2
301	HexNAc <sub>6</sub> Hex <sub>3</sub> Red-HexNAc <sub>1</sub>		2390.2576	2390.2567	0.37	1196.129	2
302	HexNAc <sub>5</sub> Hex <sub>7</sub> Fuc <sub>5</sub> Red-HexNAc <sub>1</sub>		3831.9706	3831.9756	1.29	1278.3308	3

## 8. Acknowledgment

First and foremost, I would like to express my sincere appreciation and heartfelt gratitude to my supervisor, Prof. Hartmut Schlüter, for giving me the opportunity to conduct N-glycan project and supervising my work in his group at Universitätsklinikum Hamburg-Eppendorf (UKE) and most of all, for his invaluable guidance given throughout the duration of my research.

I am also very grateful to Prof. Neumann Julia and Dr. Voß Hannah, who advised me on my project and initiated this research project with my supervisor. They not only provided precious tissues and cell lines, but also invested their time and effort to ensure the research project was aligned with potential clinical outcomes in medulloblastoma cancer.






My PhD experience would not have been complete without the help and support of members from the Mass Spectrometric Proteomics group headed by my supervisor. Specifically, I would like to express my sincere gratitude to Dr. Yudong Guan for his invaluable technical advice on the use of mass spectrometry and N-glycan data analysis. I would also like to acknowledge present group members, Riedner, Dr. Maria, Moritz Manuela, Harder Soenke, Bente Siebels, Mair Thomas, Roza Haghiri and Zhao Shanshan for their friendship and support. I am also grateful to officemates, Englert Hanna and Luis Brito for their kind assistance as well as various snacks and participating in interesting and informative conversations in the office.

I would also like to thank the Guangzhou City Government for providing the Oversea Study Program of the Guangzhou Elite Project for three years.







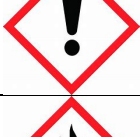






I am so thankful to have wonderful parents and friends who have continually been my source strength, motivation and love.







## 9. Risk and safety

Risk and safety pictograms of potentially hazardous chemicals used throughout this study, based on the Globally Harmonized System of Classification and Labelling of Chemicals (GHS), GHS hazard and precautionary statements.

Compound	GHS symbol	GHS hazard	Hazard statements	Precautionary statements
Methanol (LiChrosolv®)		GHS02 GHS06 GHS08	H225 H301 H311 H331 H370	P210 P240 P280 P302+P352 P304+P340 P308+P310- P403+P233
Ammonium bicarbonate		GHS07	H302	P301+P312+P330
Dithiothreitol		GHS07	H302 H315 H319 H335	P261 P305+P351+P338
Iodoacetamide		GHS06 GHS08	H301 H317 H334	P261 P280 P301+P310 P342+P311
Formic acid		GHS02 GHS06 GHS05	H226 H302 H314 H331 EUH071	P210 P280 P301+P330+P331 P304+P340 P305+P351+P338 P308+P310



Acetonitrile (LiChrosolv®)	 	GHS02 GHS07	H225 H302 H312 H332 H319	P210 P240 P302+P352 P305+P351+P338 P403+P233
Trypsin	 	GHS07 GHS08	H315 H319 H334 H317 H335	P264 P272 P280 P302+P352 P305+P351+P338 P312
Iodomethane	 	GHS06 GHS08	H301 H312 H315 H331 H335 H351	P261 P280 P301+P310 P311
Sodium deoxycholate		GHS07	H302	P301+P312+P330
Acetic acid	 	GHS02 GHS05	H226 H314	P210 P280 P301+P330+P331 P305+P351+P338 P308+P310
n-heptane	   	GHS02 GHS07 GHS08 GHS09	H225 H304 H315 H336 H410	P210 P273 P301+P310 P304+P340 P331 P403+P235

Ethanol	 	GHS02 GHS07	H225 H319	P210 P233 P305+P351+P338
Sodium hydroxide beads		GHS05	H290 H314	P233 P280 P303+P361+P353 P305+P351+P338 P310
Chloroform	 	GHS06 GHS08	H302 H315 H319 H331 H351 H361d H372	P202 P260 P302+P352 P304+P340 P305+P351+P338 P308+P313
Dimethyl sulfoxide		GHS02	H315 H319 H335	P261 P264 P264+P265 P271 P280 P302+P352 P304+P340 P305+P351+P338 P319 P321 P332+P317 P337+P317 P362+P364 P403+P233 P405 P501

## 10. Declaration

### Declaration on oath

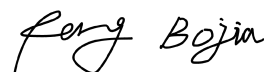
I hereby declare that this thesis has been generated by me from my own research and experiments. I have not used or written other than the acknowledged resources and aids. The submitted written version corresponds to the version on the electronic storage medium. I hereby declare that I have not previously applied or pursued for a doctorate (Ph.D. studies).

### Eidesstattliche Versicherung

Hiermit erkläre ich, dass ich diese Arbeit eigenständig anhand meiner eigenen Forschung und Experimente verfasst habe. Ich habe keine anderen als die anerkannten Quellen und Hilfsmittel verwendet. Die eingereichte schriftliche Version entspricht der Version auf dem elektronischen Speichermedium. Weiterhin versichere ich, dass diese Arbeit noch nicht an anderer Stelle als Abschlussarbeit vorgelegen hat.

Hamburg, 28 November 2023

Bojia Peng



---

Place and Date

Signature